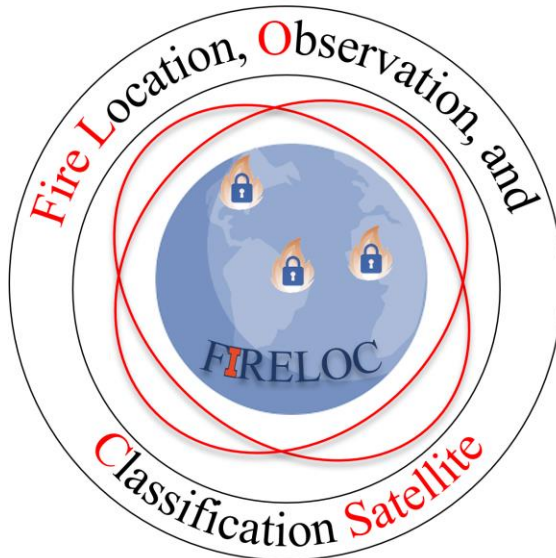


# Task 5.8 Fire Detection Constellation

Fire-LOC: Fire Location, Observation, and Classification Satellite



Team 5

Lucas Alava Peña [Orbital] L. Alava Peña

Corwin Carroll [Ground Stations] Corwin Carroll

Emilio Garcia Gordon [Power] Emilio G

Neil Limaye [C&DH/COMMs] Neil Limaye

Dean Romanchek [Team Lead] Dean Romanchek

David Salmi [Structures/Thermal] David Salmi

Rachit Singhvi [ADCS] Rachit

John Stecker [Propulsion] J Stecker

## 1. TASK ORDER

### 1.1. MISSION BACKGROUND

The Natural Geographic (NatGeo) released a study on March 21<sup>st</sup>, 2019 revealing shocking information regarding the wildfire epidemic caused by urbanization, expansion, and modernization which has invoked rapid climate change in the past several years<sup>[1]</sup>. This section will attempt to use this information to prove that the world is in danger and that not even the United States (US) can subdue this enemy. Based on this study, NatGeo estimates that there are more than 100,000 wildfires every year in the US alone, consuming up to 5 million acres (approximately 7,812 square miles – two thirds of the entire landmass of Haiti) of land every year<sup>[1]</sup>. In recent years, these statistics have soared to an estimated 9 to 10 million acres with damages including nearly a dozen firefighter fatalities every year since 2014 with an increase from 1,953 to 12,306 structures burned in just four years<sup>[2]</sup> according to the Congressional Research Service. With further investigation, based on statistics provided by the US Fire Administration (USFA), over the last ten years, an average of \$14.37 billion dollars in damages are directly attributed to US wildfires with this average leaping a staggering 12% from 2008 accounting for \$23 of the \$143.7 billion (or ~16%) of the damages over the last decade<sup>[3]</sup>.

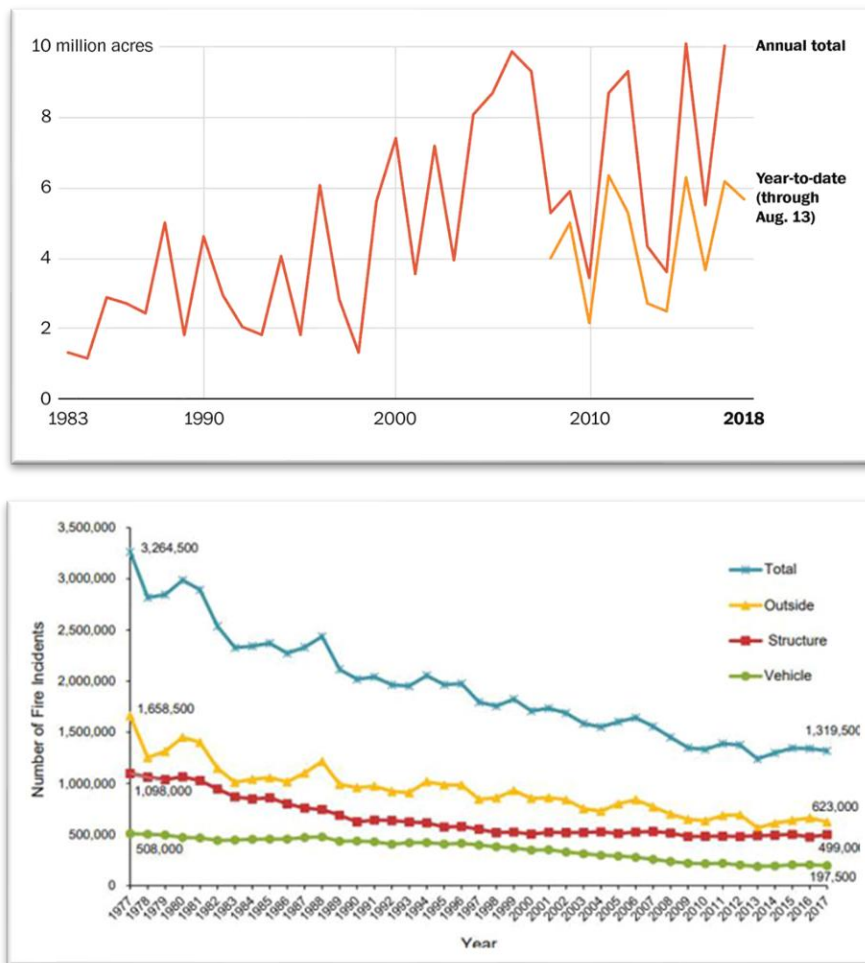


**Figure 1. Fire Activity.** Annual Total Burned Acres<sup>4</sup> (Top) and Fire Type Frequency<sup>5</sup> (Bottom).



USFA has clearly stated that there were 1,319,500 fires in the United States (US) in 2017<sup>[3]</sup>, but this trend has decreased by over six percent since 2008. In fact, based on findings from the National Fire Protection Agency (NFPA) which are shown in *Error! Reference source not found.*, fires of all types have decreased drastically over the last 30 years – outside fires by 62.43%, structural fires by 54.55%, and vehicle fires by 61.12% (totaling a 59.58% decrease)<sup>[5]</sup> – thus the recent surge in wildfire frequency and damage accumulation is greatly troubling. Although fewer fires happen on average, the damage and death that ensure continue to rise despite the US boasting some of the most advanced fire detection and regulation systems in the world. In just a few scattered events in Northern California in 2018, \$10.342 billion<sup>[3]</sup> can be attributed to the August Carr Fire<sup>[6]</sup> (causing over \$1.654 billion in damages and consuming 229,651 acres) and the July Ferguson Fire<sup>[7]</sup> (causing over \$345 million in damages and consuming 96,901 acres), which can be seen in *Error! Reference source not found.*. According to recent studies, wildfires spread at an average of 6.7 miles per hour in forest and 14 miles per hour in grassland<sup>[11]</sup>, thus assuming fires expand at a constant rate circularly, in the matter of an hour, wildfires can spread up to 90,000 acres in forest and 392,000 acres in grassland from a single point of origin as shown in *Error! Reference source not found.*.

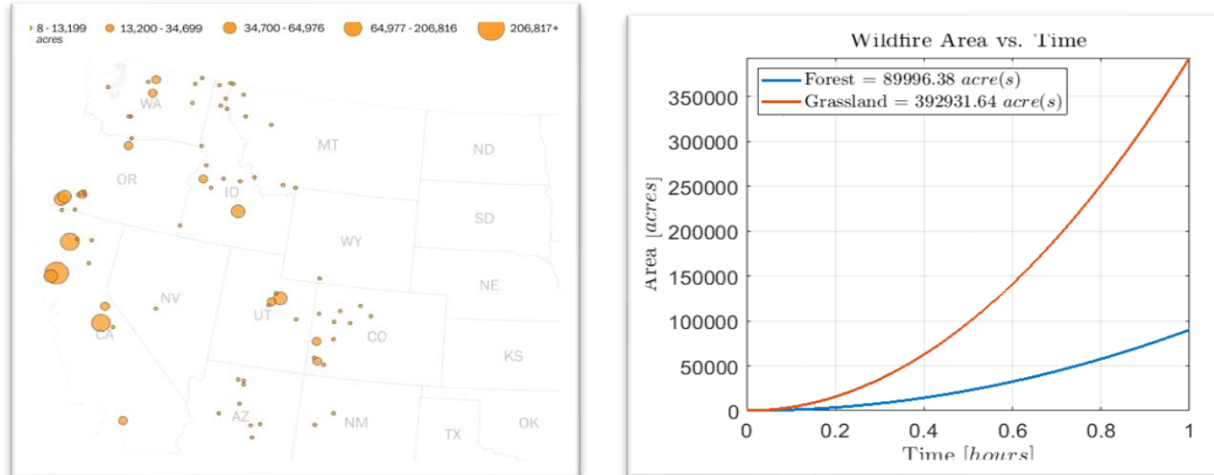


**Figure 2. Wildfire Spreading Information.** Wildfires Active in August 2018<sup>4</sup> (Left) and Wildfire Growth Rate (Right).

Based on the requirements and recommendations made in the Request For Proposal (RFP) and by the teaching staff of this course, the Fire-LOC system is planned to be a constellation of CubeSats accommodating an Infrared (IR) payload to locate, observe, and classify ground-based wildfires. This project and this mission detailed in this Preliminary Design Review (PDR) report are managed, developed, and operated through, and with the assistance of, the Laboratory for Advanced Space Systems at Illinois (LASSI) facilities. The Fire-LOC constellation provides 95% landmass coverage between the 70°S and 70°N lines of Latitude with a revisit period well below 24 hours, serving as a vigilant first warning system for the detection of potentially dangerous developing fires.

In an attempt to develop quick, reliable, and affordable communications, payload data will be relayed through a Space Based Communications System (Space COMMs) to selected ground stations to minimize response time while expanding the frequency which potentially lifesaving information can be transmitted.



The payload for this mission is capable of detecting ground fires at a 30-meter resolution while maintaining under the required 50-meter resolution with the assistance of advantageous orbital metrics and a highly accurate and sensitive Attitude Determination and Control System (ADCS). The CubeSat is purposefully not designed to locate and observe urban fires, as it is a redundant measure due to the currently in-place fire safety measures in urban environments.

## 2. MANAGEMENT APPROACH

### 2.1. TEAM ORGANIZATION

The Fire-LOC team has adapted the collaborative organizational hierarchy that was originally detailed in the project proposal. Following several design iterations, it was determined that a propulsion system may not be necessary, thus a heavier emphasis was placed on payload design. This organizational scheme attempts to optimize the team work flow by introducing a primary team lead, a secondary member (or 1<sup>st</sup> liaison), a tertiary member (or 2<sup>nd</sup> liaison), and so on. This allows for redundancy in design morphology and constant peer evaluation to maintain a tight schedule while adapting to feedback and design alterations quickly. Finally, this team organization assists sub-teams in maintaining a similar level of research and progress since secondary and tertiary members maintain the ability to shift from project to project based on their independent level of progress. **Error! Reference source not found.** shows the chain of command for this team and the high degree of collaboration and cooperation between sub-teams for the Fire-LOC system. Each team was assigned a key letter and color (for example, the Payload team uses red and the character Y) to label documents and trade studies for ease of navigation during the design process.

### 2.2. ROLES AND RESPONSIBILITIES

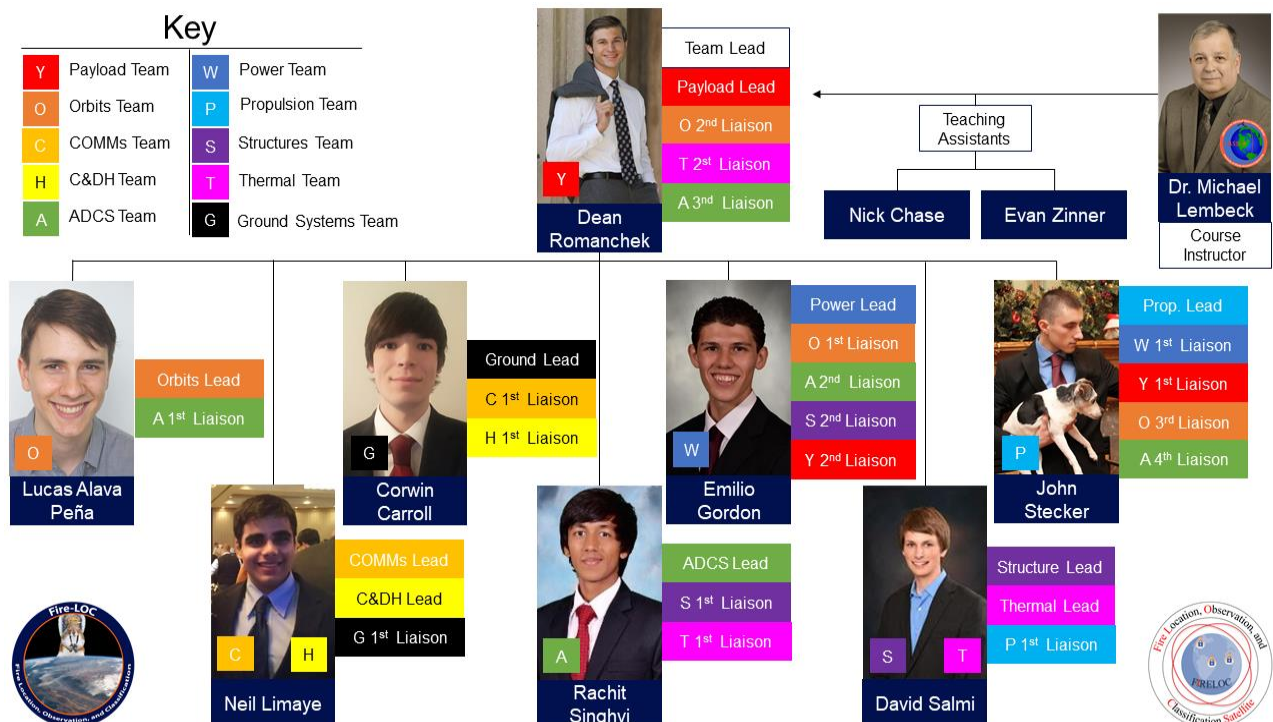


**Figure 3. Organizational Chart.** A high-level summary of the interconnections of various subsystems showing each team lead and the sub team liaison responsibilities for each member.

Operating as the Team Lead and payload lead, Dean Romanchek has been involved in cutting edge research and development, both within and beyond his academic focus. He has served Illinois Robotic in Space (IRIS) as secretary, chief mechanical engineer, project manager, president, and consulting engineer for mechanical and autonomous subsystems. Each year, IRIS enters NASA's annual Robotic Mining Competition (RMC) which entails the autonomous navigation and control of a rover-type vehicle to collect specified samples in a simulated, controlled, lunar environment. During his involvement, the IRIS team placed first in systems engineering twice, outperforming fifty top-ranked engineering universities and has pushed IRIS to reimagine their engineering process, emphasizing optimization and organization. Within the Koki Ho research group, Dean has focused primarily on computer aided design (CAD) and thermal simulations to design personalized passive thermal control systems in the SYNERGEO/SCEPTER project which focuses on the development of a software package to autonomously plan and design a unique constellation of CubeSat sized payloads. Within the Fire-LOC group, Dean's responsibilities include designing the payload and ensuring all other subsystems are designed, simulated, and meet the requirements of the RFP.

Operating as Power Lead, Emilio Gordon has been involved in a number of projects outside of the academic regime. For three years, Emilio served the Satellite Development Organization (SatDev) as director of member enrichment, thermal team lead, and volunteer under the (ADCS) subsystem. In his first year, Emilio worked on the proposal for the NASA Undergraduate Student Instrument Project (USIP) for both the Cooling, Annealing, and Pointing Satellite (CAPSat) and SpaceIce, two missions that University of Illinois Urbana-Champaign (UIUC) are currently undergoing. Outside of SatDev, Emilio has led a six-person team to design a fully electric, lunar space tug for the 2017 NASA BigIdea Challenge. In the 2016 NASA Micro-G NEXT challenge, his team developed and tested a tool for asteroid sample collection in micro-gravity that received positive feedback from the astronaut-trained divers. Within the Joshua Rovey research group, Emilio Gordon has assisted in the development of multi-mode propulsion, advancing the technology from a technical readiness level (TRL) of TRL3 to TRL5. Within the Fire-LOC group, Emilio's responsibilities include designing the power system, determining operational modes, power budgeting, solar panel placement, and power system component selection.

Operating as Structures/Thermal lead, David has experience working with Siemens NX Compter Aided Design Program for four years on a number of various projects. David worked on a Senior Design Project his freshman year where he modeled a satellite for an asteroid observation mission. David joined the Illinois Space Society competition team, Micro-G NEXT where he helped model and build an asteroid rock chipping sampler for micro-gravity environments. During the same year, David joined the SatDev program where he led the Harness team in constructing flight ready harnesses to all components for the Lower Atmosphere/Ionosphere Coupling Experiment (LAICE). David also helped with the Thermal Vacuum Chamber (TVAC) and some testing towards the final stages before satellite completion. Besides his club activities, David has experience working at the MakerLab, a 3D printing facility on campus where he teaches workshops on 3D modeling and printing. Within the Fire-LOC group, David's responsibilities include bulk thermal simulations, computer aided design, structural modeling, high fidelity thermal simulations, and thermal component selection and P-PODS compliance.



Operating as Propulsion lead, John Stecker has participated in a number of relevant and useful registered student organizations and research projects. With SatDev, over the first three years of undergrad, John worked with the TVAC and Testing, Harness, and Thermal Simulation and Design teams, spending the majority of the time with the TVAC and Testing team. On the TVAC and Testing team, John acquired practical knowledge of testing procedures, equipment upkeep, and characterization of testing equipment. Working with the Harness subteam, John learned Creo Parametric's Cabling tool, and proceeded to teach the rest of the team the tool's capabilities. In his second year, John participated in the NASA Student Competition Payload and Structures teams, where he helped to design a landing system for a large model rocket, as well as design, select, and assemble components of the rocket. Under the Undergraduate Research Opportunities Program (UROP), John worked in a paid capacity on the five CubeSat missions LASSI had operating, contributing materials to the CDRs for SpaceICE, CAPSat, and SASSI<sup>2</sup>. Meeting with subteam leads, gathering information, John independently constructed MOAGs of power and data connections between subsystems, as well as detailed graphics for each subsystem components, for SASSI<sup>2</sup>, SpaceICE, and CAPSat. Within the Fire-LOC group, John's responsibilities include all interface control diagrams (ICD), the feasibility analysis of a propulsion system, and assisting all other subteams that require additional manpower due to his incredible breadth of knowledge on the topics at hand.

Operating as ADCS team lead, Rachit Singhvi is a part of a diverse group of registered student organizations on campus. Most recently, he has served as co-program manager for LASSI's CubeSail mission that was launched aboard RocketLab's Electron rocket as a part of the ELaNa mission in December of 2018. He is also a part of the program management team for LASSI's LAICE CubeSat as well as a part of the ADCS team for a few other CubeSat missions. Understanding the importance of disciplined organization and efficient planning are at the heart of all missions, was a key result of his experience working at LASSI. He also developed a strong technical base in the continually advancing field of CubeSat ADCS. Rachit was also involved in the 2017 NASA BIG IDEA Challenge where his team developed a fully electric, modular, and extendable lunar space tug. Within the Fire-LOC group, Rachit's responsibilities include all attitude control simulations, component research and placement, and attitude determination component selection.

Operating as Orbital Mechanics team lead, Lucas Alava Peña has a variety of relevant experiences. Lucas participated in the Drone Dash 2 competition. He helped his team achieve a novel implementation to achieve the task of the competition that involved a remote-controlled electromagnet. As a result, his team won the biggest payload award. Moreover, he has relevant experience in using GMAT experience from his space system course. This experience includes a variety of different implementing a variety of different maneuvers. As part of a UTC Rolls Royce partnership between the Composites UTC center in Bristol and the light weight UTC in Dresden, Lucas conducted research in the realm of modelling the bonding of over-molded thermoplastics. Thereafter, the model was implemented using MATLAB, this script involved reading Moldflow outputs and creating a statistical model of the over-molding process based on experimental data that Lucas has conducted from numerous Dynamic Stability Control (DSC) runs to emulate the actual modelling process. Within the Fire-LOC group, Lucas' responsibilities include all orbital mechanics calculations, trade-off analysis, orbital phasing, ground coverage calculations, eclipse and shading, and final orbital selections.



Operating as Command and Data Handling (C&DH) team lead, Neil Limaye has extensive experience in the field of computer science and software architecture for varying applications. Extensive experience with multiple programming languages including Java, C, C++, Python, JavaScript, Ruby, and MATLAB as well as a deep understanding of the fundamental operations of both UNIX and Windows-based operating systems inform the mindset with which to approach the requirements for command and data handling for the Fire-LOC satellite. Neil's experience constructing homeostatic thermodynamic systems with limited equipment and funds as well as his assembly and programming of an Arduino-powered automated valve qualify him to understand the requirements for the necessary commercial off-the-shelf (COTS) equipment to complete this task. Within the Fire-LOC group, Neil's responsibilities include data compression and storage research, communications research, operating system and data handing research, and final component selection for all communications and command and data handling apparatus.

Operating as Ground Systems lead, Corwin Carroll has experience working with the CubeSat CAPSat in LASSI. Corwin has seen the radiator payload from concept to assembly and testing. In addition to this, Corwin has experience in computer science, having taken a multitude of computer science courses. This has led to experience in C, C++, Java, Python, and Rust that can be put to use in designing the ground systems of the Fire-LOC satellite. Within the Fire-LOC group, Corwin's responsibilities include all ground station phases, operations, and contact schedules as well as ensuring all ground station and communications linkages are properly planned to ensure a feasible subsystem.

### **2.3. FIRE TRADE STUDY APPROACH**

For organization, the Fire-LOC team has implemented a tested and established trade study organization and management system known as the FIRE model. The FIRE model is a revision of the Decision Matrix Document (DMD) model implemented in the 2016 NASA BigIDEA challenge. By implementing this model, the team was able to meet tight deadlines while managing to maintain organization and meet the requirements established in the challenges RFP. By following the FIRE (Foresee, Investigate, Record, and Execute) model, every trade study conducted using the tree diagram in **Appendix C. Iterative Design Approach** allows a standard template for documentation and review known as the FIRE Document. By following the FIRE model, trade studies are guaranteed to be conducted in a systematic and organized way. The FIRE Doc. is written by the supervisor of the specific trade study and follows a standardized template with four key pillars:

- 1. Foresee:** The first section of a FIRE Doc. defines the problem statement the trade study plans to investigate. This establishes a clear outline for the rest of the document and allows the reader to understand what is gained from reading the document.
- 2. Investigate:** After establishing intent, the next step is to investigate. Every trade study involves research and discovery. The findings, whether through research or experimentation are listed in this section in great detail with appropriate citations. The “investigate” portion involves a major bulk of the different sources and discoveries made when conducting the trade study.
- 3. Record:** With the completion of a thorough investigation, the record section acts as a summary and final decision made from the trade study. The record section is concise and provides reasoning for the decision.
- 4. Execute:** This section subjects the supervisor of the trade study to peer review. Here the trade study supervisor, sub team liaison, and team lead must approve and sign-off at the conclusions



reached. Once a FIRE document has been signed off, the trade study is considered complete. If rejected by any party for any reason, the supervisor must revisit and fix the corrections or expand on the trade study.

By implementing the FIRE model, trade studies and the resulting decisions are easily retraceable and conducted in accordance with the dates and deadlines schedules in the team Gantt chart shown in **Appendix F. Gantt Chart**. In addition, the FIRE model introduces an element of peer review and responsibility for every trade study which ensures all members are informed of pertinent design decisions and re-evaluated design criterion which could affect the morphology of the entire satellite which multiple members keep subsystems on schedule.

### 3. INTERFACE CONTROL DIAGRAM

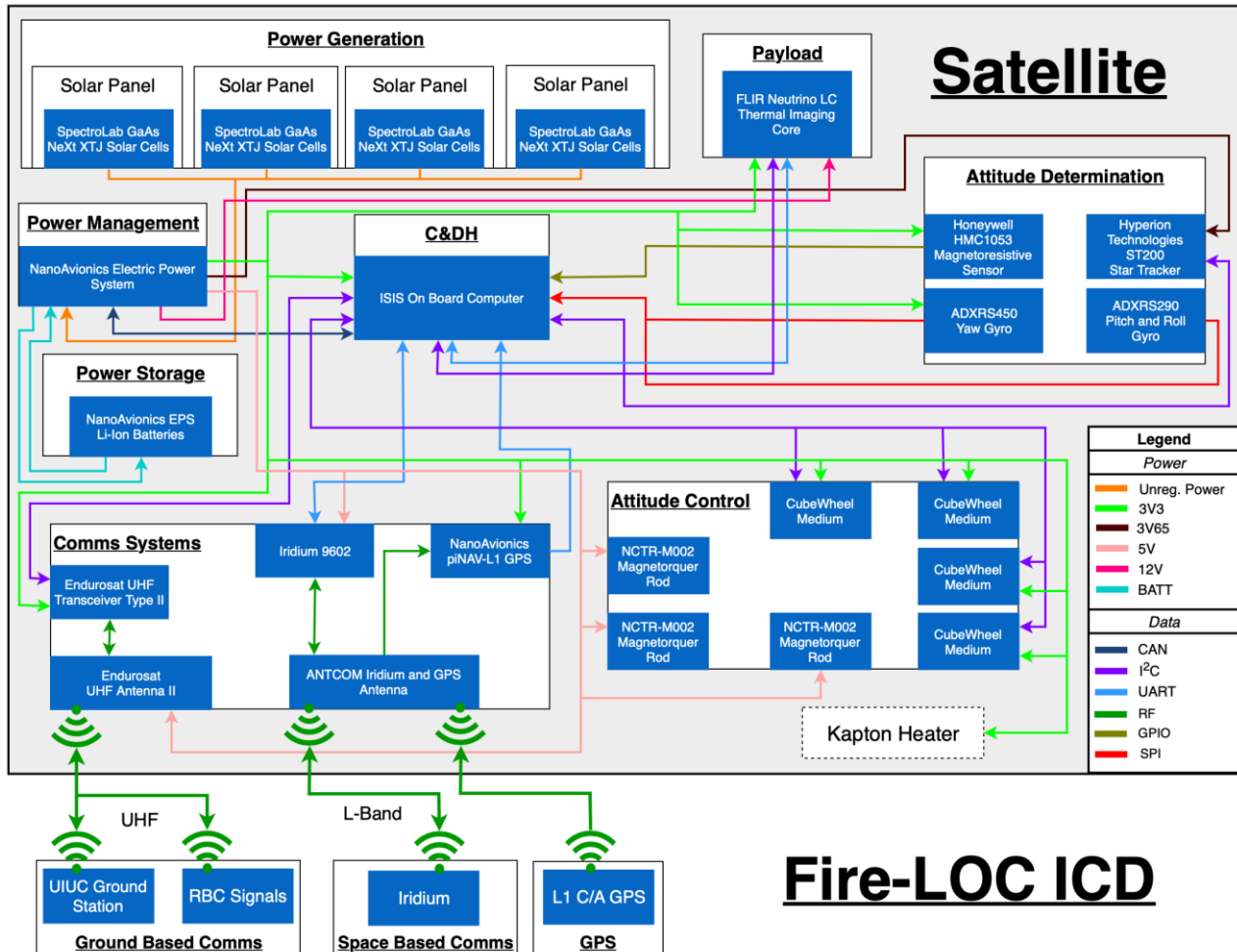


**Figure 4. Fire-LOC ICD:** This diagram demonstrates the data and power connections between the various subsystems, as well as basic connections between the satellite and its comms targets

The Interface Control Diagram (ICD) seen above in **Error! Reference source not found.** demonstrates the interconnectivity of the various subsystems comprising the Fire-LOC satellite. With regards to power output from the power management system, the NanoAvionics Electric Power System, there are four available regulated voltage rails, two at 3V3 and 5V, and the other two configurable between 3V and 18V



<sup>[14]</sup>. These two configurable channels would be set to 3V65 for the star tracker, and 12V for a possible thermal system for the modified FLIR, if necessary. If any additional voltages are required, buck or boost converters could be used to lower or raise the voltage as necessary.

Data connections are all feasible with the ISIS On-Board Computer (OBC), which allows SPI, UART, I<sup>2</sup>C, and GPIO connections, with two important notes <sup>[15]</sup>. One, CAN bus is not directly supported by the OBC, though bridges do exist that can control CAN using SPI interfaces, such as the MCP2515 <sup>[16]</sup>. Second, only 2 UART connections are available on the OBC, though, again, bridges exist to convert SPI or I<sup>2</sup>C to UART, such as the SC16IS7xx <sup>[17]</sup>.

## 4. PAYLOAD

### 4.1. SYSTEM REQUIREMENTS

Based upon the mission presented in the Error! Reference source not found. and **Appendix D.** sections, the payload operational requirements will dominate the iterative design process for this mission. A great majority of the mission objectives are oriented towards the success of the payload design, thus slight alterations in design or system configuration will greatly affect the operation of each of the other subsystems discussed in the Error! Reference source not found. section. The level one and level two system requirements in **Table 1** below will serve as a preface to inform the reader as to the purpose of the alterations in design between payload iterations. Paramount to the success of this project are requirements dictating payload operations and execution, namely the use of Infrared (IR) imagery, re-visitation time below 24 hours, landmass coverage, and ground resolution. **Table 1** lists the level one and two requirements updated to the specifications of the final payload design.

**Table 1. Payload Requirements.** Enumerated Level 1 and Level 2 Requirements for the Payload as specified by the Request for Proposal (RFP).

Req. #	Requirement	Verification
<b>Y:1</b>	<b>Each CubeSat shall carry a minimum of one payload/instrument.</b>	<b>Inspection</b>
<b>Y:2</b>	<b>The payload shall detect fires.</b>	<b>Test</b>
Y:2.1	The payload/constellation shall have a re-visitation time of 24 hours or less.	Analysis
Y:2.2	The payload shall have 95% landmass coverage between 70°S and 70°N lines of Latitude.	Analysis
Y:2.3	The payload shall be at an altitude of 500 km.	Analysis
Y:2.4	The payload shall gather data in the form of infrared (IR) imagery.	Test
Y:2.5	The payload shall map ground fires at 50 m resolution per pixel.	Analysis
<b>Y:3</b>	<b>The payload shall accept commands from the C&amp;DH system.</b>	<b>Test</b>
<b>Y:4</b>	<b>The payload shall communicate with the C&amp;DH System.</b>	<b>Test</b>
Y:4.1	The payload shall send IR data to the C&DH system.	Test
Y:4.2	The payload shall send status of health data to the C&DH system.	Test
<b>Y:5</b>	<b>The payload shall receive power from the power system.</b>	<b>Test</b>
Y:5.1	The payload shall receive $\leq$ 8 W from the Power System.	Test
<b>Y:6</b>	<b>The payload shall have its temperature regulated by the thermal system.</b>	<b>Test</b>
Y:6.1	The payload shall maintain a temperature between -40 and 70 °C.	Test

### 4.2. FIRST DESIGN ITERATION



Resolution determination was the cornerstone of the first Fire-LOC design iteration and was arguably the criterion that drove the entire system design. Additionally, the delicate balance between orbital altitude and ground resolution determines the operational conditions for nearly every other sub-team. Based on our requirement to utilize IR imagery, this first design iteration aims to narrow the possible resolutions, fields of view, power, and data requirements to enable future iterations to make an informed decision on possible combinations of optical systems for the purpose of orbit to ground based fire detection constellations. The Payload team initialized its research by learning more about infrared (IR) technology, in particular, how the IR wavelengths are divided, categorized, and studied. From our research, in general, the wavelengths of light in the IR band are divided into five major sub-divisions as shown in **Table 2**.

**Table 2. IR Band Divisions.** A compiled list of the most frequently cited divisions of the Infrared bands.

DIVISION NAME	ABBREVIATION	WAVELENGTH	FREQUENCY	TEMPERATURE
<b>NEAR-IR</b>	NIR, IR-A <i>DIN</i>	0.75–1.4 $\mu\text{m}$	214–400 THz	3,864–2,070 K (3,591 to 1,797 °C)
<b>SHORT-WAVELENGTH IR</b>	SWIR, IR-B <i>DIN</i>	1.4–3 $\mu\text{m}$	100–214 THz	2,070–966 K (1,797 to 693 °C)
<b>MID-WAVELENGTH IR</b>	MWIR, IR-C <i>DIN</i> ; MidIR, IIR	3–8 $\mu\text{m}$	37–100 THz	966–362 K (693 to 89 °C)
<b>LONG-WAVELENGTH IR</b>	LWIR, IR-C <i>DIN</i>	8–15 $\mu\text{m}$	20–37 THz	362–193 K (89 to –80 °C)
<b>FAR IR</b>	FIR	15–1000 $\mu\text{m}$	0.3–20 THz	193–3 K (–80.15 to –270.15 °C)

From this we learned that IR cameras are usually specialized to one of these divisions with the capability of imaging in the nearest band above and below the focus as well. This set of divisions, however, changes with the academic community as shown in **Table 3**, **Table 4**, and **Table 5**; for instance, the astrophysics community defines Mid-Infrared (MIR) as light between wavelengths of 5–40  $\mu\text{m}$  while the ISO 20473 division lists MIR between 5–50  $\mu\text{m}$ . This could result in design complications when researching the current capabilities of IR detectors if each sensor found refers to a different division scheme. In general, the following are also accepted subdivisions of the IR Bands within district academic communities:

**Table 3. CIE IR Divisions.** The IR division scheme utilized by the International Commission on Illumination (CIE).

Abbreviation	Wavelength	Frequency
IR-A	700 nm – 1400 nm (0.7 $\mu\text{m}$ – 1.4 $\mu\text{m}$ )	215 THz – 430 THz
IR-B	1400 nm – 3000 nm (1.4 $\mu\text{m}$ – 3 $\mu\text{m}$ )	100 THz – 215 THz
IR-C	3000 nm – 1 mm (3 $\mu\text{m}$ – 1000 $\mu\text{m}$ )	300 GHz – 100 THz

**Table 4. ISO 20473 Divisions.** Another common division scheme for IR bands for Optics and Photonics.

Designation	Abbreviation	Wavelength
Near-IR	NIR	0.78–3 $\mu\text{m}$
Mid-IR	MIR	3–50 $\mu\text{m}$
Far-IR	FIR	50–1000 $\mu\text{m}$

**Table 5. Astronomy division scheme.** The IR division scheme utilized by most deep space sensors.

Designation	Abbreviation	Wavelength	Page Number
Near-IR	NIR	(0.7–1) to 5 $\mu\text{m}$	9
Mid-IR	MIR	5 to (25–40) $\mu\text{m}$	
Far-IR	FIR	(25–40) to (200–350) $\mu\text{m}$	



This information is incredibly useful when designing an IR imaging payload since the specific use of the payload will define the particular bands of the IR spectrum are attainable with commercial off the shelf (COTS) components like cameras, lenses, and filters. Since this mission is tailored towards fire detection, an investigation was initiated into possible methods for positive fire detection that are currently in use. In general, the National Fire Protection Association (NFPA) suggests using Rate-of-Rise heat detection systems to determine if temperatures in the immediate vicinity are rising higher than the present rate per time factor (or in laymen's terms: if an area is increasing its temperature more rapidly than its surrounding areas). This solves the issue of the Fixed Temperature Detection system that only determines if a fire has reached a certain intensity.

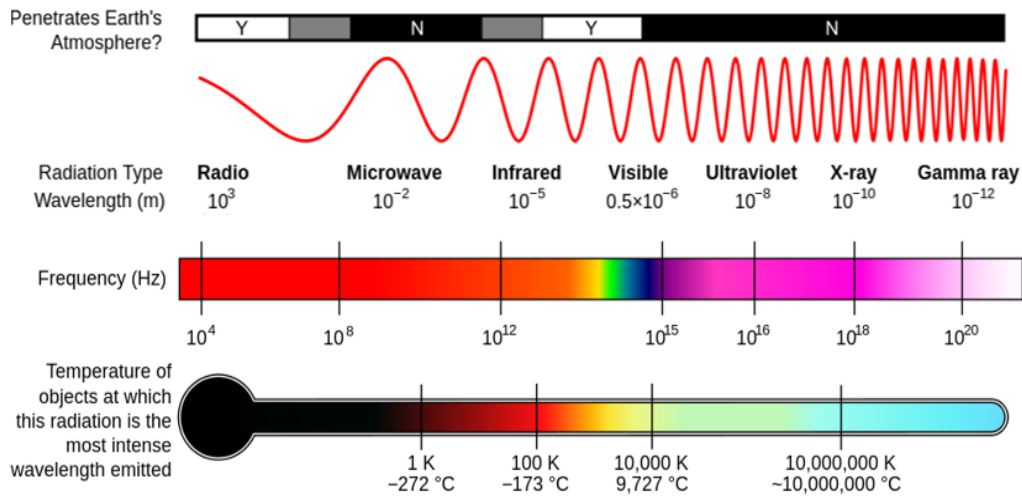


**Figure 5. Electromagnetic Spectrum. Light Spectrum Highlighting Temperature, Frequency, Radiation Type, and Earth Atmosphere Penetration [18].**

For maximum fire detection capabilities, the Fire-LOC team has determined that a Rate-of-Rise system will be the most effective for the mission at hand. Additionally, it has been shown by the NFPA that IR cameras can quickly and reliably detect fires by searching for a few select tell-tale signs of wild fires, namely the resonance frequency of carbon. When a combustible substance is ignited, it releases subtle amounts of carbon which becomes increasingly visible as a fire becomes more intense. It has been shown that this region lies between 4.3-4.4  $\mu\text{m}$  which places it firmly within the MWIR (or IR-C and MIR in other definitions) band of the IR spectrum. This greatly reduces the number of imaging devices capable of this level of accuracy, thus a few, select COTS photo-cells or imaging devices to act as the basis of the design for the Fire-LOC Payload.

Finally, our research shows that for IR sensors, refrigeration is key. These sensors usually require temperatures in excess of -200°C to operate nominally, but with the use of lasers based on indium antimonide (InSb), a realistic, near-room temperature IR-based gas analysis device can be created for the purpose of fire detection by focusing on the resonance frequency of carbon to search for tell-tale signs of growing fires using a Rate-of-Rise system. However, a quantum cascade laser must be used to detect wavelengths in this band, but that makes it an ideal photo-acoustic spectrometer for gas analysis and companies like QCSense have already pioneered this field.



Many sources identify key ingredients to the propagation of wildfires, namely the fire triangle: fuel, oxygen, and heat. The Error! Reference source not found. and **Appendix D.** sections should have clearly defined the Fire-LOC constellation's purpose is the localization, observation, and classification of wildfires. Thus, since fuel and oxygen concentration are nearly impossible to detect in critical amounts using IR cameras from orbit, heat is the most viable candidate for successful detection. In the field of forensic analysis, many cite the flash point (or the point at which something ignites) of various types of wood between 463.15 and 533.15 K (or 160-260 °C)<sup>[19]</sup>. At this temperature, a great deal of IR radiation is emitted, and the wavelengths of this light register as Mid-Wavelength Infrared (MWIR) radiation in the most common division scheme which can be seen in **Figure 5**.

Based on this knowledge, a thorough investigation into the effect of possible resolutions based on available IR technology on the payload ground resolution based on variance in Field of View (FOV) and orbital altitude was conducted. **Figure 6** summarizes these findings in a graphical setting. For an accurate determination of the feasibility of our payload design, a proper, justifiable, realistic field of view must be selected. To maximize coverage, a large field of view must be selected. However, the farther away from Earth a satellite is, the greater the number of pixels required to obtain the same or similar resolutions as spacecrafts at lower altitudes. Based on this information, an orbital altitude between 400 km and 600 km is desirable. However, it is difficult to determine and justify a possible field of view and resolution for the

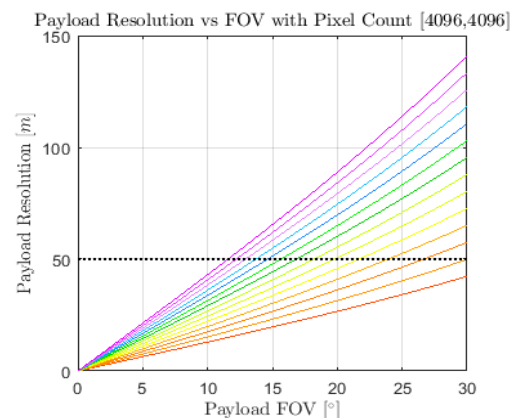
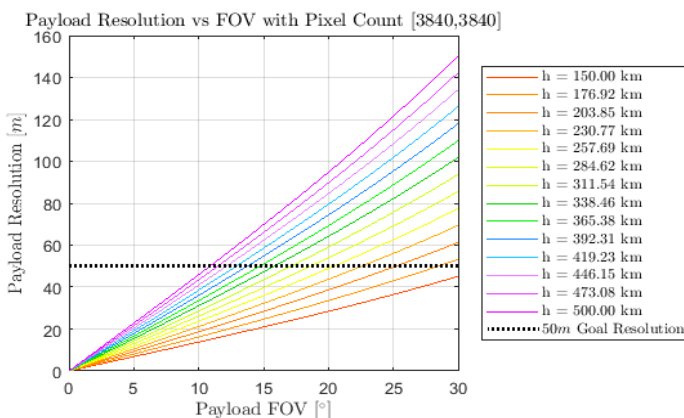
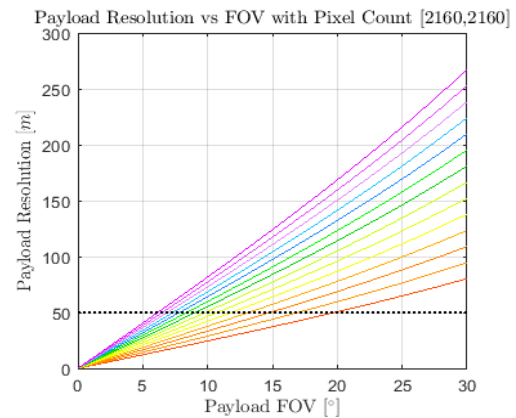
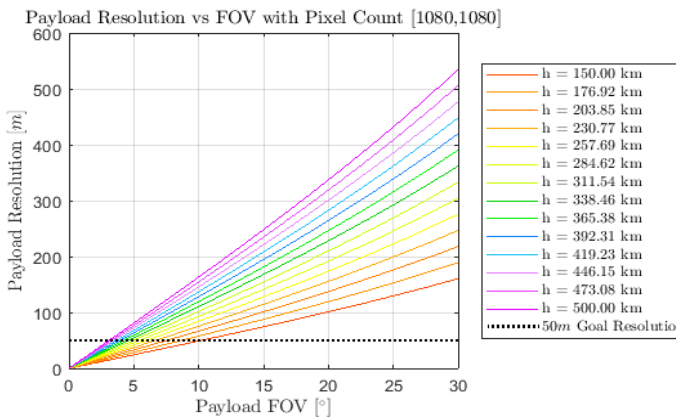


**Figure 6. Payload Resolution vs. FOV. The effect of Pixel Count (1080-4096) on Ground Resolution Based on Variance in Altitude and Possible Fields of View for Available Technology.**



customized IR payload for the Fire-LOC system at this stage due to the staggering number of pixels required for 50-meter ground resolution at even the lowest altitudes tested as shown in **Figure 7**, but there is a strong correlation between altitude, field of view, and ground resolution. It has been determined that a minimum resolution allowable for accurate detection of the smallest fire, a Class A fire as shown in **Appendix A. Fire Classification**, would make each pixel 30 by 30 m. As a comparative metric, the payload team has decided to use “number of passes end-to-end over the United States (US)” to quantify the effect of possible pairings of orbital altitudes, ground coverage, and field of view. Continuing the assumption of a square resolution, the following figure was generated.

As it can be deduced, as the number of orbital passes decreases, the East to West Length of the image must increase in order to preserve a 30 m resolution. For reference, a modern 4K camera has upwards of 16 million pixels. To minimize the revisit time, a smaller number of orbital passes is preferred, but it is unlikely that a number of passes over the US with a single payload below 40 passes is not possible with today’s technology using square image resolution. This information allowed the payload team to reinvestigate the correlation between field of view and payload resolution. Based on the findings of this study, square image resolution will not be utilized in the payload design.

#### 4.3. SECOND DESIGN ITERATION

The incredible restrictions on field of view determined in the previous design iteration has led to a decrease to the frequency of re-visitation which increases the risk of undetected fires while holding the number of satellites in the constellation constant. Therefore, a non-square resolution has been selected to both increase the area traced by the payload and to decrease the total number of satellites required to achieve the desired landmass coverage. Based on the available technology discussed, a common resolution for IR detection is  $640 \times 512$  which yields 327,680 total pixels. If these pixels are rearranged to a  $20 \times 16,384$  configuration, this allows for a 30 m ground resolution satisfying **Y:2.5** and a total field of view below  $95^\circ$  at 600 km and below  $70^\circ$  at 400 km which are capable of satisfying the arbitrary

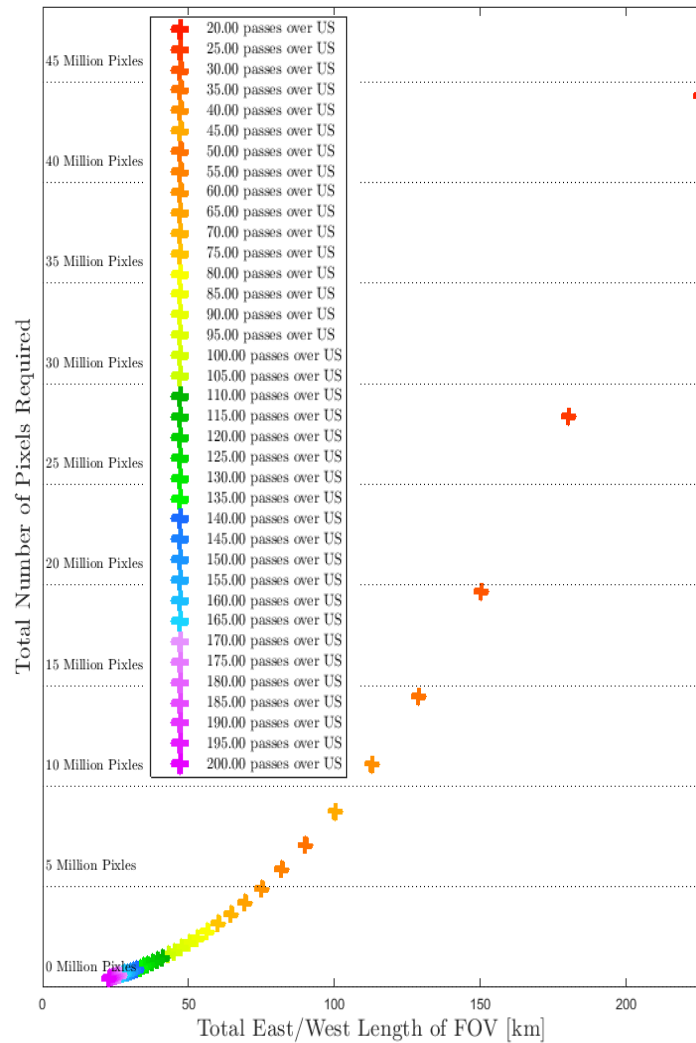


**Figure 7. Pixel Count vs. East/West Ground Track Length.**  
Correlation Between Number of Passes Over the US and Total Number of Pixels Required for A Square Image.



benchmark for imaging the continental United States in 15 passes or less. As orbital altitude increases, the field of view required to achieve this resolution will decrease, which allows for design iteration to improve the overall performance of the system. In order to achieve a system capable of detecting fires with a reasonable number of satellites in the constellation, and an appropriate image resolution for detecting Class A fires, an IR sensor that satisfies those requirements, and is capable of detecting wavelengths determined in the previous design iteration, shall be determined in this iteration.

Having determined that a square image would not be feasible for a reasonable constellation size, the IR sensor will be a rectangular, nearly linear imaging array. In order to determine the practicality of a miniaturized MWIR sensor, commercial options were initially investigated. **Figure 8** shows the FLIR™ Neutrino™ SWaP+C Series, a commercially available MWIR camera which will be used as the backbone to create a realistic design for this payload. This miniaturized sensor has a mass of 380 grams, dimensions of 7.4 cm x 4.6 cm x 6.1 cm, and power consumption of 4 W nominally and 8 W while powering up. Given the high level of feasibility of this imager, the Fire-LOC thermal imager will be modeled similarly. However, the Neutrino™ SWaP+C has a resolution of 640 x 512 pixels, which much too low for the Fire-LOC mission. Therefore, the Fire-LOC sensor will have an imaging array with the same number of pixels, but reoriented to provide a better, push broom style of coverage for the constellation.

To further explore the possibility of this push broom set-up, image distortion and imaging rates were

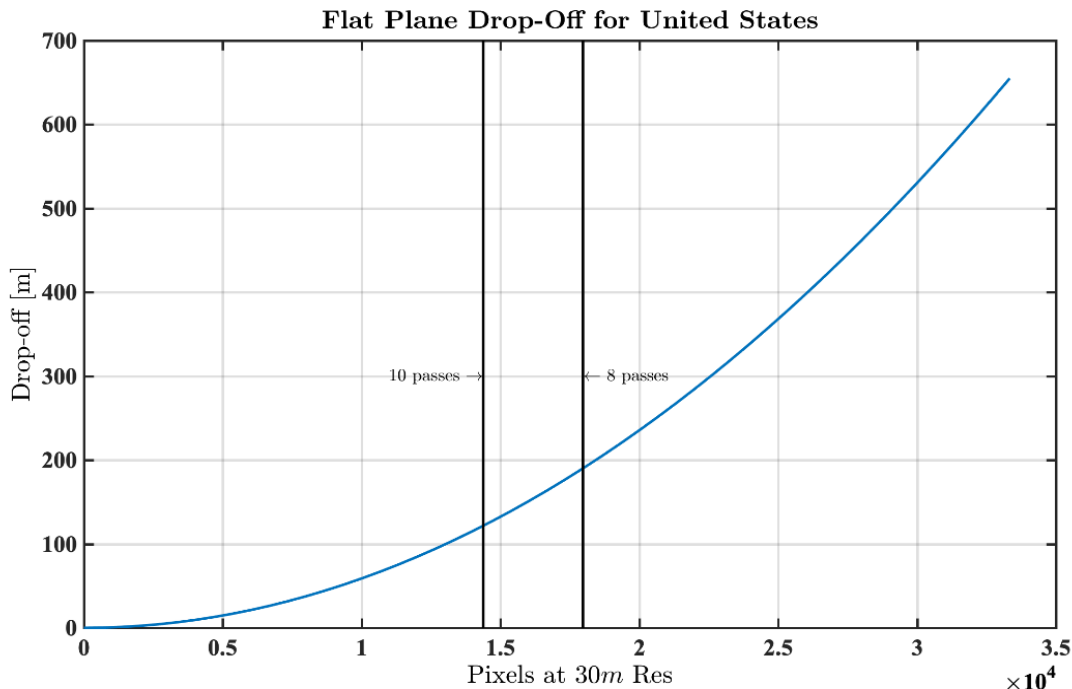


**Figure 9. Earth Horizon Drop-Off vs. Horizontal Pixel Count.** Correlation Between Number of Passes Over the US and the Drop Off of Resolution due to the Immense Size of the Imager's Ground Track.



examined. **Figure 9** shows the “flat plane drop-off” for a specific pixel width at the desired 30 m resolution. This “flat plane drop-off” is the difference between the assumed flat imaging plane, and the actual curvature of the earth. Pixel widths associated with 10 and 8 passes needed to cover the U.S. end to end have been marked off. It can be seen that the drop off is negligible compared with the size of the image in this range, meaning that at the scale investigated, image perspective distortion should not be too large a factor. As for the imaging

rates, the Neutrino™ SWaP+C has a max imaging rate of 60 Hz. In the graph in **Figure 10**, imaging rates required for various orbit altitudes have been plotted against image widths. A wider image would make the image for the push broom shorter height wise and would require a higher imaging rate. The 60 Hz limit has been drawn, and the pixel widths corresponding to 10 and 8 passes needed to cover the U.S. end to end have been marked off. Given a setup within 8 to 10 passes, in the altitudes further tested in the **ORBITAL ANALYSIS** section, the imaging rate is more than reasonable for an IR imaging sensor of construction similar to the Neutrino™ SWaP+C, in a push broom configuration.

From these plots, a push broom pixel width between the marked 8 and 10 passes is a feasible option. At a pixel width of 16,384 pixels, the height of the imaging array is 20 pixels. This results in the same number of pixels as the 640 x 512 imager from FLIR™. In order to reduce the likelihood of any false positives,

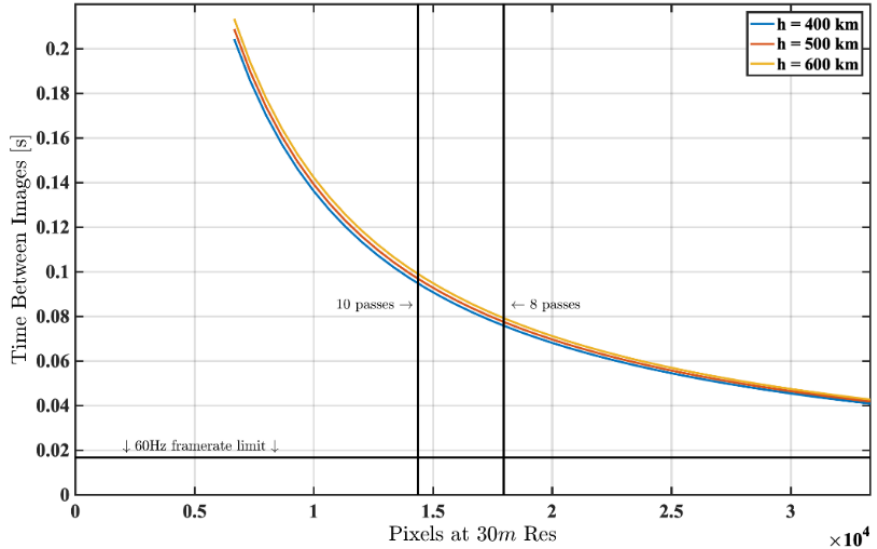


**Figure 10. Imaging Rates vs. Horizontal Pixel Count.** Imaging Rates Required for Various Pixel Configurations for an IR Payload at Several Orbital Altitudes.

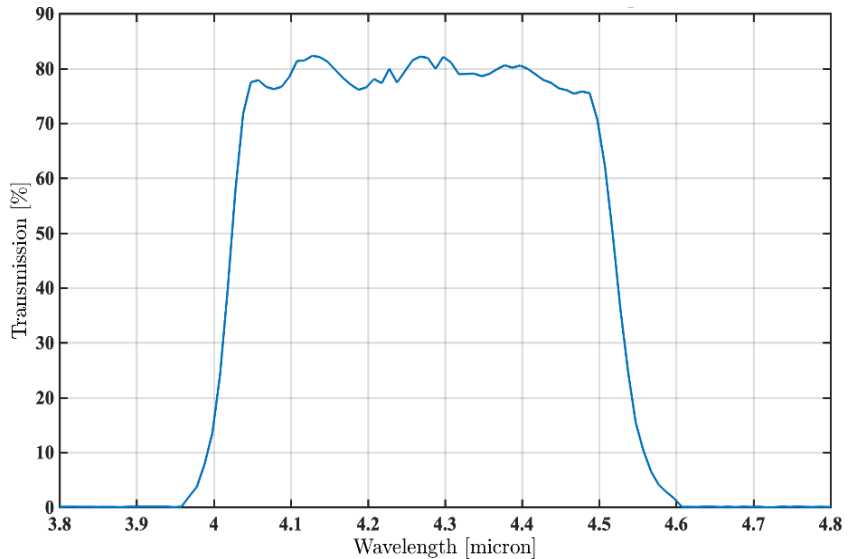


**Figure 11. Filter Light Passage.** Transmission Wavelengths for the FB4250-500 IR Bandpass Filter from THORLABSTM.

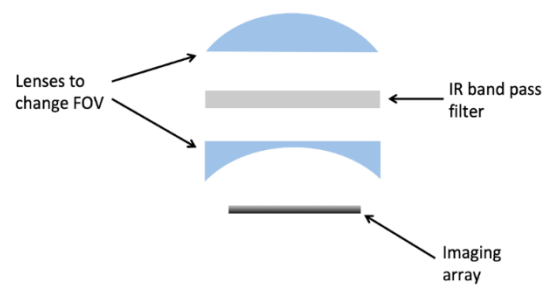


**Figure 12. Estimated Lens Configuration.** Plano-Convex/Filter/Plano Concave Payload Lens Pairing Configuration.



the FB4250-500 IR Bandpass Filter from THORLABSTM can be used to block out any unnecessary wavelengths of light. The transmission plot for the filter can be seen in **Figure 11**, which only allow the wavelengths identified in design iteration one to pass through to the IR sensor which reduces the likelihood of false positives by limiting the amount of radiation capable of being detected.

The final additional pieces of the IR sensor are the lenses necessary to achieve the FOV determined in by the altitude selected. Based on the evidence presented in this document, a thorough investigation into the effect of possible resolutions based on available technology on the payload ground resolution based on variance in image size and orbital altitude was conducted. **Figure 13** shows the basic construction of the payload configuration determined in this design iteration, with lenses to adjust the FOV, and the IR filter to ensure fewer false positives with possible image rates shown in **Figure 13**.

#### 4.4. FINAL DESIGN ITERATION

Based on the findings of the previous two design iterations, an IR filter was chosen to remove all light not within 4,000-5,000 nm on the MWIR band (the resonance frequency of CO<sub>2</sub> and the flash point of most wood).

As a result, the incoming visual data to the payload will either be black or heat data between 89-693°C, successfully detecting fires satisfying **Y:1**, **Y:2**, **Y:2.4**, **Y:2.5**. For ease of data interpretation, this data will be grey scaled to reduce the depth of the image from [255 × 255 × 255] to a single “intensity” reading between 0-255. This will reduce each pixel to a depth of 1 byte (8 bits), which makes the entire image approximately 400 kilobytes (as discussed in the **COMMAND & DATA HANDLING** section). For seamless coverage, the payload would need to capture an image every 0.08 seconds between 400-600

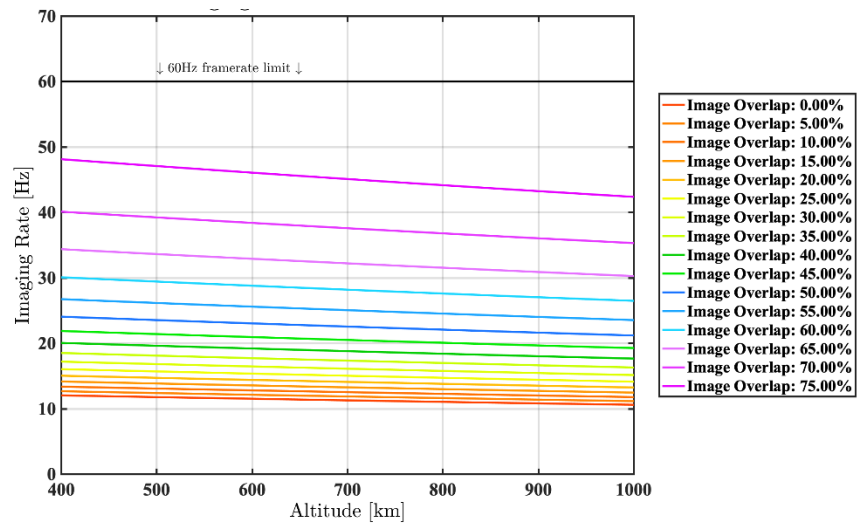


**Figure 13. Imaging Rates at Various Altitudes.** The correlation between altitude, imaging rates, and the percentage of overlap between images being captured by the payload system.

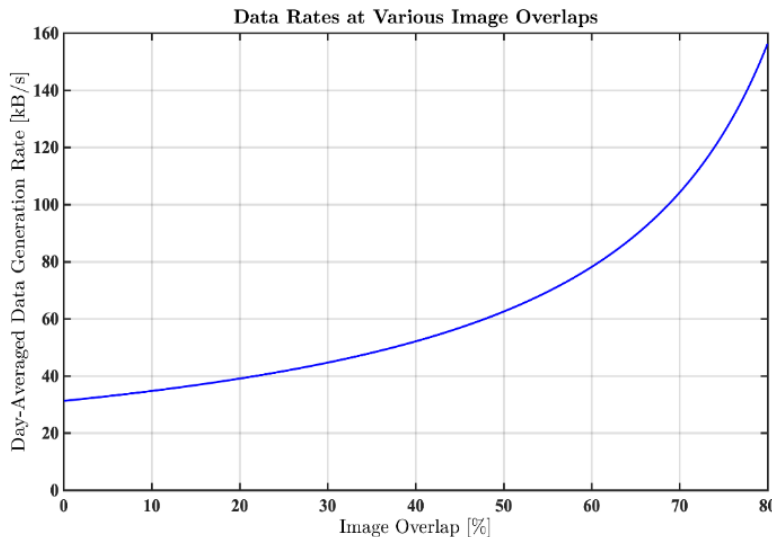


**Figure 14. Possible Payload Data Rates.** High level estimate of possible payload data generation rates using the fringe case of 4,500 detected per day per satellite.



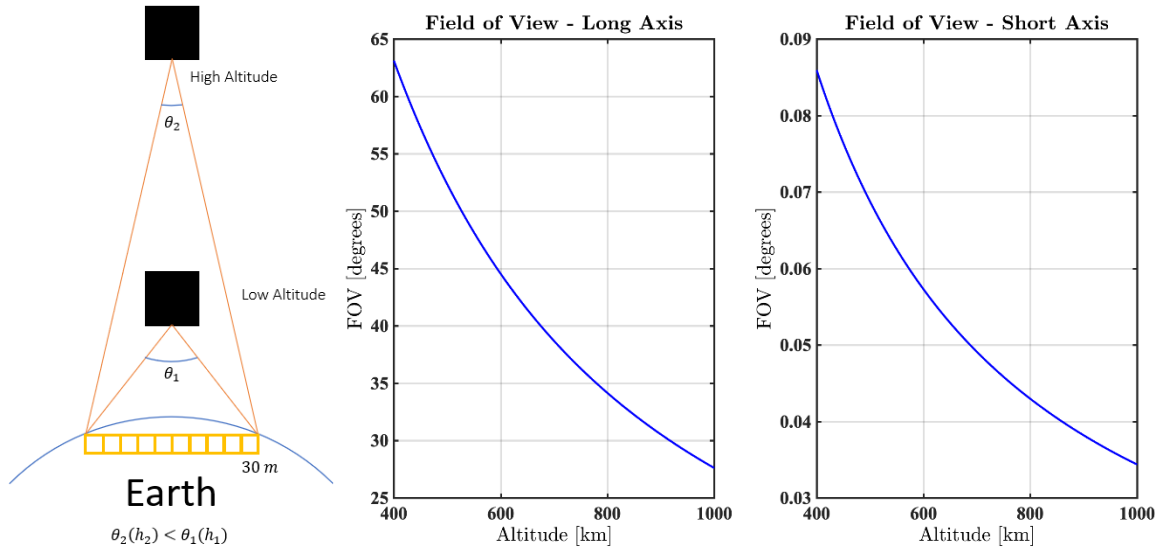


**Figure 15. Payload Field of View Determination.** Field of View Required Metrics at Various Altitudes for a payload with constant ground track.

km altitude, but for image overlap to reduce the possibility of a false positive, images would need to be taken much faster. These findings are corroborated in **Figure 14**.

Based on information present in National Geographic's online webpage<sup>1</sup>, an average of 100,000 wildfires occur every year in the United States. Extrapolating and assuming similar conditions for the propagation of wildfires globally, one would assume that around 1,628,187.17 wildfires would occur every year. Continuing, this would equate to 4,457.73 fires per day. The chance a single satellite would detect every one of these fires in one orbit is nearly zero, but we will assume it is possible as a fringe case to further design the system. This would create a total of 1.78 gigabytes of data per day of non-discarded IR images with the data recording rate dictated by the altitude of the spacecraft. **Figure 15** demonstrates the day-averaged data rates per second for the spacecraft, assuming an average fire size of 50 acres, 4,500 fires in a day, and that every fire is captured by the same satellite, providing a high estimate for data generation. The payload team has discerned that a non-square resolution is mandatory to achieve a realistic coverage estimate. However, for every altitude selected, a possible field of view is obtainable based on the team's research. **Figure 16** demonstrates the correlation between altitude and required field of view.

**Table 6. Initial Payload Characteristics.** Payload characteristics based upon research from design iteration two.

Altitude	Mass	Power	Volume	FOV (16,384 pixels)	FOV (20 pixels)	NADIR Pointing Req.	Orbit Normal Pointing Req.	Third Axis Pointing Req.
400 km	~650 g	4-8 W	10×10×20 cc	63.13°	0.086°	± 0.0699°	± 27.74"	± 30.94"
500 km	--	--	--	52.35°	0.069°	± 0.0699°	± 23.01"	± 24.75"
600 km	--	--	--	44.55°	0.057°	± 0.0699°	± 19.58"	± 20.63"
700 km	--	--	--	38.69°	0.049°	± 0.0699°	± 17"	± 17.68"



For precision pointing requirement enumeration, a geometric analysis was conducted to correlate the angular offset from the NADIR axis with the angular distortion of the fringe pixels in the payload field of view. This study was conducted to find the degree to which the payload could tilt before the requirements of ground resolution are not properly met, however, several answers were identified. The payload team attempted to justify extreme pointing requirement, how far the spacecraft can tilt before the image is shifted by the length of two pixels, to force nearly ideal operational conditions. This result is much smaller than the one obtained to break the 50 m ground resolution requirement and **Figure 17** shows this correlation more clearly.

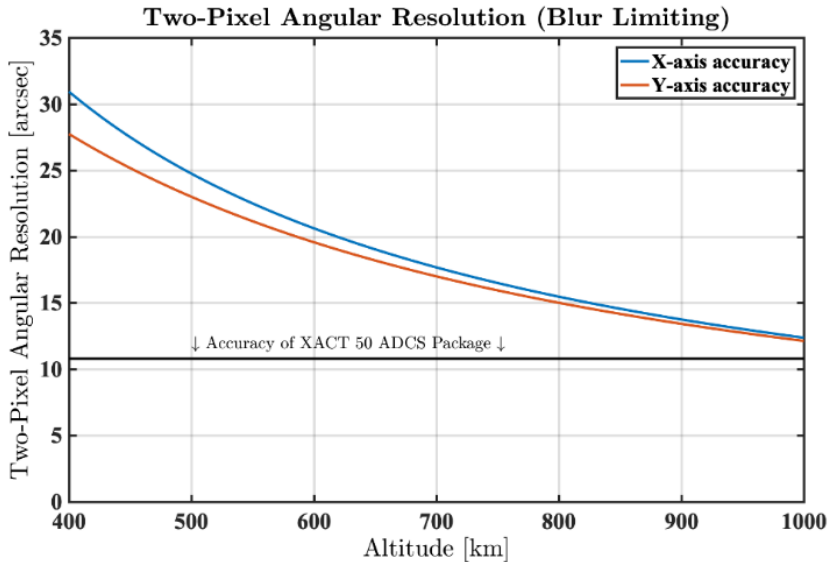


**Figure 16. Payload Pointing Requirements.** Possible payload pointing requirements based upon two-pixel blur limitations and angular distortion from orbital attitude.

This would limit the amount of blurring in the image immensely, and, compared to the XACT 50 ADCS package, these tolerances would seem like a possible baseline for the Fire-LOC ADCS system. Another limiting factor would be maintaining the ground resolution of the image. Any rotation of the satellite will cause edge pixels to distort, and we would like to limit this increase in resolution to less than 38 meters. Given this, below is the angular pointing requirements for the Fire-LOC system, with the y-axis pointing orbit normal (aligned with the long axis of the image – 16,384 pixels), and the x-axis being the resulting cross product of the orbit normal y-axis and the nadir pointing z-axis, as above, which has no physical significance in the system.

Given the incredibly coarse required accuracy of the resolution pointing requirement, the limiting requirement will be the two-pixel angular resolution to limit image blurring. For the z-axis, the pointing requirement would be defined as that which is required to prevent a loss in ground track coverage:  $\arctan(20 \text{ pixels} / 16384 \text{ pixels}) = 0.0699^\circ$ . **Table 6** was created to summarize the findings to this point of the current design iteration which

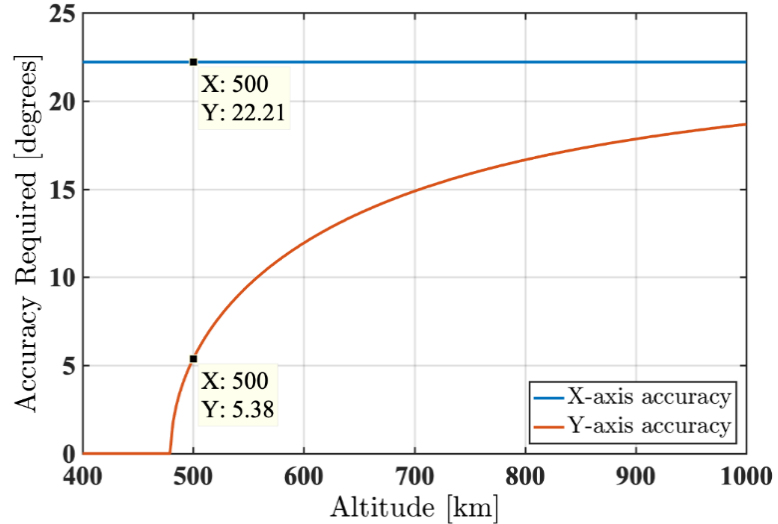


**Figure 17. Amended Pointing Requirements.** Field of View Required Metrics at Various Altitudes derived from previous attempts.



include extreme pointing requirements which were later reduced for a more achievable system.

From previous design iterations, and the information present in the **ORBITAL ANALYSIS** section, it was determined that the Fire-LOC constellation shall operate at an altitude of 500 km with 22 satellites in 22 planes operating with 3 at 20° inclination, 6 at 30° inclination, 6 at 40° inclination, 5 at 50° inclination, and 2 at 65° inclination. This allows for an average revisit time of 1.5 hours over one day. Previous research in this section demonstrates that at this selected altitude, the payload would require a long axis field of view of 52.35° and a short axis field of view of 0.069° as shown in . Since the long axis FOV is larger, it will be the fringe case that drives the design of the optics.

The payloads team launched a thorough investigation into astronomy telescope optics and has decided that a double plano-convex anti-symmetric lens is the most optimal for this design for a number of reasons. Firstly, its compact design is a fraction of the weight and size of other astronomical lens pairings making it ideal for CubeSat compliant payloads. The primary reason this configuration is not more prevalent is due to its limited focal length. Most astronomical lenses require high resolution at multiple millions of kilometers whereas this mission only requires a resolution of a few hundred kilometers (500 km to be exact). Secondly, this configuration allows for simple integration of the selected Infrared (IR) filter selected since the plano-convex nature of the lenses utilizes perfectly flat contact faces used as principal planes allowing for simple application of Snell's Law to account for the refractive index of the vacuum of space ( $n = 1$ ), the glass lenses ( $n = 1.6$ ), and the IR filter ( $n = 1.747$  due to the sapphire substrate). Since the payload requires a field of view that accommodates the fringe case, the radius of curvature of the outmost lens is fixed. The normal vector associated with the outmost edges of the lens dictate the field of view and the maximum diameter of the lens must fit within the 1U face of a CubeSat, thus a diameter of 85 mm was selected to maximize the viewing area while maintaining a feasible design. Since the field of view must be accounted for by the front lens' geometry, we can say that the radius of curvature of the red lens (in **Figure 16**) must be found this way:

$$R_2 = \frac{85/2 \text{ mm}}{55^\circ/2} = 92.0414 \text{ mm}$$

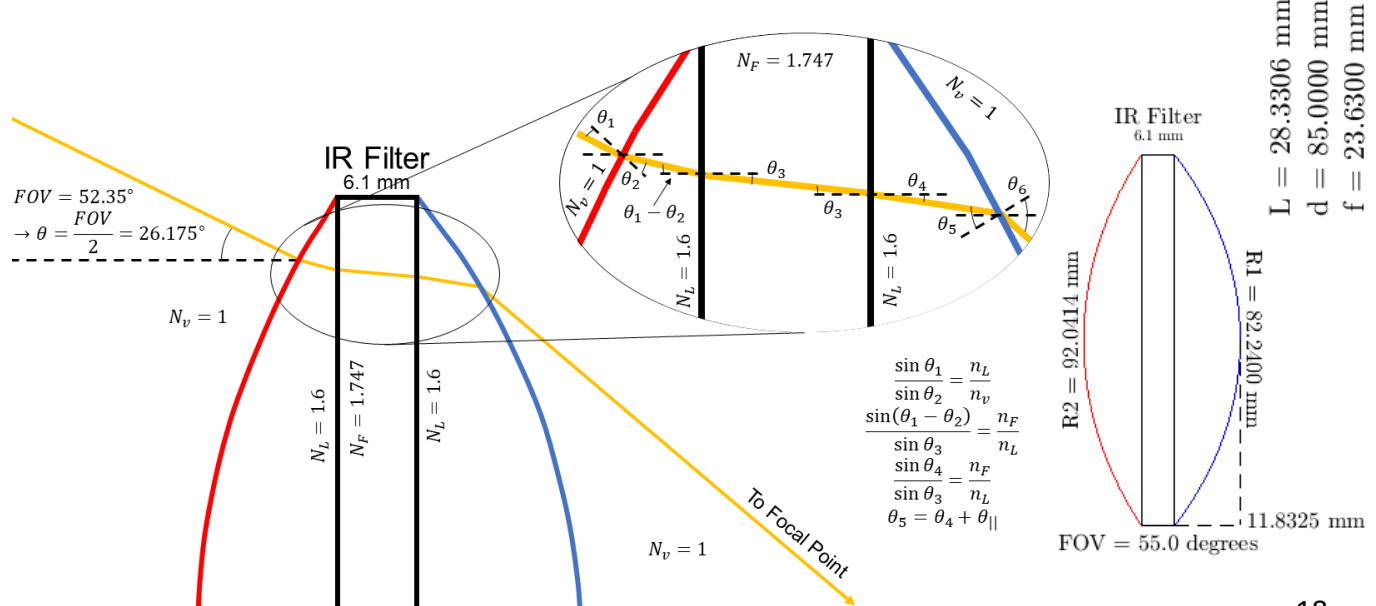


**Figure 18. Payload Optics Design.** Light Ray Interaction with Lens Geometry and Selected Geometry for Payload Optics.

The values for the indices of refraction for each of the materials are also known so using the process in **Figure 18**, the remainder of the angles and lens radii can be found. Using a custom-made program using the computer language MATLAB, the process described above was turned into an iterative design loop which would consider many rays of light originating throughout a cone with the desired field of view to create the double convex lens shown in **Figure 18**. The information in **Table 7** illustrates the component breakdown, including mass, volume, and pricing information. Also included are the minimum and maximum operating temperature of each element of the payload and **Table 7** shows the final characteristics of this design.

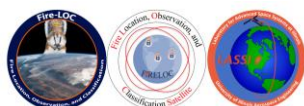
**Table 7. Payload Budgeting.** Final payload configuration and statistics used for final system configuration.

Larger Part	Mass [g]	Margin of Error	Mass Guess [g]	Volume [cc]	Tmin [C]	Tmax [C]	Price
<b>IR Sensor</b>	380	1.50	570	215.67	-40	71	~\$27,000.00
<b>Focus Lens</b>	0.176	2.50	0.441	0.031823	--	--	\$1.72
<b>IR Filter</b>	22.68	1.10	24.95	3.935476	-50	80	\$321.48
<b>Inlet Lens</b>	0.00025 5	2.50	0.006	22.0267	--	--	~ \$1.00

In **Table 8**, the maximum allowable X, Y, and Z rotations can be seen. The rotation limits for X and Y were determined as the angle that would push ground resolution past a certain threshold, decided as 35m to ensure the payload never approaches violation of the 50m requirement. The Y axis pointing requirement is determined to be finer than the X axis, as a significantly wider field of view will make angular perturbations more impactful on ground resolution. The Z axis was determined as the amount of rotation required to force the diagonal of the image to be perpendicular to the direction of travel. Any rotation after this point would cause coverage to be lost.

**Table 8. Payload Metrics.** A summary of all relevant metrics for the payload configurations.

Metric	Value
<b>Altitude [km]</b>	500 km
<b>Mass [kg]</b>	0.595 kg
<b>Volume [cc]</b>	1,087.3 = 1.08 U
<b>Length, Width, Height [cm]</b>	10cm, 10 cm, 10.8730 cm
<b>Price [USD]</b>	\$27,232.20
<b>Tmin [°C]</b>	-40°C
<b>Tmax [°C]</b>	71°C
<b>FOV (16,384-pixel axis) [°]</b>	52.35°
<b>FOV (20-pixel axis) [°]</b>	0.06875°
<b>Maximum allowable X, Y, Z Rotation [°]</b>	[22.22°, 5.41°, 0.0699°]



## 5. ORBITAL ANALYSIS

### 5.1. ORBITAL REQUIREMENTS

The orbital requirements are derived from the relevant payload requirements which are enumerated in the **Systems Requirements section**. The specific requirements pertaining to orbits are req. **Y:2.1**, **Y:2.2**, and **Y:2.3** which pertain to characteristics of the payload that are determined by the constellation. Specifically, referring to having a re-visitation time of 24 hours or less, providing 95% landmass coverage between the 70°S and 70°N lines of Latitude, and being in LEO respectively.

Second, given the requirements from the RFP of the mission, the altitude of the constellation would have to be within Low Earth Orbit (LEO). LEO is defined as an altitude below 2000 km, however, typically for satellites, there is a lower bound of an altitude of 160 km as otherwise, they would have a useless orbital lifetime. Thus, setting initial bounds for the altitude of our orbits. Fortunately, the range of altitudes described by LEO have no significant effects as a result of radiation, since the Van Allen radiation belt is far further up, as its lower boundary starts at roughly 6000 km.

Third, the constellation's characteristics should be designed so that it detects the maximum amount of fires to be as useful as possible, therefore, should have better re-visitation times in areas with more fires. The selection of the orbits for the constellation primarily depended on the choice of the payload which according to our iterative design process tree (see **Figure 50**), was the first step and the most important step of the analysis. Therefore, the choice and analysis from the payload impose orbital design choices, to ensure that the payload is feasible.

### 5.2. INITIAL ALTITUDES BOUNDS

The initial bounds as given by the RFP are between 160 and 2000 km. However, one factor which significantly impacted our choice of altitude would be the impact of the altitudes is the deorbit time. According to RFP, the mission must have an operational phase of 9 months. Therefore, the choice of altitude for the constellation must ensure at least a 9-month lifetime. As a result of the earth's atmosphere, spacecraft in LEO would experience atmospheric drag, this is particularly significant at lower altitudes. The drag is a force that acts in the opposite (and parallel) to the direction of travel. Consequently, reducing both its velocity and energy. This eventually leading it into an unstable state, in which it rapidly loses altitude. The most important factor for determining lifetime besides the altitudes itself would be the ballistic coefficient. The ballistic coefficient is a function of its mass and geometry of the spacecraft and density of the medium, while the altitude impacts the properties of the atmosphere, specifically of interest would be its density. The shape and thus its ballistic coefficient, affect the interactions between the atmosphere and the spacecraft.

The ballistic coefficient can be defined as:

$$\beta = \frac{\text{mass}}{C_D \text{Area}_{\text{cross-sectional}}}$$

The reference area to compute the drag coefficient is the cross-section in the direction of travel. The relevant cross-sectional area will depend on the chosen orientation of the CubeSat and its designed size (e.g. 1U vs 3U) and its mass will depend on a variety of other factors. Assuming a typical 3U sat with a long face pointing NADIR and with the other parallel long face pointing in the direction of the orbit



Alava Pena

normal. The following parameters were used for an initial calculation: mass = 4kg, 3U size and a drag coefficient of 2.2, typical for such a spacecraft; this yielded a ballistic coefficient of about  $180 \text{ kg/m}^2$ . Referring to **Figure 19**, this resulted in a minimum starting altitude of between 300 km and 400 km (see the solar minimum and maximum bounds of the graph in **Figure 19**). Therefore, the lower bound was found to be 400 km (worst case scenario starting at solar maximum), to ensure some margin.

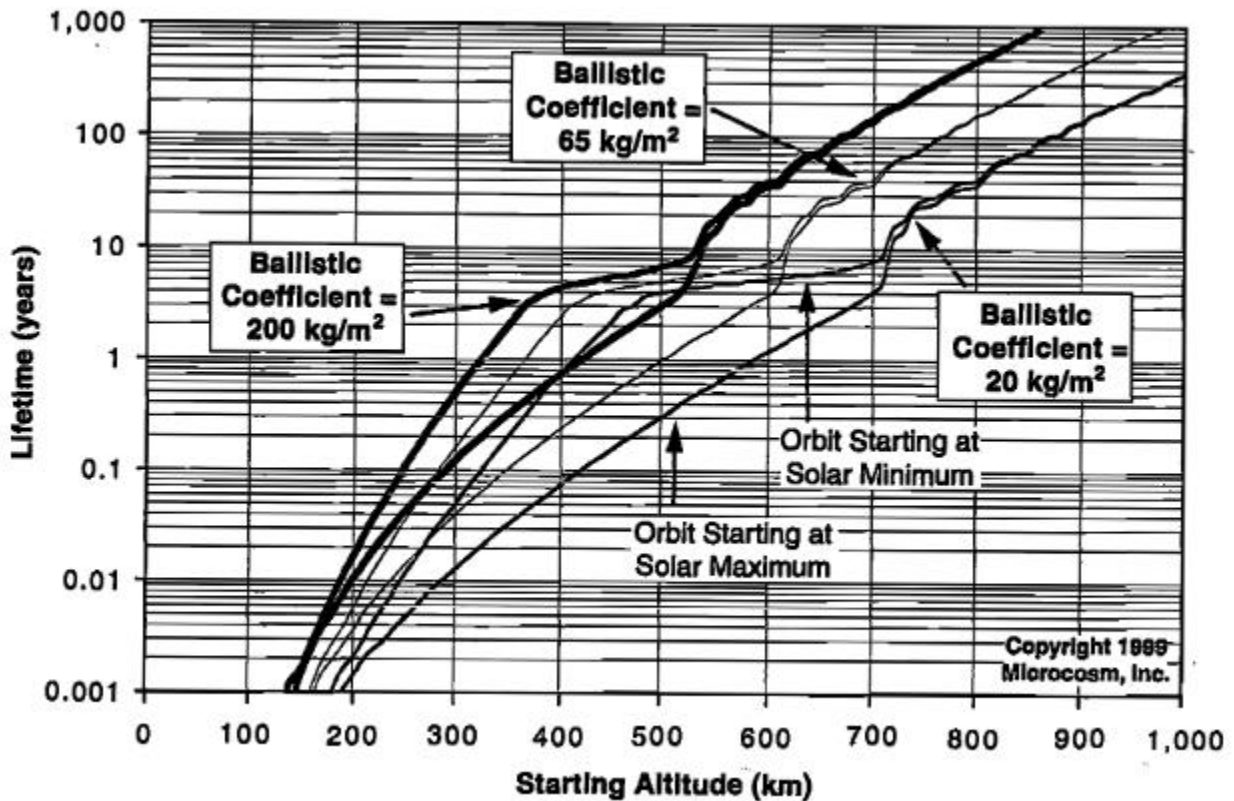


**Figure 19. The Lifetime of Satellite given its Starting Altitude:** Lifetime of satellites (years) vs Starting Altitude (km) for various satellites with varying ballistic coefficients and solar activity are seen plotted. from Space Mission Analysis and Design (Wertz) [20]

The analysis regarding deorbit time will later be refined in future through the use of FreeFlyer which has an in-built atmospheric model and is able to compute these parameters to a higher degree of accuracy. Moreover, FreeFlyer is able to have more realistic emulation of solar intensity as it can extract the relevant section of the solar cycles pertaining to our operational mission phase rather than simply give us the range (between starting at solar minimum and solar maximum). The Solar cycles also impacts the lifetime of satellites as seen in **Figure 19**. The variation in solar activity results in a variation of density that is particularly significant, specifically at the altitudes ranges of 400 km and 800 km, there is a density change of two magnitudes. Noting that at solar maximum, the density is larger.

Furthermore, the effect of the altitude needs to be considered. It was important to consider that it would be unfeasible to have a payload at a very high altitude, which would consequently require extremely small and unfeasible fields of views as seen in **Figure 20**. This, as a result, would demand unreasonable resolutions. For further information please see the **FIRST DESIGN ITERATION**.



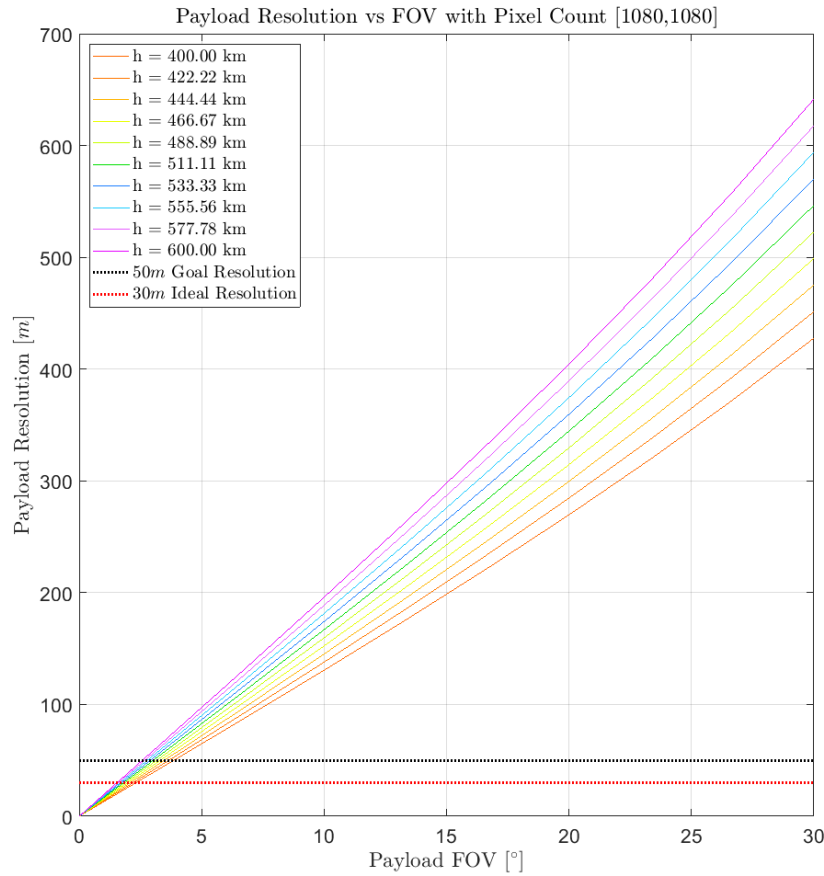


**Figure 20. Payload resolution vs FOV:** Payload resolution(m) vs Payload FOV (degrees) is plotted. The lower the resolution the smaller the required FOV of the payload to meet our resolution requirement.

Note that further lines could be plotted for **Figure 20**. However, they are deemed as unreasonable, in terms of the required FOV one would require to achieve. Therefore, the upper bound of the orbit can be set to be 600 km.

### 5.3. CHOICE OF ORBITAL ANALYSIS TOOL

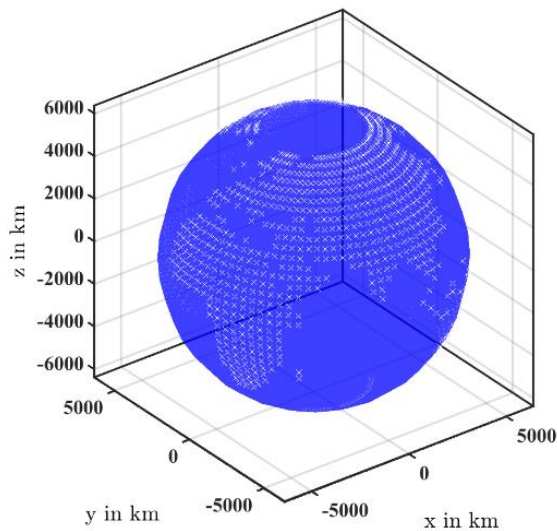
The orbital analysis was conducted using software produced by FreeFlyer. FreeFlyer is a reliable software as it has been both independently verified and validated. Additionally, some of the industry leading companies/organizations such as NASA, USAF, and NRO have used FreeFlyer for their space systems design.<sup>[21]</sup> Furthermore, it has many built-in functionalities relating to computing coverage and revisit times, and a powerful scripting interface to perform more complex analysis, if required. Thus, it is well suited for being the main orbital analysis tool of the Fire-LOC mission. However, if need be, additional tools can be used, such as MATLAB scripts.

### 5.4. INITIAL COVERAGE ANALYSIS FOR A SINGLE SATELLITE

Alava Pena

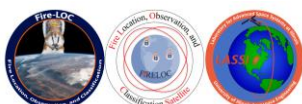


Coverage, in FreeFlyer, can be obtained by using Point Groups, which are a collection of points spread evenly around a body of interest. However, in our mission, specifically interested in measuring the coverage over the landmass areas between 70°S and 70°N lines of Latitude, FreeFlyer, unfortunately, does not have such an option (measuring coverage by landmass) by default. Therefore, additional work was required in the form a MATLAB script which generates the points of interest, which then can be imported as individual points by declaring them in the FreeForm script. Points in FreeFlyer are defined by their latitude and longitude, it is important to note that one cannot simply generate evenly spaced by taking their ranges and evenly splitting it up, as these longitudes and latitudes must be mapped then onto Earth which is a spheroid. First, using spherical coordinates, evenly spaced points on a sphere are generated. Moreover, their corresponding latitudes and longitudes are computed, as required for FreeFlyer and for the MATLAB mapping. Then through using the MATLAB mapping toolbox, each point (in form of latitude and longitude) can be checked if it is within or outside of a landmass. Thereafter, if it is outside of landmass, it is removed from the vector of points that are returned. To aid visually both of representation of the points (part of the group points) in 3D space in an Earth Frame and their corresponding latitudes and longitudes are plotted in **Figure 21** and **Figure 22**.



Alava Pena

**Figure 21. Coverage Points generated in 3D space for the points of interest - Coverage Points in 3D from 5000 points originally spread-out evenly around a sphere, to originally verify that the code was working as intended.**



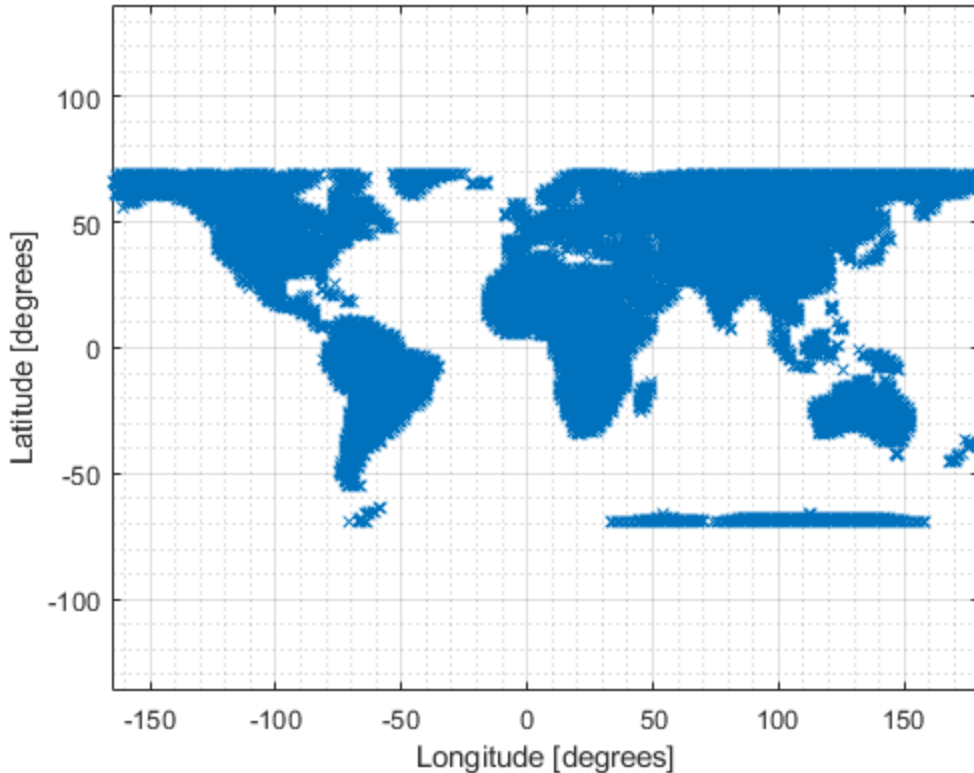


**Figure 22. Latitude and Longitude location of the points of interest- Coverage Points displayed in terms of latitude and longitude from 50000 points, at the locations of interest that is landmass between 70 °S and 70 °N Latitude**

In FreeFlyer, a script (using FreeForm) was implemented to compute the coverage using the aforementioned GroupPoints while propagating the single spacecraft for 24 hours in 10 seconds increments. The GroupPoints are then imported through using another MATLAB script which generates the code required in FreeFlyer to generate and specify individual points. Different inclinations were iterated over for circular orbits at altitudes of 400, 500 and 600 km to obtain the most ideal coverage, the inclination of 69 degrees obtained the most desirable inclination in terms of coverage. This resulted in 50.8 %, 56.44 %, 63.1% coverage in each of the respective altitudes. Furthermore, note that all the orbits investigated in the **ORBITAL ANALYSIS** section will be circular since for detecting the most fires, covering as much area as possible in evenly is more important than staying in one area significantly longer. Additionally, this greatly simplifies payload related analysis, given that in a circular orbit case, the payload would have a single (constant) resolution as the altitude is constant, thereby making it easier to ensure we meet our resolution requirement. Coverage will further be discussed in the **CONSTELLATION DESIGN** section.

## 5.5. ALTITUDE JUSTIFICATION

To further narrow down the altitude, that currently is bounded between 400 and 600 km, the primary factors, deorbit time and payload feasibility, impacting the altitude were reevaluated. From the point of view of the payload, the lower the orbit the easier and cheaper to design and manufacture the payload. At this point in time, more metrics regarding the satellite's configuration were found, thus, allowing more



accurate deorbit times to be computed using FreeFlyer by introducing a force model to model the atmosphere, allowing the drag to be incorporated. Deorbit times were computed between 400 km until 500 km, at which the time to deorbit was deemed acceptable with significant margin given that deorbit time is a critical mission risk. At 400 km, the satellite deorbited after 6 months (182 days). Moreover, by choosing a higher altitude for the risk mitigation reason, we were able to have more coverage as seen in the **INITIAL COVERAGE ANALYSIS FOR A SINGLE SATELLITE** section. At an altitude of 500 km, the deorbit time was 816 days (2.23 years). Thereby, maintaining the payload feasibility and meeting the 9-month operational mission phase requirement. Furthermore, this altitude meets our requirement of being in LEO.

## **5.6. SHADOW CHARACTERISTICS**

For the chosen altitude and a circular orbit at 500km altitude, the shadow events, that are Earth Penumbral and Umbral Event were simulated for the entire duration of the mission using FreeFlyer. The duration (in min) of Shadow events can be summarized in **Table 9** (see below).

**Table 9. Earth Shadow characteristics:** Statistical big 5 analysis for the any Earth Shadowing events, Earth Penumbral, and Umbral events over the duration of the entire operation mission phase.

Type of Shadow Event	Any	Earth Penumbral	Earth Umbral
<b>Count</b>	7491	3754	3737
<b>mean</b>	31.364510	31.522882	31.205418
<b>std</b>	5.501528	5.511528	5.487600
<b>min</b>	1.077150	1.077150	1.205083
<b>25%</b>	29.772942	29.959712	29.572250
<b>50%</b>	33.359367	33.521000	33.195317
<b>75%</b>	35.200683	35.356192	35.063483
<b>max</b>	<b>35.937500</b>	35.937500	35.653333

These numerical results can be compared and thus verified with analytical calculations. The first equation used in the calculation of the eclipse time of a Fire-LOC spacecraft is the eclipse fraction:

$$f_E = \frac{1}{\pi} \cos^{-1} \left[ \frac{\sqrt{h^2 + 2Rh}}{(R + h) \cos \beta} \right]$$

Where R is the earth's radius, h is the orbit altitude and  $\beta$  is the angle between the sun and the orbit plane. Since the maximum eclipse fraction is required for this study, the beta angle,  $\beta$ , is assumed to be equal to zero. The resultant equation can be written as:

$$f_E = \frac{1}{\pi} \cos^{-1} \left[ \frac{\sqrt{h^2 + 2Rh}}{(R + h)} \right]$$

Once the eclipse fraction has been determined, the orbital period, P, must be calculated by first finding the mean motion, n, which is a function of the standard gravitation constant for Earth and the semi-major axis of our orbit.

Alava Pena



$$n = \sqrt{\mu/a^3}$$

$$P = \frac{2\pi}{n}$$

With the eclipse fraction and period of the orbit, we can calculate the maximum eclipse period,  $T_{E,max}$ .

$$T_{E,max} = P f_{E,max}$$

For an orbit of 500km, the maximum eclipse time is 35.92min with 15.24 cycles per 24hr time span. This implies the simulation was carried out correctly since there is just a 0.04% between the simulation results and the analytical calculation.

## 5.7. CONSTELLATION DESIGN

The FreeFlyer script was extended to create and propagate an entire constellation rather than a single satellite to give a greater understanding of how the coverage statistics would increase with different permutations and combinations of planes, inclinations, and numbers of satellites. Moreover, re-visitation frequency for each point of the Point Group could be computed allowing for additional statistics to be gathered, such as the average re-visitation period for each location.

The first constellation that was attempted had 6 planes with 2 Satellites Per Plane (SPP) with the inclination that most ideal for a single satellite, 69 degrees. Note that the satellites in the same plane would have 180° separation in their orbit. For the remainder of this trade study, whenever a set of satellites are said to be in the same plane, it should be assumed that they are evenly spread out along their plane — i.e.: each satellite will have a separation of  $360^\circ/n$ , where  $n$  is the number of satellites in that plane. This configuration achieved coverage of 84.4%, significantly less than the desired coverage. Thereafter, additional planes were added to try to increase coverage, yielding a constellation with 8 planes and 2 SPP which achieved a 100 percent coverage of points and revisited 99.88% of the points. While this meets our requirements, the distribution of the re-visitation is not ideal. The current inclination is 69°, which results in the higher altitudes being revisited the most, which is not that useful for a fire detection constellation since a great majority of global fires take place much closer to the equator (which will be discussed later).

A satellite configuration was tested with 1 plane and 10 SPP. Interestingly, this obtained 99.3% percent coverage. Despite the high overall percent coverage, this approach would be unfeasible for our project as the distribution of the points that would have been revisited is not well spread out and in close proximity to fires and the percentage of points that were revisited was at 94.1%, lower than required. From here, it was evident that a greater variety of inclinations was necessary. Moreover, the number of satellites in a constellation could be reduced to just nine, with a constellation configuration of 3 planes with 3 SPP. This yielded 97.15% coverage and a re-visitation percentage in 95.4%, much closer to the desired result with fewer satellites.

Alava Pena



Given the various constellation choices that meet the scope of the mission, the distribution of the re-visitation times of specific locations on earth that are more susceptible to fires became a priority. The reason for this choice in constellation design evaluation is to ensure that the constellation can be as useful as possible, that is to detect as many fires as it can in a reasonable time, therefore, being able to revisit areas that typically (historically) have a trend of having a lot of fires. According to Global Fire Watch, the majority of the fires that occur on Earth lie between 40°S and 40°N lines of Latitude [22]. Additionally, for communication purposes, it would be of use to pass the United States as frequent as possible, in order to downlink large amounts of data, if required. Thus, a program written for MATLAB was developed to plot the distribution of the number of times each point (of the Group Points) was visited in a visual, informative manner was created, an example of which can be seen in the records section. This tool will be used in combination with the coverage percentage and re-visitation percentage in a 24h timespan.

Moreover, with this tool, the impact of extending the simulation times on the distribution of the re-visitation frequencies for each point can be investigated. It is expected that the distribution stays roughly the same in terms of the ratios, however, obviously, the number of times each point is revisited should increase if the time of the simulation is increased. In **Figure 23** and **Figure 24** the same simulation (3 planes, 3 SPP) is run with the only difference being the time the constellation is propagated, with the simulation timespan being 1 day and 7 days respectively, based on the figures, it can be seen that both the distribution is the approximately same and even the average and standard deviation are extremely close to the standard deviation varying by 2.2% and the mean by less than half of a percent. This seems logical since the orbital period of at 500 km for a circular orbit is 94.8 mins, therefore, in a day it would have completed already 15.19 orbits, enough to be able to average out the results.

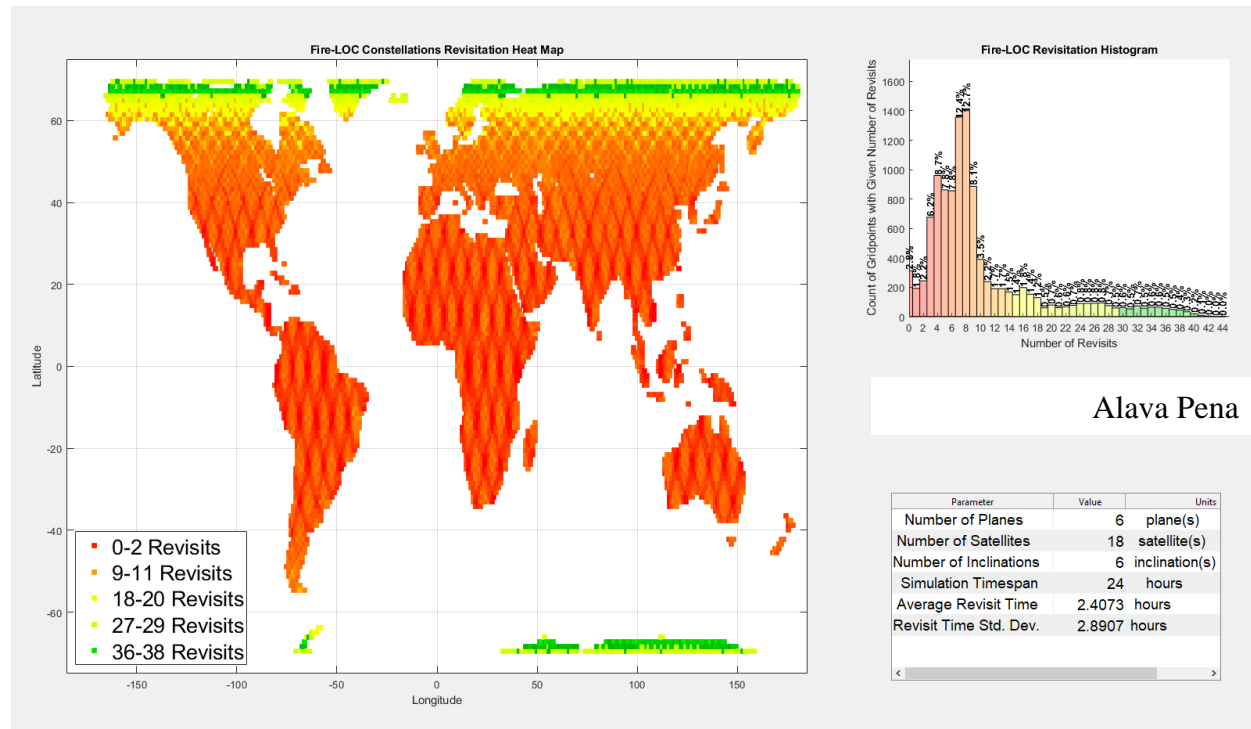


**Figure 23. Re-visitation Metrics for 24 hours of a Constellation for: with 6 planes with 3 satellites per plane**



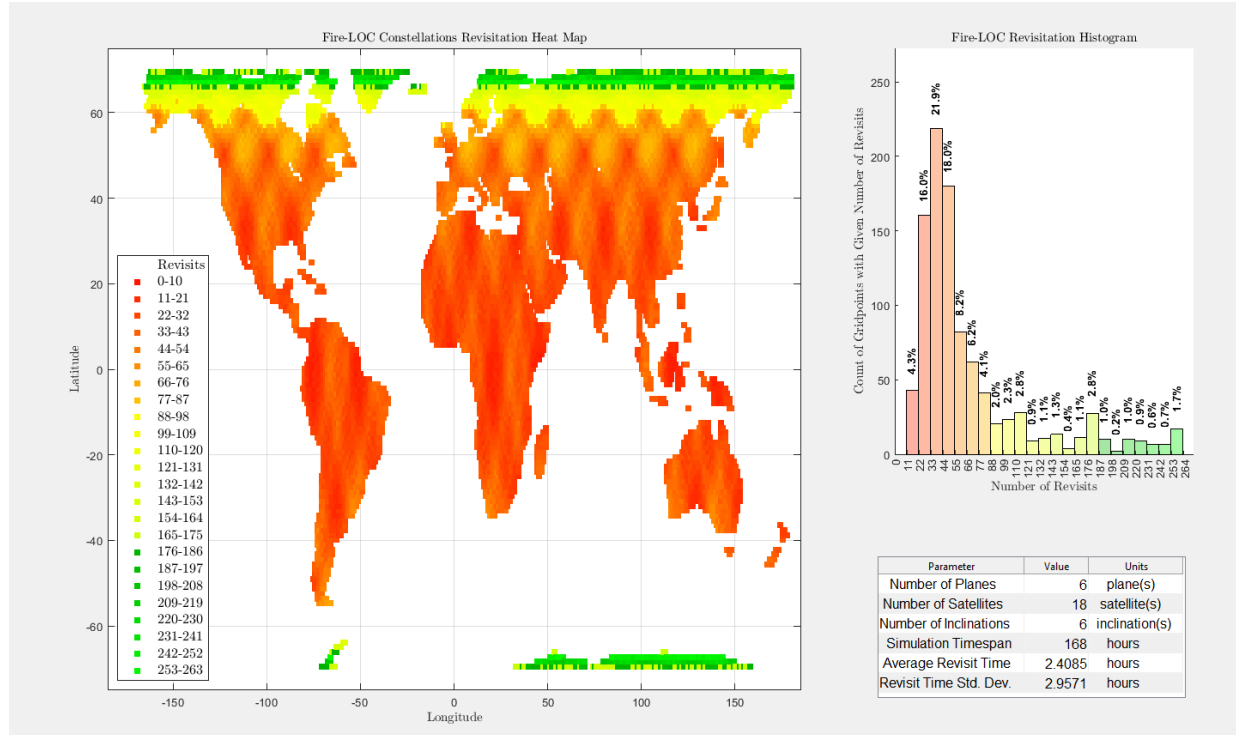


**Figure 24. Re-visitation Metrics for 168 hours of a Constellation:** with 6 planes with 3 satellites per plane

Additionally, it can be seen that constellations which only have a single inclination will only revisit certain areas numerous times, in the case of both **Figure 23** and **Figure 24**, given the high inclination of  $69^\circ$ , it visited most locations close to the  $70^\circ\text{S}$  and  $70^\circ\text{N}$  lines of Latitude. This suggests that combinations of planes need to be attempted to be able to revisit more areas. But, after attempting to use various inclinations, it was also found that the number of satellites for each inclination. The reason for this being that various inclinations are not as much of interest to us, specifically the higher ones, as these typically revisit points closer to the higher latitudes, which tend to have a much lower frequency of fires that occur.

Alava Pena

This process was iterated with various amounts of satellites to bring the re-visitation times down to below one hour in areas in which fires are prevalent, given the quick manner fire can spread and the number of satellites in certain inclinations with varying inclinations. Furthermore, the satellites in the same inclinations would have constant angular separations between them, thus, have varying true anomalies. Additionally, to further vary the points that are visited, the RAAN can also be varied. As long as the inclinations are within the expected latitudes of fires and the other orbital parameters are varied significantly enough should, the intersection of the orbits will result in a variety of different locations being visited in areas that are of interest to us.

The final constellation test was determined to have the best fit for the Fire-LOC mission which consisted of a constellation of 22 satellites in 5 different inclinations ( $27^\circ$ ,  $35^\circ$ ,  $44^\circ$ ,  $54^\circ$ , and  $68^\circ$ ). Moreover, it had 2, 6, 6, 5, 3 satellites in each respective inclination, in order to gain more coverage in the latitudes of interest. It achieved a total coverage above 95% between  $70^\circ\text{S}$  and  $70^\circ\text{N}$  lines of Latitude and the re-visitation every point in the PointGroup within 24 hours. Specifically, it delivers coverage of 98.89% with

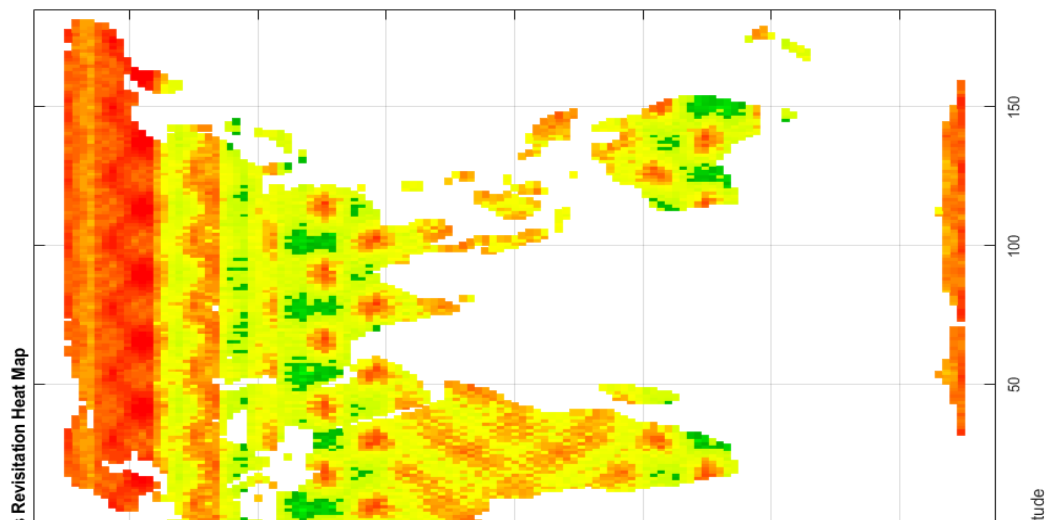
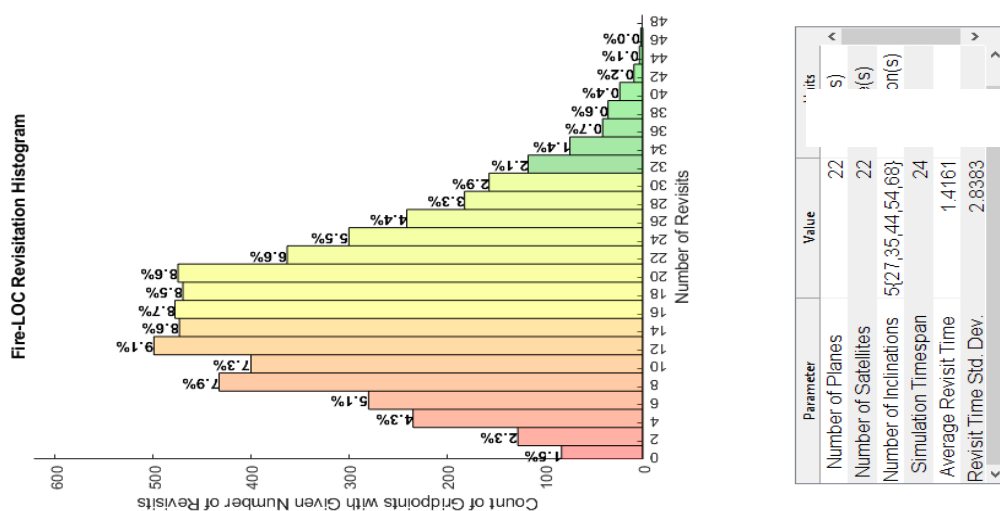


98.49% re-visitation every point in the PointGroup. Thereby, meeting our coverage and re-visitation requirements. This yields a revisit time of 1.4161 hours on average and with a standard deviation of 2.8383 hours, most importantly it has very frequent re-visitation in areas prevalent to fires as seen in **Figure 25**. In addition, it has particularly frequent re-visitation in certain areas of the United States such as California, that would be useful if communication with the ground is required. These desirable characteristics can be seen in **Figure 25** on the following page or in **Table 10**.

**Table 10. Constellation characteristics:** *This table describes many key parameters of the final constellation after all the analysis was carried out.*

Metric	Configuration
<b>Number of Satellites</b>	22
<b>Altitude [km]</b>	500
<b>Inclinations [degrees]</b>	5 {27,35,44,54,68}
<b>Number of Satellites in each Plane</b>	{2,6,6,5,3}
<b>Coverage Percentage</b>	98.89%
<b>Revisit Percentage</b>	98.49%
<b>RAAN and argument of periapsis</b>	Varying linearly for each satellite

Alava Pena



Alava Pena  
Revisit Metrics for final Constellation Designed with 22 satellites that varying inclinations simulated for a timespan of 24 hours

## 5.8. PERCENTAGE OF PAYLOAD ACTIVITY

In order to perform additional analyses regarding other subsystems, specifically the payload, power subsystems, and the concepts of operations, the percentage of time the payload is active is required. This is due to the fact that the activity of the payload greatly drives many factors in the design of the mission. Therefore, the percentage of time the sensor is gathering data was investigated, i.e. when it is over a landmass that is between the 70°S and 70°N lines of Latitude. Moreover, it shall do so for the varying inclinations chosen in the **CONSTELLATION DESIGN**, given that it is the main factor impacting the percentage.

Simulations will be run for all the different inclinations of the constellation that were designed in **CONSTELLATION DESIGN**, the reason for that being that the differences in other orbital parameters are rather minimal. To show that this is the case, an orbit with an inclination of 68 degrees with a RAAN and argument of periapsis of 0 degrees and with an orbit with an inclination of 68 degrees with RAAN and argument of periapsis of 180 degrees. The differences in the result were rather minimal, the percentage difference in a week-long simulation between both simulations were just 0.03%, suggesting that our assumption that mainly focusing on the inclination is a valid approach. Moreover, the later results displayed in **Table 11**, suggest that inclinations do have a much larger impact than the 0.03% difference of changing other orbital elements.

The simulations run for the duration of a week, the reason for this being, that the percentage of time over land for that specific orbit has safely converged to a specific value. Additionally, to confirm this, the same simulation was run for a month for an inclination of 35 degrees. This yielded a percentage over the landmass of 30.90 %, just a 0.43 % difference from the week-long simulation that resulted in 30.37% (see **Table 11**). The results of the FreeFlyer simulations can be summarized in **Table 11**.

**Table 11. Percentage Payload if active:** meaning that it is over land and on for various inclinations (since that is the main factor impacting the activity), simulated for the duration of a week.

Inclination	Percentage of time Payload is active. [1 week simulation]
27	29.802748
35	30.3668557
44	29.4588383
54	30.6509482
68	35.7914056



## 6. ATTITUDE DETERMINATION SYSTEM

### 6.1. SYSTEM REQUIREMENTS

The attitude determination system (ADS) derives its functional requirements from the mission task order. The ADS is imperative in the qualitative aspect of the mission. The level 1 and level 2 requirements presented in **Table 12** lay down the framework upon which the iterative design process is based. The task order defines fire detection and location as its primary objective which requires exigency in response. To this note, it is essential that the ADS functions within a very stringent error margin to precisely downlink fire location to ground. This creates a need for detailed process to determine an efficient sensor suite to fulfill the qualitative requirements as well as dependent requirements such as power, mass, and structural integrability of the ADS.

**Table 12. ADCS Requirements.** *Enumerated Level 1 and Level 2 Requirements for the ADCS as specified by the Request for Proposal (RFP).*

Req. #	Requirement	Verification
<b>A:1</b>	<b>ADCS shall receive commands from C&amp;DH</b>	<b>Demonstration</b>
A:1.1	ADCS shall change satellite attitude as commanded by C&DH.	Demonstration
<b>A:2</b>	<b>ACS shall provide attitude stabilization</b>	<b>Demonstration</b>
A:1.2	The ACS shall achieve a drift rate of the yaw axis to within $\pm 0.032$ degrees/sec	Test
A:1.3	The ACS shall achieve a drift rate of the pitch axis to within $\pm 0.069$ degrees/sec	Test
A:1.4	The ACS shall achieve a drift rate of the roll axis to within $\pm 0.089$ degrees/sec	Test
<b>A:3</b>	<b>ADS shall determine satellite attitude using onboard sensors</b>	<b>Demonstration</b>
A:3.1	The ADS shall determine attitude of the yaw axis to within $\pm 0.06$ degrees	Test
A:3.2	The ADS shall determine attitude of the pitch axis to within $\pm 0.008$ degrees	Test
A:3.3	The ADS shall determine attitude of the roll axis to within $\pm 0.008$ degrees	Test
<b>A:4</b>	<b>ADCS shall generate status telemetry for C&amp;DH</b>	<b>Demonstration</b>
<b>A:5</b>	<b>ADCS shall receive power from the Power System</b>	<b>Demonstration</b>
<b>A: 6</b>	<b>ADCS shall be capable of integration into CubeSat</b>	<b>Demonstration</b>

### 6.2. SENSOR SUITE

In order to determine a baseline for the sensor accuracy requirements, analysis had to be conducted to determine the effect of orbital altitude on sensor accuracy in relation to error on the ground. Essentially, the increase in area due to angular drift affecting the attitude determination of the satellite was to be determined. For this purpose, it was observed that considering an orbital altitude of 500 km in the LEO, an angle of  $1^\circ$  would linearly equal to 8.7275 km (2.4241 m per arcsec) on the ground. Using this metric, the “search” area values were observed against different values of angular error. Here, the term “angular error” is used to define the smallest error to which a sensor can determine the attitude of the CubeSat. As shown in **Figure 26**, an exponential increase in search area was observed with increase in angular error. For an error of  $0.25^\circ$  (common accuracy level for earth and sun sensors), a minimum search area of  $4.7605 \text{ km}^2$  was observed.



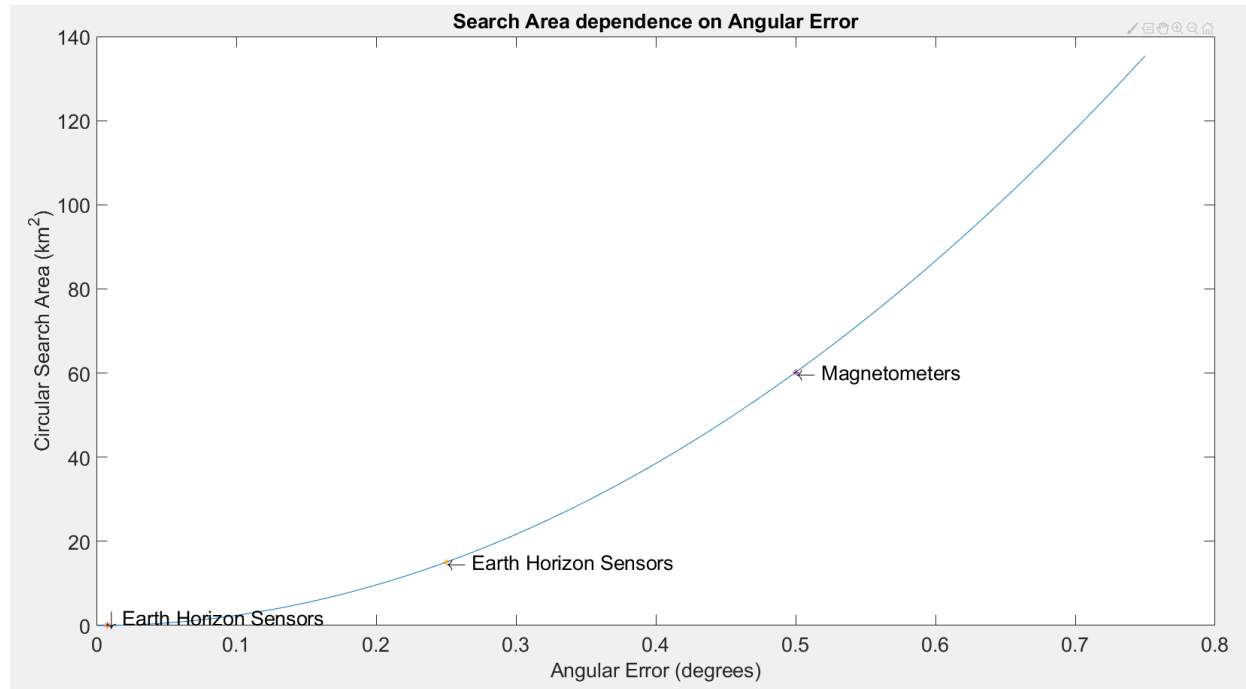


**Figure 26. Search Area dependence on Angular error at 500 km.** Exponential increase in search area is observed with decrease in angular determination accuracy of sensors. Star trackers provide the best accuracy possible.

The Fire-LOC payload can detect fires that span 0.001 km<sup>2</sup> (class A), which makes the previously mentioned search area highly vague in terms of “pin-pointing” the location of the fire and could cause a delay in response, especially in remote areas. To prevent this disparity, highly accurate inertial and body fixed rotational sensors are needed. NADIR pointing requirement of the payload limits the inertial sensors choices to star trackers, Earth horizon sensors, and fine Earth sensors. But, as discussed previously, due to a demanding accuracy requirement, a star tracker was chosen as the on-board inertial sensor for the constellation in order to satisfy the ADS requirement of determining satellite attitude as stated in A:3. Inertial sensors are usually combined with body fixed sensors that provide angular rate measurements that are later input into a Kalman filter to determine the attitude of the satellite. Gyroscopes provide highly accurate angular rates about the 3-axes. Having determined the primary ADS, we analyzed the various parts for their critical failure causes and it was noted that star trackers have an inherent disability of being blinded by objects in their line of sight. Further, gyroscopic failures are plausible sources of failure, however uncommon. To this end, a 3-axes magnetometer was added to the sensor suite to provide fault tolerance and redundancy. **Table 13** provides a detailed description of the COTS parts to be deployed on the Fire-LOC satellites.

**Table 13. Sensor suite components.** The COTS parts were chosen primarily based on their performance. The secondary measures of distinguishing competitive parts were power consumption and size.

Part Name	Company	Performance	Dimensions	Power Consumption
			[mm]	mW
ST-200 Star Tracker	Hyperion Technologies	<30 arcsec Pitch and Yaw accuracy	29 x 29 x 38.1	600



		<200 Roll axis accuracy		
ADXRS 290 MEMS	Analog Devices	200 LSB/sec Pitch and Roll sensitivity	4.5 x 5.8 x 1.2	39
ADXRS 450 MEMS		80 LSB/sec Yaw sensitivity	9 x 9 x 4	53
HMC1053 Magnetometer	Honeywell	0.01° orthogonal sensitivity	1 x 3 x 3	30

The final ADS configuration along a complete flow chart for the ADCS is shown below in *Figure 27*.

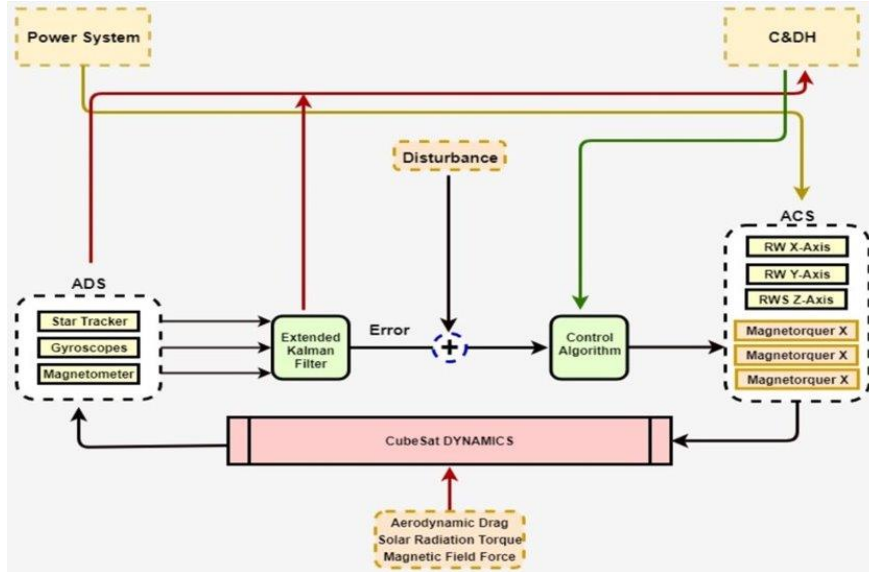


**Figure 27. ADCS Process flow diagram.** Distributed ADS and ACS processes with inter-subsystem connections along with added effects of external parameters on subsystem.

## 7. ATTITUDE CONTROL SYSTEM

### 7.1. PASSIVE CONTROL

Provided the fine pointing requirements required by the payload, the use of passive control of the Fire-LOC satellites attitude was out of question. However, for modes when the satellite's payload is not operational, switching to passive control could offer power savings and increase the lifespan of the selected control actuator. The purpose of many of the trade studies conducted by the ADCS team was to derive criteria on the moment of inertia elements ( $J_1$ ,  $J_2$ ,  $J_3$ ) that guarantee marginal passive gravity-gradient stabilization for a spacecraft in low earth orbit. The results of this trade study generated criteria for the possible geometries of the space craft that would enable the use of gravity gradient stabilization for periods when the payload is off, thus saving power and reducing the loads on the control system. This is only possible if gravity gradient is utilized to keep the satellite within an acceptable pointing range while in eclipse. To begin, the following three constants were defined:

$$a_1 = \frac{J_2 - J_3}{J_1} \quad a_2 = \frac{J_1 - J_3}{J_2} \quad a_3 = \frac{J_2 - J_1}{J_3}$$

From these three constants, six inequalities involving  $a_1$  and  $a_3$  were derived which guaranteed marginal passive gravity gradient stability for a space craft in low earth orbit. These six inequalities are as follows:

1.  $1 + 3a_1 + a_1a_3 > 0$
2.  $(1 + 3a_1 + a_1a_3)^2 - 16a_1a_3 > 0$



3.  $a_1 a_3 > 0$
4.  $a_1 > a_3$
5.  $|a_1| < 1$
6.  $|a_3| < 1$

Inequalities 1,2 and 3 relate to the spacecraf's roll and yaw stability by using the equations of motion for roll and yaw. Inequality 4 relates to the spacecraf's pitch stability by using the equations of motion for pitch. The final two inequalities were derived using the definition of moments of inertia. **Figure 28** below shows the resulting constraints for  $a_1$  and  $a_3$ . The shaded region represents the  $a_1$  and  $a_3$  values for stability. Each inequality region is labeled with respect to the related inequality equation listed above. With the moments of inertial derived from the CAD model,  $a_1 = 0.962$  and  $a_3 = 0.017$  meaning the design of the Fire-LOC satellites is marginally stable using a gravity gradient approach.

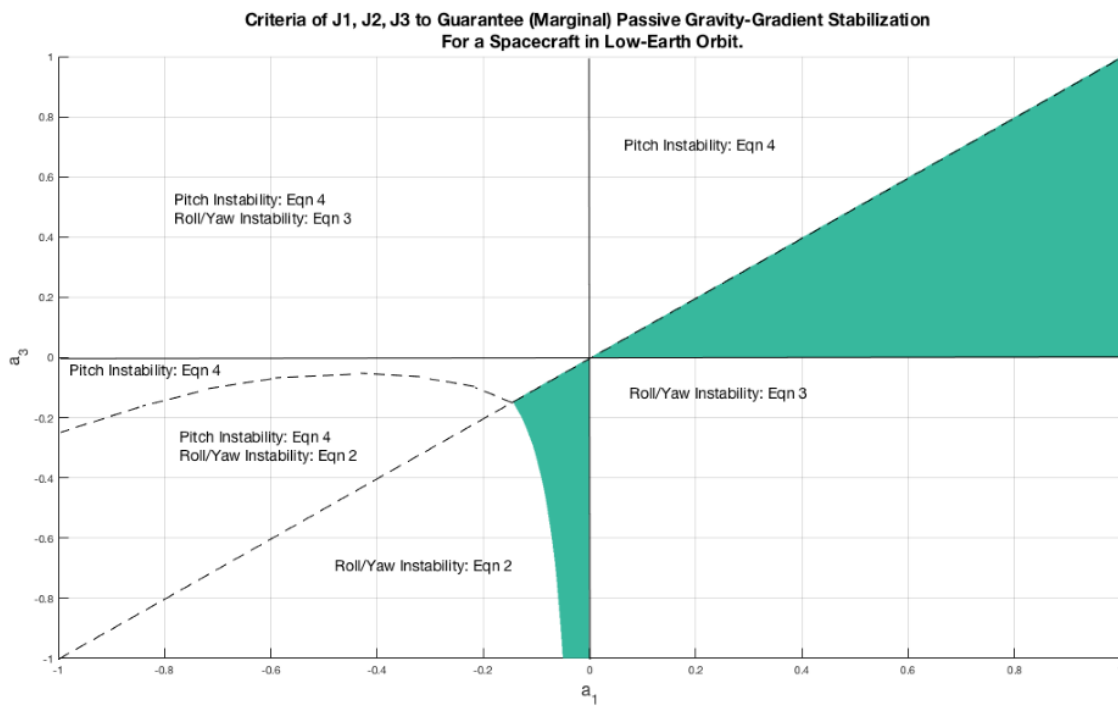


**Figure 28. Criteria for J1, J2, J3 to guarantee (marginal) passive gravity-gradient stabilization for a spacecraft in low-earth orbit.** Moments of Inertia derived from the cad model, indicate  $a_1 = 0.962$  and  $a_3 = 0.017$  making the design of the craft marginally stable

The moment of inertias derived from the CAD were tested in simulations that propagated the satellites attitude with time provided the equations of motion and initial conditions for the attitude and angular rates.

## 7.2. ACTIVE CONTROL

In the search for actuators for active control, focus was placed on commercial-off-the-shelf (COTS) reaction wheels for CubeSats. The reaction wheels were tested in simulation to examine any given reaction wheels ability to control the space craft. The simulation uses the equations of motion of the spacecraft and reaction wheels for each axis to simulate the motion of the craft propagating in time, taking



into consideration max torque, max spin rate and the wheels moment of inertia. A database was collected of different CubeSat reaction wheels and, with information provided from previous trade studies. This database was narrowed down to the best three reaction wheels, basing the decision off the maximum torque provided, power requirements, mass, momentum storage, and finally rpm accuracy. The three selected reaction wheels are shown in **Table 14**.

**Table 14. Three best-case reaction wheels for control.** The reactions wheels in this table were selected based on maximum torque provided, power consumption, mass, momentum storage and accuracy.

Part Name	Company	Max	Max	Max	Mass	Power Consumption		
		Torque	Speed			Momentum Storage	[W]	Idle
		[Nm]	[RPM]	[Nms]	[g]		SS	Peak
SatBus 4RW0	Nano-Avionics	0.0032	6500	0.02	137	0.045	0.15	3
CubeWheel Medium	CubeSat Shop	0.001	6000	0.0108	150	N/A	0.19	1.3
RWP050	Blue Canyon Tech	0.007	N/A	0.05	240	N/A	0.5	1

With these three selected reaction wheels, several simulations were tested to validate their ability to control the Fire-LOC satellites. From simulating these three reactions wheels the following their listed operational parameters, **Table 15** provides the results of the simulations listing the total torque applied and settling time. By linearly interpolating the steady state and peak power of the several reaction wheels, a torque-to-power relation was derived. By multiplying the power from a respective torque value to the time-interval it was applied, provides the W-s. Taking the sum over the entire simulation and dividing by the simulation duration provides an approximation for the power required to perform the maneuver. All simulations had the same controller gains and initial conditions  $\theta_1 = 22^\circ, \theta_2 = 5^\circ, \theta_3 = 0^\circ, \omega_1 = 0.1 \frac{\text{rad}}{\text{sec}}, \omega_2 = 0.1 \frac{\text{rad}}{\text{sec}}, \omega_3 = 0.01 \frac{\text{rad}}{\text{sec}}$ .

**Table 15. Simulation results for the three best-case reaction wheels for control.** The reaction wheels were simulated and had their settling time and power consumed for going from  $\theta_1 = 22^\circ, \theta_2 = 5^\circ, \theta_3 = 0^\circ, \omega_1 = 0.1 \frac{\text{rad}}{\text{sec}}, \omega_2 = 0.1 \frac{\text{rad}}{\text{sec}}, \omega_3 = 0.01 \frac{\text{rad}}{\text{sec}}$  to a steady state equilibrium position .

Part	Max Torque [Nms]	For 4 Wheels			Settling Time [sec]	Power Consumed		
		Nominal Power [W]	Peak Power [W]	Mass [g]		X-Axis [W]	Y-Axis [W]	Z-Axis [W]
SatBus 4RW0	0.0032	0.6	6	700	15	0.151	0.15	0.15
CubeWheel Medium	0.001	0.76	2.6	450	25	0.191	0.19	0.19
RWP050	0.007	2	4	960	10	0.501	0.5	0.5
								1.5



The CubeWheel Medium manufactured by CubeSpace offered the best balance of power consumption and torque applied to satisfy the ACS requirement to provide attitude stabilization as shown in requirement **A:2**. The CubeWheel Medium reaction wheel had a slower settling time than the 4RW0 and RWP050 but offered the same stability at a lower power and mass cost. In addition, the CubeWheel medium has had more rigorous testing for space-flight capability and offers a better controllability accuracy of up to 3rpm. The results for the CubeWheel Medium simulation are shown in **Figure 29** for the moment of inertia derived from the finalized CAD model.

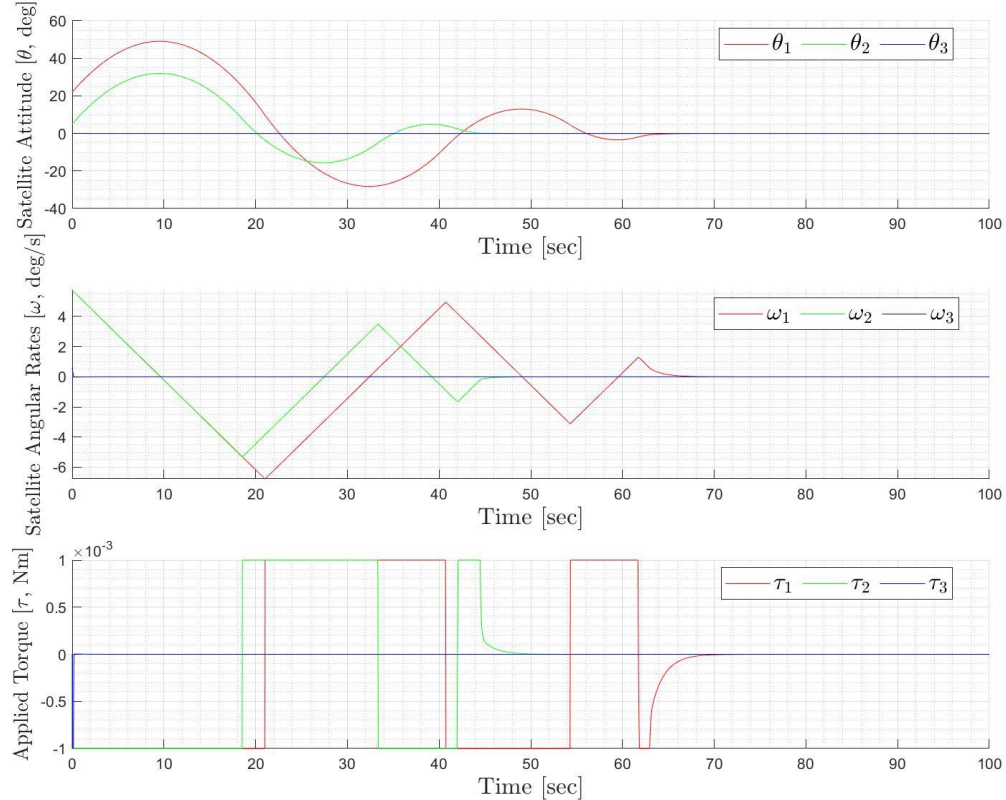


**Figure 29. Simulated Fire-LOC satellite control using CubeWheel Medium reaction wheels.** Settling time was observed to be 70 seconds. Satellite began at the same initial conditions previously stated however now is using the MOI derived from the CAD model.

Following the decision to go with the CubeWheel Medium, a simulation was performed switching from active control to passive gravity gradience. Here, the gravity gradient was initialized at a worst-case scenario for the payload to be pointing at an attitude of [22, 5, 0] degrees. The simulation ran using passive gravity gradience from 0 to 500 seconds and then switched to using the reaction wheels at 501 before turning off again at 600 seconds. After which, passive control ran from 6010 second to 700 seconds.. Finally, reaction wheel turned back on and were operational till the end. From this simulation, it was proven that these reaction wheels can regain control from the CubeSat after being powered off and allowing passive gravity gradience to take over.



### 7.3. PERTURBATION AND MOMENTUM DUMPING

The operational orbital altitude of the Fire-LOC constellation makes the satellites susceptible to various sources of perturbations including Aerodynamic drag, magnetic field torque due to internal components, and solar radiation torque. These sources of perturbation are described below:

- Aerodynamic Drag: Active below the 650 km altitude threshold and produces a decelerating force on the orbit normal face of the CubeSat.
- Magnetic Field Torque: The onboard electronics of the CubeSat create a magnetic dipole along the length of the CubeSat, which interacts with the Earth's magnetic field, producing a torque on the satellite.
- Solar Radiation Torque: Solar radiation and particles strike the surface of the CubeSat and the resultant force produces a torque on the satellite.

To counteract these perturbing torques, reaction wheels need to work overtime for attitude corrections. This continual production of acceleration by reactions wheels may saturate them with momentum over time and this requires desaturation. For the Fire-LOC CubeSats, three magnetic torquers shall be used for performing momentum dumping. These torquers will be aligned with the axis of the momentum wheels for a simple and efficient design. To perform momentum dumping, magnetorquers must produce a higher torque than the sum of torques due to the perturbing forces. Magnetic torquers use the Earth's magnetic field to function. The field strength decreases as a function of height shown below:

$$B = \frac{m_d}{r^3} \quad (6)$$

Where  $r$  is the radial distance from center of the Earth and  $m_d = 7.96 \times 10^{15}$  Wbm is the magnetic dipole strength of the Earth. To calculate the total torque produced by specific magnetometers can be calculated as follows:

$$\tau_a^b = m \times B \quad (7)$$

Where  $m$  is the magnetic moment produced by the magnetic torquers and can be calculated as  $m = i_c N A$ , where  $i_c$  is current supplied,  $N$  is no. of turns in the coil and  $A$  is coil area. The approximate numerical values for these perturbing torques and the minimum torque requirement for magnetorquers are listed in **Table 16** below.

**Table 16. Sources of perturbation and maximum torques on CubeSat.** Using pre-defined mathematical models and historical data for constants[25], maximum torques produced by sources of perturbation were calculated and summed to approximate minimum torque needed from magnetorquers.

Source	Approximate Maximum Torque (Nm)
Aerodynamic Drag	$1.557 \times 10^{-7}$
Solar Radiation Torque	$2.305 \times 10^{-8}$
Magnetic field	$1 \times 10^{-6}$
<b>Required Magnetorquer Torque</b>	<b><math>&gt;1.1787 \times 10^{-6}</math> Nm</b>



## 8. COMMUNICATIONS

### 8.1. SYSTEM REQUIREMENTS

The mission details from the Error! Reference source not found. and **Appendix D. Iterative Design Approach** sections dictate how the Communications system will have to be designed to be the most appropriate for the mission. This system will need to communicate information to the relevant networks in order to be effective. The most important level one and level two requirements are detailed in Table 17

**Table 17. COMMs Requirements:** *Enumerated Level 1 and Level 2 Requirements for the COMMs system as specified by the Request for Proposal (RFP).*

Req. #	Requirement	Verification
C:1	<b>The COMMs System shall consist of commercial off-the-shelf components</b>	Demonstration
C:2	<b>The COMMs system shall transmit telemetry data</b>	Test
C:2.1	The COMMs system shall format telemetry for transmission according to CCSDS protocols	Demonstration
C:2.2	The COMMs system shall transmit at specific frequencies in the L-Band and UHF-Band	Demonstration
C:2.3	The COMMs system shall not exceed a transmission loss of 5 dB	Demonstration
C:3	<b>The COMMs system shall receive telemetry data</b>	Test
C:3.1	The COMMs system shall receive data with a gain of 3 dB	Test
C:4	<b>C&amp;DH shall accept commands from the Ground System</b>	Test
C:5	<b>Satellites from the Fire-LOC constellation shall share the same command frequency</b>	Demonstration
C:6	<b>Fire-LOC satellites shall be identified with satellite IDs</b> <i>Note: With satellite ID in the uplink packets identifying which satellite is to process the command message.</i>	Test

### 8.2. BANDWIDTH DETERMINATION

Section 9.2 determined that the most reliable system for transmitting fire information would be to utilize both ground and space-based communications systems based on the signal that needs to be sent. Therefore, the bandwidth restrictions for the satellite will be based on the limitations of available networks as well as the availability and readiness of antennae equipped for such.

According to NASA, different bandwidths have different applications in existing communications infrastructure. VHF and UHF bands are the most frequently used and reliable bands for communicating to ground stations as it has the most TRL (Technology Readiness Level) 9 components as seen in Table 18, meaning they are appropriate for deployment to missions. Since we are also using Amazon's AWS based ground stations, the antennae need to be compatible with its bandwidths as well. AWS uses S-band, X-band, and UHF for its satellite communications. Therefore, using the UHF band for communicating with ground stations is the best solution.

**Table 18. CubeSat UHF Antenna components:** *UHF-Band Antenna Components ranked & detailed by NASA*

Product	Manufacturer	TRL Status
Lithium-1	Astronautical Development LLC	9
CSK Phasing Board	Astronautical Development LLC	9
VUTRX	Clyde Space Ltd.	9



UHF Antenna	Endurosat	9
UHF Transceiver Type II	Endurosat	9
ETT-01EBA102-00	Emhiser Research, Inc.	9
NanoCom AX100	GOMSpace ApS	8
NanoCom ANT430	GOMSpace ApS	9
NanoCom SDR	GOMSpace ApS	7
P/N 17100	Haigh-Farr, Inc.	9
Helios Deployable Antenna	Helical-Communications Technologies	6
TRXUV	ISIS B.V.	9
TRXVU	ISIS B.V.	8
Deployable Antenna System for CubeSats	ISIS B.V.	9
Cadet	L3 Communications, Inc.	9
SatCOM TP0	LY3H	9
SatCOM UHF	NanoAvionics	9
UHF Antenna	NanoAvionics	9

Space communications networks like Iridium and GlobalStar utilize the L-band radio waves for communications, therefore an additional antenna operating on the L-band will be required for all space-based communications. The choices for CubeSat-compatible L-band components are detailed in Table 19.

**Table 19. L-Band Components:** *L-Band Antenna Components ranked & detailed by NASA [26]*

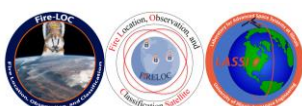
Product	Manufacturer	TRL Status
Helios Deployable Antenna	Helical Communications Technologies	6
9602 SBD	Iridium Communications, Inc.	9
EyeStar-S2	NearSpace Launch, Inc. (NSL)	9
EyeStar-D2	NearSpace Launch, Inc. (NSL)	9
Antenna SYN7391-B (Iridium)	NAL Research Corporation	Unkn.
STX2 Simplex	sci_Zone, Inc.	9

The final decision for determining the bandwidth for communications operations is to use two antennae – one operating in the UHF Band for ground station communications and one operating in the L-band for space-based communications.

### 8.3. NETWORK CHOICE

#### Ground Communications Network

As FIRELOC is exempt from the requirement that all communication to ground stations be to those in the United States, the opportunity to interface with commercial ground station service providers opens up. The provider with the most worldwide coverage and locations. In addition, the communications strategy



in 9.3 stated that space-based communications systems would be necessary to maximize the speed at which detected fires are reported. Therefore, the most reliable and cost-efficient providers for both infrastructures need to be found.

RBC Signals features commercial ground station infrastructure in full operation with coverage across the continents of Europe, North America, and Asia as well as multiple stations in the southern hemisphere.



**Figure 30: RBC Signals Coverage Map** <sup>[27]</sup>: *Map of RBC affiliated ground stations and their coverage*

This provides the opportunity for multiple uplinks and downlinks per day if necessary, as the coverage of the orbits determined by 5.7 in Figure 31 found that the revisits at each location per orbit was high around the same areas as the RBC Ground Stations in Figure 30.



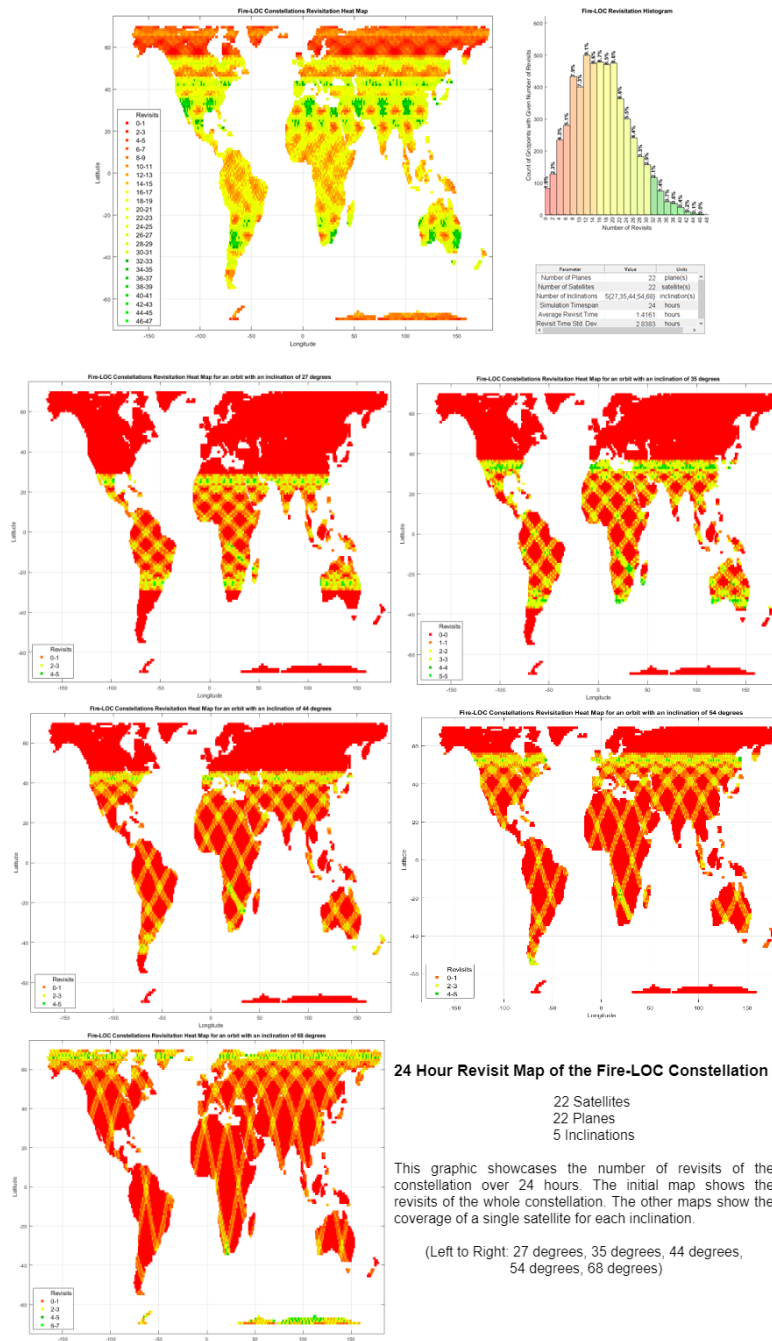


**Figure 31: 24-Hour Inclination Coverage Map:** Coverage of a single satellite over 24 hours for each inclination used by the constellation.

The pricing for RBC is custom tailored to the needs of the customer as per their website, therefore the most cost-efficient option since an optimal contract can be reasoned and negotiated.



**Space Communications Network**

Companies that provide space communications infrastructure have pricing schemes that prioritize different aspects of network usage. This information in Table 20 was summarized by Unidata[26] and informs the selection of which network and pricing model is optimal for FIRELOC

**Table 20. Space COMMs Pricing Schemes:** *Comparison of Space-Based Communications Network Pricing Schemes*

<b>GlobalStar Model - Airtime</b>	<b>Very Low Data Volume</b>	<b>Low Data Volume</b>	<b>High Data Volume</b>	<b>Medium Res Photo</b>	<b>High Res Photo</b>
Monthly Base Price	\$30.00	\$30.00	\$30.00	\$30.00	\$30.00
Comms Frequency	1 daily	1 hour	5 minutes	1 hour	1 hour
Bytes per Comms	224	224	230	25,000	110,000
Bytes per second	818	818	818	818	818
Packets per Comms including 2 OH	2	2	2	33	136
10 Seconds per Comms	1	1	1	4	14
Comms per Month	31	732	8784	732	732
First 10 Second Packets per Month	31	732	8784	732	732
Next 10 Second Packets per Month	0	0	0	2196	9516
Cents per First 10 Second Packets	4	4	4	4	4
Cents per Next 10 Second Packets	16.67	16.67	16.67	16.67	16.67
Monthly Packet Price	\$1.24	\$29.28	\$351.36	\$395.35	\$1,615.60
Minus Monthly Included Calls	(\$10.00)	(\$10.00)	(\$10.00)		
(\$10.00)	(\$10.00)				
Monthly Total Price	\$30	\$30	\$371.36	\$415.35	\$1,635.60
<b>Inmarsat BGAN (Session-Based)</b>					
<b>BGAN M2M 12 Month Plan</b>	<b>Very Low Data Volume</b>	<b>Low Data Volume</b>	<b>High Data Volume</b>	<b>Medium Res Photo</b>	<b>High Res Photo</b>
Comms Frequency	1 daily	1 hour	10 minutes	1 hour	1 hour
Payload Bytes per Comms	222	222	240*1	25,000	110,000
Billing Bytes per Month	30,500	732,000	4,392,000	31,671,976	136,867,892
Monthly	\$36.70	\$36.70	\$53.90	\$136.70	\$136.70



<b>Subscription Cost</b>					
Monthly Allowance	2MB	2MB	5MB	20MB	20MB
\$/MB Out of Bundle	\$23.35	\$23.35	\$13.30	\$6.80	\$6.85
Monthly Total Price	\$37	\$37	\$54	\$216	\$937
<b>Inmarsat BGAN (Per-Day basis)</b>					
<b>BGAN M2M 12 Month Plan</b>	<b>Low Data Volume</b>	<b>High Data Volume</b>	<b>High Data Volume</b>	<b>5 Minute Data+ Medium Res Photo</b>	<b>5 Minute Data + Medium Res Photo</b>
Comms Frequency	1 daily	5 minutes	1 minute	1 per day	3 per day
Payload Bytes per Comms	240	240	240	25,000	25,000
Billing Bytes per Month	1,055,080	2,109,160	10,541,800	2,969,604	5,977,657
Monthly Subscription Cost	\$36.50	\$36.50	\$95.00	\$53.90	\$53.90
Monthly Allowance	2MB	2MB	10MB	5MB	5MB
\$/MB Out of Bundle	\$23.35	\$23.35	\$9.50	\$13.30	\$13.30
Monthly Total Price	\$37	\$39	\$100	\$54	\$67
<b>Iridium per 10 Byte Block SBD Rate Plans</b>	<b>Very Low Data Volume</b>	<b>Low Data Volume</b>	<b>High Data Volume</b>		
Comms Frequency	1 daily	1 hour	5 minutes		
Payload Bytes per Comms	8	8	8		
Data Bytes per Month	248	5,952	71,424		
Monthly 10 Byte Blocks	248	744	8928		
Monthly Subscription Cost	\$16.50	\$27.50	\$66.00		
Monthly Allowance (Bytes/Block)	3,000/300	8,000/800	30,000/3,000		
Bytes Out of Bundle	0	0	41,424		



\$/10 Bytes Out of Bundle	\$0.11	\$0.07	\$0.03		
Monthly \$ Out of Bundle	\$0	\$0	\$196		
Monthly Total Price	\$17	\$28	\$262		

Since the space-based communications network is for immediate data transmission upon detection of a fire, limiting the satellite to a set number of contacts per day is counterproductive. In addition, the asynchronicity of any communications over space-based networks means sizing for airtime is irrelevant. What drives the requirement for space communications is the need for immediate and reliable connection for low-data signals. Therefore, the most appropriate service plans are Iridium's per-10 Byte block plan and Inmarsat's Session-based plan. Sections 9.2 and 9.3 conservatively estimate threat detection will require 100 Bytes for reporting the section threat level and 10B per command, therefore their monthly volume will need to be on the order of thousands of bytes.

The best choice of networks in addition to the University of Illinois ground station is the RBC ground station network and the Iridium satellite network's \$28/month plan. The RBC system stands out in its worldwide reach and high revisit times while the Iridium network offers the best per-unit data plan out of all the options.

#### **8.4. UPLINK/DOWNLINK SCHEDULING**

It is first necessary to see what opportunities a given satellite will have to transmit data. Two types of data transmissions will occur, a mass image transmission of full-size images or a section threat level. The second type will be sent via Space COMMs and can always be assumed to be in contact. In addition, section threat levels are sent when a fire is spotted, and as such are not predictable making scheduling these transmissions pointless.

In addition to downlinks, uplinks may also occur. These are rarely urgent and are much smaller than any image transmission. As such these can be bundled into any attempt at downlinking and will not be taken into account for scheduling.

This leaves the task of scheduling mass image transmissions. These will be sent directly to a ground station and consist of full-size images containing potential fires gathered since the last transmission. For a transmission to occur, the satellite must pass over a ground station while also at a high enough elevation to have enough time to transmit all data.

Figure 32 shows how often the entire constellation revisits areas over 24 hours by the entire constellation as well as the 5 individual orbital inclinations. Comparing this to Figure 31 shows that each inclination will be able to revisit multiple RBC ground stations over a 24-hour period. therefore, there are several options for each satellite to transmit over 24 hours, and it must be determined whether a satellite should attempt a downlink whenever possible, or schedule them over a time period.



From section 5.3, the payload can point about 22 degrees off-axis without disrupting the sweep. This either limits the satellite to passes 75+ degree pass or suspending imaging during a transmission. Both limit potential transmission opportunities and should be minimized.

The mass image transmissions are designed to support a world-wide wildfire map with a 24-hour delay at most. To minimize the number of downlinks, the satellite will attempt a downlink every 12-hour period. Computers ground side will predict the transmission opportunities over this period, decide the optimal pass. This data will be uploaded to the satellite every time a transmission occurs. In the worst cases, there will be a 24-hour gap between transmissions, within our limit. A buffer of the next 30 days of transmission opportunities will be stored in a buffer on the satellite.

Ground systems will simulate the orbit of each satellite, up to a month in advance. The best opportunities for each 12-hour period will be prepared to be sent to the target. This data will have to be updated once a month and can be bundled in a convenient transmission opportunity. In the next pass, this information will be transmitted to the satellite, preparing it for the upcoming transmissions. Data will be transmitted down sometime in a 12-hour block, ensuring a worst-case delay of 24 hours.

### **8.5. ANTENNA SIZING**

The communications components are subject to various restrictions. First, they must conform to the dimensional and volume constraints of a CubeSat. They must also communicate along the frequency bandwidths determined in 8.1 in order to be useful. These components must also not interfere with the IR-detecting payload during operation and adjusting for this may require re-orientation of the craft which may also interrupt any data gathering.

As per, the craft can be assumed to always be in contact with space-based communications networks. Therefore, the positioning of the antenna for space-based communications can be placed anywhere on the body of the craft such that its signals will not enter the field of view of the payload. This allows for more freedom in the form factor of the final component. The antenna must operate on frequencies compatible with the network chosen in 8.3. There is additional benefit to using one recommended or provided by that network as potential low-level incompatibilities between an L-Band transceiver and the network will have already been addressed. Since commands can be transferred over the space communications network, this antenna will need to always be on to be ready to receive.

In addition, section 8.4 requires an antenna capable of transmitting along the UHF frequency bandwidth for communication with ground stations. This will require potential re-orientation of the craft during operation and configured such that its chassis will not interfere with the payload's data collection. The maximum adjustment is 15 degrees off-axis as stated in section 5.3. This antenna will only need to be turned on for periods of communication with ground stations, which are stored in a buffer of 30 days' communications.

**Table 21. UIUC Ground Station Downlink Budget**

<b>Property</b>	<b>90 Degree Pass</b>	<b>45 Degree Pass</b>	<b>15 Degree Pass</b>
Satellite Power Output	30.00 dBm	30.00 dBm	30.00 dBm



(P_t)			
Satellite Antenna Gain (G_t)	1.36 dBi	1.36 dBi	1.36 dBi
Satellite Losses (L_t)	1.00 dB	1.00 dB	1.00 dB
Free Path Space Loss (L_fs)	137.30 dB	140.10 dB	146.60 dB
Misc Loss (L_m)	2.00 dB	2.00 dB	2.00 dB
Ground Station Antenna Gain (G_r)	13.30 dBi	13.30 dBi	13.30 dBi
Ground Station Loss (L_r)	5.00 dB	5.00 dB	5.00 dB
Ground station Amplification	22.00 dB	22.00 dB	22.00 dB
Received Power (dBm)	-78.64 dBm	-81.44 dBm	-87.94 dBm
Noise Floor	-120.00 dBm	-120.00 dBm	-120.00 dBm
SNR	41.36 dBm	38.56 dBm	32.06 dBm

**Table 22. UIUC Ground Station Uplink Budget**

Property	90 Degree Pass	45 Degree Pass	15 Degree Pass
Ground Station Power Ouput (P_t)	49.00 dBm	49.00 dBm	49.00 dBm
Ground Station Antenna Gain (G_t)	13.30 dBi	13.30 dBi	13.30 dBi
Ground Station Losses (L_t)	5.00 dB	5.00 dB	5.00 dB
Free Path Space Loss (L_fs)	137.30 dB	140.10 dB	146.60 dB
Misc Loss (L_m)	2.00 dB	2.00 dB	2.00 dB
Receiver Antenna Gain (G_r)	1.36 dBi	1.36 dBi	1.36 dBi
Receiver Loss (L_r)	1.00 dB	1.00 dB	1.00 dB
Received Power (dBm)	-81.64 dBm	-84.44 dBm	-90.94 dBm
Noise	-120.00 dBm	-120.00 dBm	-120.00 dBm
SNR	38.36 dB	35.56 dB	29.06 dB

The University of Illinois ground station requires that for both uplink and downlink, the satellite antenna have a gain of 1.36 dBi.

Finally, among the base requirements for FireLoc is that it be equipped with a GPS unit to determine its location along the Earth's surface. This is useful because it allows for controlled data collection over the Earth's surface, as looking for fires in the ocean is unnecessary. This GPS unit will also quickly provide location information in the event that a fire is detected. To compensate for the worst-case scenario, the GPS must be capable of updating information once every two seconds.



Three components for the Communications system need to be used: One for GPS, one for communicating with ground stations at UHF frequencies, and one for communicating with the space-based communications network at L-Band Frequencies. All components must be appropriate for the dimensional constraints of CubeSats. The UHF ideally does not require more than 15 degrees of reorientation and that it be capable of a gain of 1.36 dBi. The ideal L-Band antenna is provided or recommended by the network of choice in order to reduce potential problems. The GPS antenna need only update its location once every two seconds. For these reasons, the COMMs system shall use the EnduroSat UHF Antenna + Transceiver and the Antcom Iridium as they are capable of enough gain to communicate with their relevant networks.



## 9. GROUND SYSTEMS

### 9.1. SYSTEM REQUIREMENTS

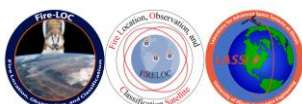
Based upon the mission presented in the **Task Order** and **Concept of Operations** sections, the ground system requirements are focused on receiving mission data from the constellation. The ground system is isolated from most subsystems, only interfacing with the communications subsystem. As such, the focus for the design was the successful retrieval of data via a seamless interface with the communications subsystem. The level one and level two system requirements in **Table 23** serve to showcase the objectives of the design process, the most important being receiving the mission data in a timely manner, minimizing cost, and interfacing with the communications system.

**Table 23. Ground System Requirements.** *Enumerated Level 1 and Level 2 Requirements for the Ground System as specified by the Request for Proposal (RFP).*

Req. #	Requirement	Verification
G:1	<b>The Ground System shall provide satellite tracking data for antenna pointing.</b>	Demonstration
G:2	<b>The Ground System shall receive satellite telemetry data</b>	Demonstration
G:2.1	The Ground System shall store satellite telemetry data.	Demonstration
G:2.2	Ground Control shall store 10 GB of telemetry data.	Analysis
G:2.3	The Ground System shall limit check telemetry data.	Test
G:2.4	The Ground System shall make telemetry data available for display.	Demonstration
G:3	<b>The Ground System shall receive mission data.</b>	Demonstration
G:3.1	The Ground System shall store mission data.	Demonstration
G:3.2	The Ground System shall provide a contact schedule.	Demonstration
G:3.3	The Ground System shall send commands to target satellite.	Demonstration
G:3.4	The Ground System shall send commands prefaced by satellite ID.	Demonstration
G:3.5	The Ground System shall send commands via UHF.	Demonstration
G:3.6	At most two contacts in a day shall be used for commands per satellite.	Analysis
G:3.7	Command support shall be based on satellite contacts visible from UIUC.	Analysis
G:4	<b>The Ground System shall maintain a record of target satellite configuration.</b>	Demonstration
G:5	<b>The Ground System shall be automated during weekends.</b>	Demonstration
G:5.1	Software shall notify operations team of any anomalies.	Demonstration
G:6	<b>Ground stations shall be worldwide.</b>	Inspection
G:6.1	RBC Signals shall be used.	Inspection
G:6.2	The LASSI ground station at UIUC shall be used.	Inspection

### 9.2. DIRECT VS INDIRECT COMMUNICATIONS

In the determination of the ground station network, it is necessary to examine the requirements of the system. The ground system must be able to receive and process the mission data of the constellation. The mission data would be images that contain potential wildfires. In a worst-case peak, this could reach up to 5 GB per day of mission data. The Fire-LOC constellation is a warning system, as such any sightings must be reported as soon as possible. It is necessary to find a ground system that can handle large amounts of information in a timely manner. There are two paths available, relying on direct downlinks, or using a space-based intermediary to relay data.



Direct communications entail a satellite directly connecting with a ground station to transmit data. This is the most common method of communication for satellites. Direct communications have the advantage of allowing large amounts of data to be transmitted cheaply. On the other hand, direct communications require a ground stations, which are expensive to build or rent. In addition, it is infeasible to have satellites be in range of a ground station at all times. As such, a fire sighting may need to wait until the satellite reaches a ground station to provide a warning. Thus, it is necessary to find a means to reduce the delay between a sighting and a warning.

Space-based communications (Space Comms) use a third-party satellite as a relay for communications. If a fire is spotted, instead of waiting for a ground station to be in range, the information can be relayed immediately. This would allow wildfire warnings to be sent to customers almost immediately. The downside would be the high data cost for using the system. This would make transmitting full-size images infeasible.

Fire-LOC will use a combination of these systems for ground system support. Mass data transmissions will be designated low priority and wait for a direct connection opportunity to transmit. Wildfire sightings will be given high priority and be sent through space comms. An overview of the system can be seen in **Figure 32**.

### **9.3. COMMUNICATIONS STRATEGY**

The Fire-LOC constellation will use a triangle communication strategy (as seen in **Figure 32**). High priority, but low size data will be transmitted via space comms. Low priority but bandwidth intensive data will wait until a downlink opportunity occurs. The typical reasons for communication can be seen in detail in **Table 24** along with the direction and estimated size. From this we can determine the division of communication between the various systems.

**Table 24. Communications Requirements:** *Direction, reason, size, and frequency of expected communications.*

Data	Direction	Reason	Estimated Size	Frequency
Command	Up	This is required in the RFP. Would encompass manual control, image requests.	10 B	On Demand
System Updates	Up	Update Satellite firmware.	1 MB	Infrequent
Contact Schedule Update	Up	Updates the contact schedule for the satellite.	1 kB	Monthly
Status Update	Down	Transmission of satellite status. (Battery Level, System Status, Memory Usage ...)	100 B	Daily
Mass Image Transmission	Down	Transmission of full-size images stored during the orbit.	100 MB	Daily
Section Threat Level	Down	Transmission of segmented images in response to fire detection.	100 B	N/A



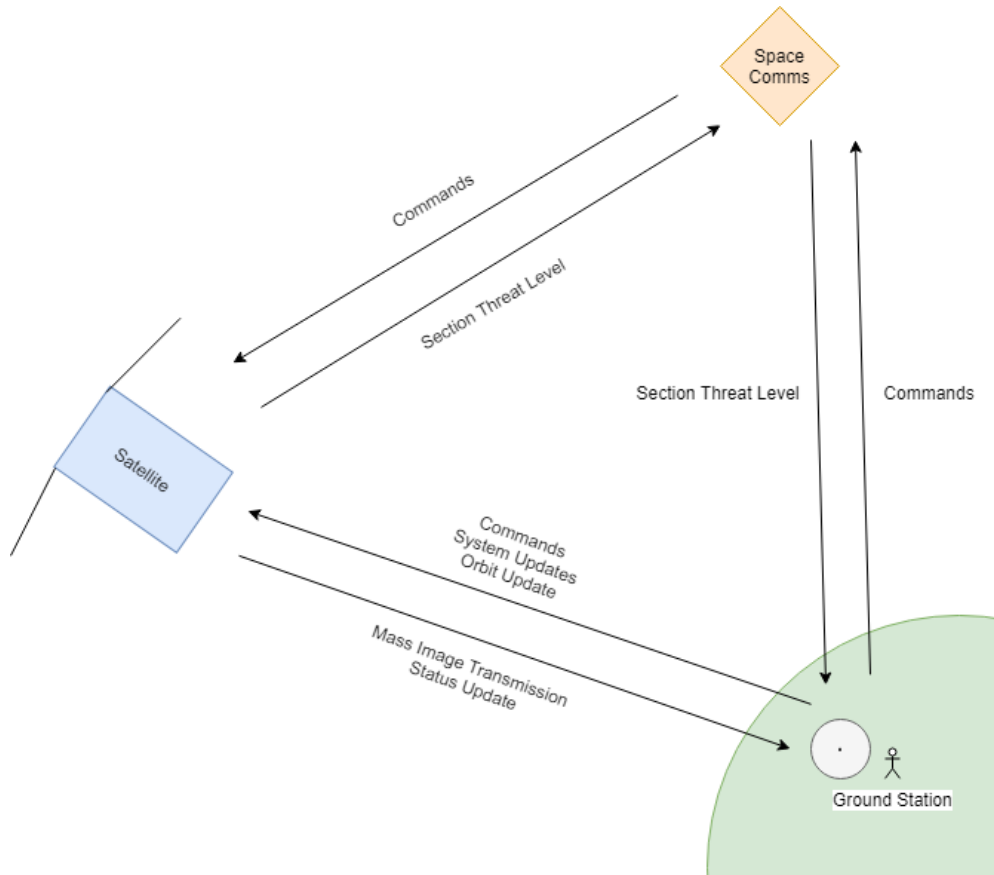
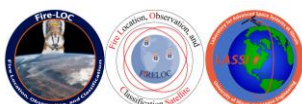


**Figure 32. Communications Strategy:** Communications strategy of the Fire-LOC Constellation, with direction of expected transmissions.

For space comms, the amount of data sent must be minimized, while still providing a worthwhile degree of accuracy for wildfire warnings. To accomplish this, lossy compression is used. The 20x16384 full-size image is compressed into a 1x128 image, or effectively an array. By analyzing the number of active pixels in a section, a threat level can be found. The various cutoff values can be found in **Table 25**. This compression scheme allows a 300 KB image to be compressed to about 500 B. As a downside, this is a very lossy method of compression, cutting resolution down from 30m to square kilometers. To help combat this, latitude and longitudes of noticeable hotspots will also be included. Two single precision floating points at a cost of 8 B will be provided for each active pixel, up to 50 in total. Active pixels will be chosen based on the concentration of active pixels. This would lead to larger clumps of fires being provided coordinates at the expense of smaller fire. A simplistic visualization of the compression scheme can be seen in **Figure 33**.

**Table 25. Threat Level Classification:** The classification scheme for the section threat level compression method. Details the number of active pixels necessary for each level.

Fire Class	Pixel Cutoff	Percentage	Threat Level
None	0	0.00 %	0



A	1	0.039 %	1
B	3	0.097 %	2
C	25	0.97 %	3
D	75	0.2.9 %	4
E	250	9.7 %	5
F	1250	48.8 %	6
G	>1250	> 48.8 %	7

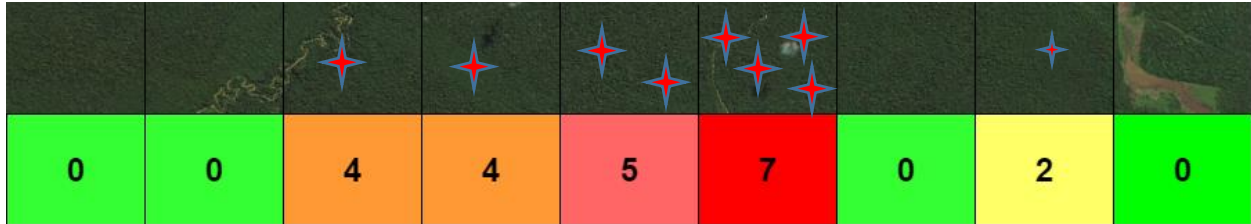


**Figure 33. Section Threat Level:** Example visualization of a section threat level. Not to scale with actual section threat level.

It is still necessary to transfer the full-size images back to earth. This data is not a high priority, and thus will wait for a scheduled downlink opportunity. The constellation will provide full res images with a maximum lag of 24 hours. In addition, a predictable schedule of contacts will vastly simplify automation of the ground systems. To accomplish this, a regular contact schedule will be established, with contacts occurring once within every 12-hour slot. The data transmitted during the contacts will be any images gathered since the last contact, status check of the systems on board, updates to the contact schedule, and any necessary commands. If any system updates are required, they will also be applied via a direct connection.

**Table 26. Division of Communications:** Details what information will be sent via space comms, and what data is transmitted directly

As an overview for the communications strategy for Fire-LOC, the data transmission requirements will be split between space comms and direct communications. The division can be seen in

Space Comms	Direct Comms
Section Threat Level	Full Size Images
Lat/Long of Wildfire	Status Checks
Commands	Commands
	Contact Schedule Update
	System Updates

**Table 26.** This strategy provides a cost-effective solution that minimizes response time to wildfire sightings, while still providing full resolution mappings of wildfires.

#### 9.4. GROUND STATION LOCATION

With the communication strategy of Fire-LOC known, it is possible to determine the location of the ground stations. This initially brings the

question of ground stations will be built or purchased. This decision mainly comes down to the desired time between contacts. More ground stations will increase the number of opportunities a



satellite will have to transmit to ground. Fire-LOC will maintain wildfire data at a lag of 24 hours at most. By looking at the projected coverage of satellites over 24 hours for every inclination of the constellation, it is possible to determine necessary locations for ground stations. This will require numerous ground stations across the world. Building ground stations for the constellation would be a massive startup cost for a system that last only a year, and as such is not a practical option for Fire-LOC.



**Figure 34. AWS Ground Station Locations:** Proposed placement of AWS ground stations

This leaves using already existing ground stations. Initially, Amazon Web Services Ground Station was considered. Amazon is planning to build ground stations to offer ground control as a service. The price for the service would only depend on the antenna time used. This would be a high-quality solution; however, the system is not yet built. Several ground stations have been built for testing, but do not provide global coverage yet. As such, this system, cannot be used by Fire-LOC.

Fire-LOC instead will use RBC Signals as its ground station provider to fulfill. RBC Signals acts as a middle-man between ground stations with extra antenna time and satellite operators looking for ground stations. As can be seen in **Figure 30**, RBC Signals can provide global coverage as specified in G:6, and numerous contact opportunities. Pricing is subscription based with several service levels. In addition, the LASSI ground station will be used as specified in G:6.2.

## 9.5.GROUND STATION AUTOMATION

The largest ongoing cost of a satellite constellation is the cost of personnel. To minimize the cost and fulfill requirement G:5, it is necessary to automate the ground systems. The automation of the Fire-LOC constellation is inspired by the automation of the NASA FAST satellite [28]. The automation scheme can be seen in **Figure 35**. In essence, a list of commands necessary for each pass is created. These commands will be sent automatically, without the need of an operator. Log files for each pass are made and are monitored for anomalies. In case of an anomaly, the immediate operating staff is notified. If no response is detected within a certain time frame, more



personnel are notified. This system of automation proved be a major success for the NASA FAST Satellite

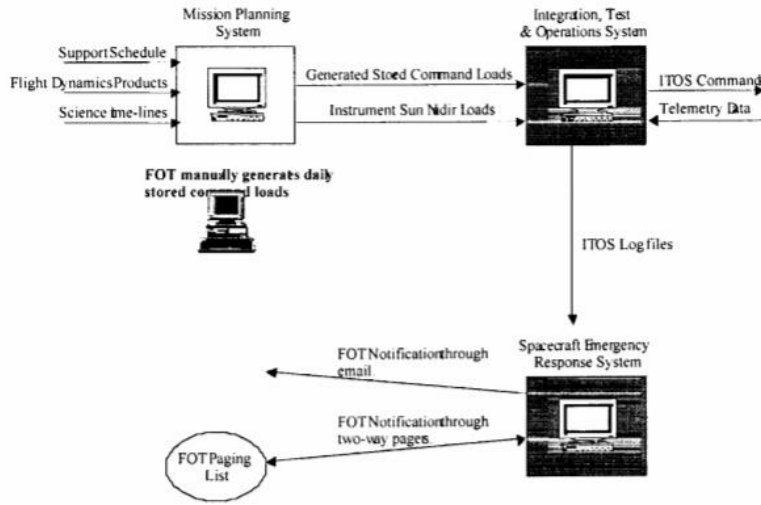


**Figure 35. NASA FAST Automation Scheme:** The automation scheme used by the NASA FAST Satellite to minimize personnel costs

Due to the unpredictable nature of wildfires, it is impractical to automate the space comms portion of the ground systems. This leaves the automation of the direct communications. The first step is to determine the scheduling of contacts. Due to the desire to maintain a lag of less than 24 hours, each data will be divided into two 12-hour sections. In each of the sections, the optimum contact opportunity will be predicted. These predictions will be done for a month in advance. This contact schedule will be uploaded to the constellation and updated once a month as required by G3.2.

The typical pass schedule can be seen in **Table 27**. The automation software will monitor several key metrics for each pass including: Battery Status, Payload Status, Orbit Status, and various other metrics. Any significant deviation will cause key personnel to be notified. Using this system will help manage costs of the Fire-LOC constellation.

**Table 27. Pass Schedule:** Details the transmissions required for a typical pass

Pass Schedule	Direction	Frequency
Status Check	Down	Twice Daily
Mass Image Transmission	Down	Twice Daily
Contact Schedule Update	Up	Monthly
Orbit Update	Up	Twice Daily
Clock Drift Check	Up	Twice Daily



## 10. COMMAND & DATA HANDLING

### 10.1. SYSTEM REQUIREMENTS

The mission details from the **Task Order** and **Concept of Operations** sections dictate how the command and data handling system (C&DH) will need to be designed in order to support the functions of all other subsystems. This system will need to interface and communicate with all subsystems in order to send commands and collect telemetry data while storing and processing IR data gathered by the Payload subsystem. The most important level one and level two requirements detailed in **Table 28** dictate the major factors in shaping the C&DH system

**Table 28:C&DH Requirements.** *Enumerated Level 1 and Level 2 Requirements for the Command & Data Handling system as specified by the Request for Proposal (RFP).*

Req. #	Requirement	Verification
<b>H:1</b>	<b>The C&amp;DH system shall receive telemetry from satellite subsystems.</b>	Test
<b>H:2</b>	<b>The C&amp;DH system shall store data.</b>	Analysis
H:2.1	The C&DH system shall store 5 GB for mission data	Analysis
<b>H:3</b>	<b>The C&amp;DH subsystem shall receive power from the power subsystem.</b>	Test
<b>H:4</b>	<b>The C&amp;DH subsystem shall be contained by the satellite</b>	Inspection
<b>H:5</b>	<b>The C&amp;DH system shall include a commercial off-the-shelf flight computer</b>	Inspection
H:5.1	The flight computer shall be an embedded computer.	Inspection
H:5.2	The flight computer shall be hardened to survive the launch environment.	Inspection
H:5.3	The flight computer shall consist of a real-time operating system (RTOS).	Inspection
H:5.4	The flight computer shall store commands for execution in the future	Inspection

### 10.2. DATA COMPRESSION

The amount of memory needed to store images taken by the FIRELOC satellite was initially estimated to be 655360 bytes per image as no integer stored in the 20x16384 array was going to be above 32,767. Finding a solution to compress data is critical as it would greatly lighten the burden of the FireLOC spacecraft. Two key components inform the solution necessary. Section 5.3 determined that the IR sensor would only output an array of limited-range integers based on the intensity of light experienced by each pixel. In addition, the C language allows for data structures to be defined such that known properties can dictate exactly how much space is allocated for each variable. Since section 9.3 determined that numbers from 0 to 255 are sufficient for describing the intensity of the detected light in the pixel, the theoretical maximum number of bits needed to store this are 8, as 00000000 represents the number 0 and 11111111 represents the number 255. In C, a data structure called bitfields <sup>[29]</sup> allows for precisely 8 bits to be allocated through the following code:

```
struct {unsigned int intensity: 8;} pval;
```

**Figure 36. Single Bitfield Storage:** *Sample code for storing a single value with bitfields*

The struct keyword defines a bitfield with variable declarations in the body designate how much memory in bits to allocate in the system for each variable. This approach is valid for single values, however the image data is stored as an array of pixel values. To minimize the data necessary to be allocated, the entire array of pixel values will need to be stored, therefore an unsigned int for each pixel value will need to be created.



```

struct {
    unsigned int p11: 8;
    unsigned int p12: 8;
    unsigned int p13: 8;
    ...
    unsigned int p2016384: 8;
} image;

```

**Figure 37. Full Image Bitfield Storage:** *Sample code for storing a full IR Image with bitfields*

The example code above has a pixel numbering system describing the pixels by their coordinates (with 11 referring to array index (1,1), I.e. the top-left corner of the array), but any numbering system can be used so long as it is consistent with the location on the sensor array.

With 327,680 pixel values at 8 bits each, the storage capacity needed per image is 2,621,440 bits, or 327680 bytes, or 328 KB. This is down to 1/2 of that needed beforehand.

### 10.3. MEMORY SIZING

Based on the RFP's data collection requirements, a rough estimate of the data being collected every 24 hours was computed. This estimation assumed the worst-case scenario where all necessary data is being collected with every sweep every second. However, from the data compression system detailed in 10.2, the data collected by the payload is significantly reduced as seen in **Table 29**.

**Table 29. Daily Data Collection:** *Amount of data collected in a 24-hour period.*

Subsystem	Data	Data Type	Quantity	Bytes
Thermal	Temperature	Float	1	4
Thermal	Heater On/Off	Boolean	1	1
Payload	Status On/Off	Boolean	1	1
Payload	Temperature	Float	1	4
Power	Remaining Battery (%)	Float	3	12
Power	Production Rate	Float	3	4
ADCS	Orientation	Float	3	12
C&DH	Memory Distribution	Float	3	12
C&DH	Time (For timestamping data)	Float	1	4
COMMS	Signal/Connection with a network	Boolean	3	3
COMMS	Transmitting fire information	Float	7	28
Ground Stations	Get Location	Float	6 (orbital elements)	24
Ground Stations	Downlink Queueing	Float	60	240
Payload	Picture	Int	327680 Pixels	655360
Payload with	Picture	Int	327680 Pixels	122880



Compression				
Data Collections per minute	30		Total without Payload	349
Data Collected per minute (bytes)	3494363.76		Payload Activity Factor	0.3544
Data Collected per Day (bytes)	5031883814			43897.672
Data Processed per Second (bytes)	58,239.4			

The data from Table 29 informs component selection as it should be capable of storing up to 5 GB of mission data per day as well as hold 59 kB of data in memory for processing.

#### 10.4. C&DH SYSTEM PARAMETERS

Section 10.3 determined that the critical requirements of the system be that it allow for at least 5 GB of permanent memory for information storage as well as the ability to run C code to use the special data storage system that when processing the payload data. Roughly 100 kB of data will be needed for any additional drivers needed for interfacing with subsystems. In addition, the base requirements of the system be that it run a Real-Time Operating System (RTOS) capable of sending commands to other CubeSat components as well as have dedicated space for computation memory and read-only memory.

The computing section must be capable of running regular commands to retrieve data from each component every two seconds as well as run the data compression code.

**Table 30. Regular Commands:** *Commands for retrieving telemetry data*

Subsystem	Command
Thermal	Turn on/off
Thermal	Get Telemetry/SOH
Payload	Turn on/off
Payload	Get Telemetry/SOH
Payload	Get Image Data
Power	Change Mode (See Table 2)
Power	Get Telemetry/SOH
ADCS	Re-Orient
COMMS	Get Telemetry/SOH
COMMS	Get GPS Data
COMMS	Uplink Process - Space
COMMS	Downlink Process - Space
COMMS	Downlink Process - Ground
COMMS	Uplink Process - Ground



There are no intensive computing requirements relegated to the computer. This system must be capable of 32-bit computing as the size of the data being processed requires enough computational space. Lastly, the computer must be hardened for the space environment. This is a given when searching for components that are compatible with CubeSat architecture.

The final system must feature the following constraints:

**Table 31. Core Technical Requirements:** *Technical Requirements for C&DH Component Selection*

Requirement	Specification
Languages supported:	C
Speed	At least 12 Commands/Second
Permanent Data Storage:	At least 6 GB
Random Access Memory Storage	At least 100kB
Computational Architecture:	32-bit RTOS
Dimensions:	CubeSat Compatible
Hardening:	Space Environment

The Command & Data Handling Subsystem has chosen to go with the ISIS On-Board Computer (OBC) as it is configurable with enough permanent memory for storing Payload data as well as a RTOS.

## 11. PROPULSION

Multiple factors were assessed to determine the need of a propulsion system. The first situation examined was the need for orbit station keeping. Meeting with the orbits lead, it was determined that there was no need for changing or maintaining orbit, as the orbit would decay after the mission end date.

Another factor investigated was the possibility of a propulsion system assisting ADCS in pointing and momentum dumping. However, pointing requirements for the payload were met by the selected reaction wheels alone, and being in LEO, momentum was covered by magnetorquers better than using a large and expendable propulsion system.

The last situation investigated was deorbiting the CubeSat. This, however, was never explicitly requested by LASSI, and, according to NASA, is “considered risky”. Therefore, it was determined that no propulsion delta-V would need to be dedicated to deorbit, especially given an already short deorbit time of 816 days. This satisfies the “25-years post mission” deorbit requirement, without the need for any active or passive deorbit system. <sup>[31]</sup>

Given the evaluation of these three factors, it was decided that no propulsion system was needed for the Fire-LOC mission, as no aspect of the mission would require its use.



## 12. POWER

### 12.1. SYSTEM REQUIREMENTS

Based upon the mission presented in the **Task Order** and **Concept of Operations** sections, the power operational requirements will dominate the iterative design process for this mission. The level one and level two system requirements in **Table 32** below will serve as a preface to inform the reader as to the purpose of the alterations in design. Paramount to the success of this project are requirements dictating power operations and execution, namely the efficiency of solar cells, power distribution to subsystems, and battery storage capabilities. **Table 32** lists the level one and two requirements updated to the specifications of the final power subsystem design.

**Table 32. Power Level 1 and Level 2 Requirements:** *Derived requirements from SRR for the power subsystem.*

Req. #	Requirement	Verification
<b>W:1</b>	<b>The satellite shall receive an uninterrupted source of power</b>	<b>Analysis</b>
<b>W:2</b>	<b>The power subsystem shall provide storage for the power generated.</b>	<b>Analysis</b>
W:2.1	The power system shall have total power storage capacity of at least 5.5 W-hr.	Test
<b>W:3</b>	<b>The power subsystem shall distribute power to all satellite subsystems.</b>	<b>Demonstration</b>
W:3.1	The power system shall distribute $\leq$ 8 W of power to the payload.	Test
W:3.2	The power system shall distribute $\leq$ 1.25 W of power to COMMS.	Test
W:3.3	The power system shall distribute $\leq$ 0.45 W of power to C&DH	Test
W:3.4	The power system shall distribute $\leq$ 0.95 W of power to the ADCS.	Test
W:3.5	The power system should distribute $\leq$ 0.15 W of power to thermal sys.	Test
<b>W:4</b>	<b>The power subsystem shall accept commands from C&amp;DH system.</b>	<b>Test</b>
<b>W:5</b>	<b>The power subsystem shall consist of photovoltaic panels.</b>	<b>Inspection</b>
W:5.1	The photovoltaic cells shall have an efficiency of at least 29.5%.	Test
<b>W:6</b>	<b>The power subsystem shall use power regulation electronics.</b>	<b>Inspection</b>
<b>W:7</b>	<b>The power board (PB) shall communicate with the flight computer.</b>	<b>Test</b>
W:7.1	The PB shall report the bus voltage for inclusion in the telemetry.	Test
W:7.2	The PB shall report the battery charge status for inclusion in telemetry.	Demonstration
<b>W:8</b>	<b>Power to the payload shall be controllable from C&amp;DH by command from the ground.</b>	<b>Test</b>
<b>W:9</b>	<b>Power shall be inhibited by two inhibits until deployment is complete</b>	<b>Demonstration</b>
<b>W:10</b>	<b>The power subsystem shall protect bus from electrical fault damage</b>	<b>Test</b>
<b>W:11</b>	<b>The power subsystem shall generate telemetry for C&amp;DH.</b>	<b>Demonstration</b>
W:11.1	The power subsystem shall send voltage data to the C&DH system.	Demonstration
W:11.2	The power subsystem shall send SOH to the C&DH system.	Demonstration

### 12.2. FEASIBILITY ANALYSIS

Presented in the **Table 33** is the component concept of operations for the typical Fire-LOC satellite. The different phases represent a different mode of operation the satellite is likely to encounter. The listed subsystems and tasks vary between phases depending on demand.



**Table 33. Subsystems and Satellite Phases:** This table lists the active subsystems during each operational phase. Each operational phase is defined by what subsystems are active.

Phase	Expected Power Usage	Payload	ADS	ACS	Thermal	Direct Downlink	GPS	Space Based Downlink
Phase A	Nominal	Active	Active	Active	Active	Disabled	Active	Disabled
Phase B	Nominal	Active	Active	Active	Active	Disabled	Active	Active
Phase C	Nominal	Active	Active	Active	Active	Active	Active	Disabled
Phase D	Nominal	Active	Active	Active	Active	Active	Active	Active
Phase E	Minimum	Disabled	Active	Minimal	Disabled	Disabled	Active	Disabled

Each phase not only represents a different set of active subsystems and tasks but also a distinct point in the concept of operations.

- Phase A – Data Gathering without Detection.
  - No need to communicate with space comms or ground stations.
- Phase B – Data Gathering with Detection not over Ground Station
  - Fire has been detected so the satellite will need to communicate with the Iridium network to send the alert that a fire has been located at said location.
- Phase C – Data Gathering without Detection over Ground Station
  - No fire has been detected within the time that the satellite has last spoken to ground station. This means it will only be sending down telemetry data.
- Phase D – Data Gathering with Detection over Ground Station.
  - A fire has been detected within the time that the satellite has last spoken to ground station. This means it will be sending down telemetry data and payload data.
- Phase E – Satellite Stand-by Mode: Over ocean or land outside coverage region

**Table 34. Power Budget:** subsystem breakdown detailing the power consumption for a given operational phase. Phase D has the highest power consumption while Phase E has the least power consumption.

Subsystem	Marginal Error	Phase A Power [W]	Phase B Power [W]	Phase C Power [W]	Phase D Power [W]	Phase E Power [W]
<b>Payload</b>	1.1	4.4	4.4	4.4	4.4	--
<b>CDH</b>	1.1	0.44	0.44	0.44	0.44	0.44
<b>ADS</b>	1.1	0.794	0.794	0.794	0.794	0.134
<b>ACS</b>	1.05	0.798	0.798	0.798	0.798	--
<b>GPS</b>	1.1	0.132	0.132	0.132	0.132	0.132
<b>Space Based Comms</b>	1.15	--	0.052	--	0.052	--
<b>Ground Station Comms</b>	1.1	--	--	1.1	1.1	--
<b>Power</b>	1.05	0.1575	0.1575	0.1575	0.1575	0.1575
<b>Thermal</b>	1.05	0.147	0.147	0.147	0.147	--
<b>Total</b>		<b>6.87</b>	<b>6.92</b>	<b>7.97</b>	<b>8.02</b>	<b>0.86</b>



These phases or modes of operation affect what subsystems are active and the state at which they operate (max power, nominal power, low power modes). An illustration defining the integration of these power phases into the con-ops is shown in **Appendix D**. The resulting power budget is shown in **Table 34**. The allotted power values come from the respective COTS parts and are reflected by requirements **W:3.1** to **W:3.5**.

As observed in the power budget, the most power required for the satellite will be when in Phase D with 8.02W. As an extra safety margin, this is rounded to 8.2W (or an additional safety margin of 2%). The margin of error implemented is between 5% to 10% due to the use of COTS parts for each subsystem. An initialization start-up phase was ignored since the RFP states we assume the satellite to already be in orbit, therefore, we assume that with full batteries and sequential startup over multiple orbits, the startup phase can be ignored. These phases were illustrated in **Figure 38** for a single orbit. From ground station trade studies, communication with the ground station is in effect for roughly 10 minutes. The figure chose to demonstrate the case for Phase D since it has the highest power usage. Following this, Phase A and Phase B were demonstrated for nominal use. Finally, Phase E was in effect for the 60% of the time the payload would be off per orbit, estimated by orbits trade studies. Each subsystem in **Figure 38** is referenced by an individual color.

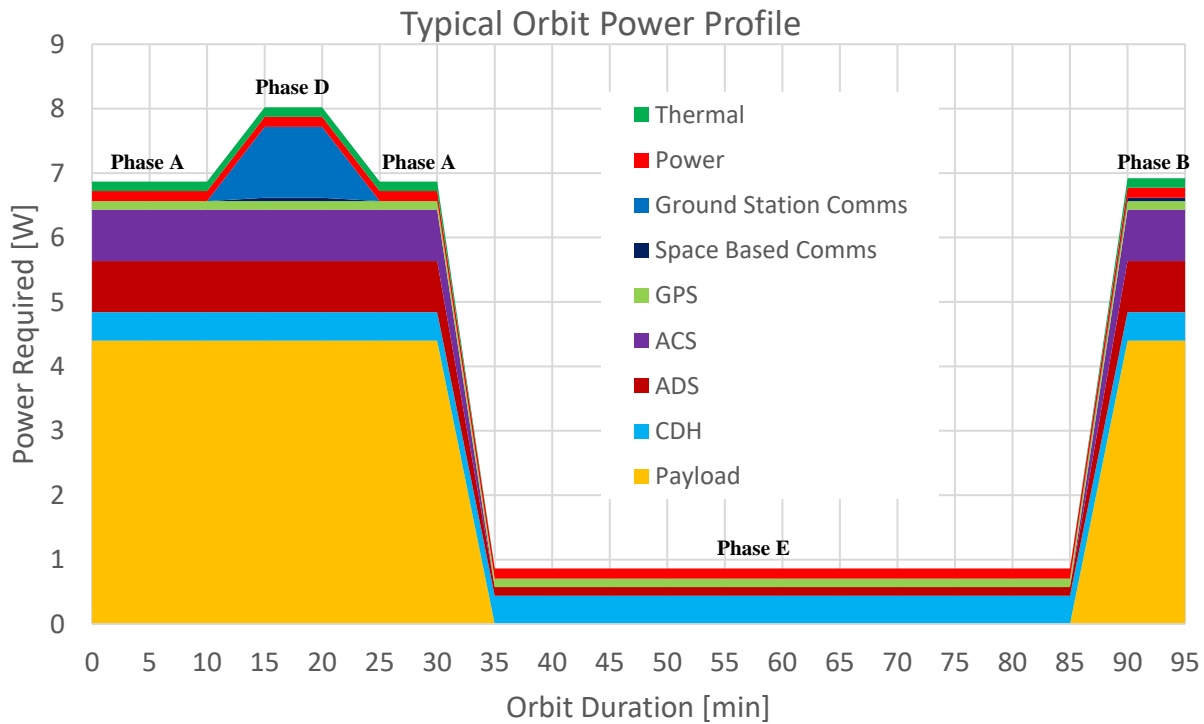


**Figure 38. Typical Orbit Power Distribution:** Over a typical orbit, this figure shows several different phases and the subsequent power loads for the length of time they are expected to be in effect.

### 12.3. POWER GENERATION

The average orbit power (AOP) was defined to be 8.2W as presented by the power budget in **Table 34** with the highest operational phase, Phase D. Phase D is the case when data gathering has detected a fire



somewhere in its orbit and is over a ground station. During this phase, it must perform a direct downlink with the ground station and send a space comms transmission with the location of the detected fire.

Since the payload is independent on the case of an eclipse, the average power required during daylight operations is the same as for during an eclipse, that is, 8.2W. At an orbit of 500km, this defines a 94-minute orbit period with ~32% of the orbit being in eclipse. Finally, the mission lifetime is designed for nine months. These parameters are requirements and constraints for the power subsystem solar array design. In designing a solar array, there is a trade-off of mass, area, cost and risk. **Table 35** provides a summary of currently available solar cell technology and their key parameters. From these options, the decision was made to go with the GaAs NeXt XTJ solar cells by SpectroLab. These cells were flight qualified by the Iridium constellation<sup>[37]</sup> and have the highest efficiency of any commercially available solar cell. This decision affected requirement **W:5.1** which defined the solar cell efficiency expected. With this value, the solar cells can be tested within the LASSI labs to verify that the solar cells can achieve at least 29.5% efficiency.

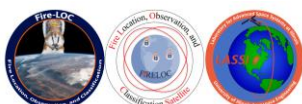
**Table 35. Several solar cell technologies and their parameters:** *These were derived from TSW0001 and resulted in the selection of GaAs NeXt XTJ solar cells by SpectroLab for the final decision of solar arrays due to its flight experience and high efficiency.*

Cell Type	Triple Junction GaAs (UTJ) <sup>[32]</sup>	GaAs (NeXt XTJ) <sup>[34]</sup>	Triple Junction Solar Cell (XTJ Prime) <sup>[33]</sup>
Efficiency (BOL) [%]	28.4	29.5	30.7
Specific Weight (cells only) [kg/m <sup>2</sup> ]	1.76 – 2.06	1.76 – 2.06	0.5-0.84
Fill Factor [%]	0.84	0.85	0.77
Performance [W/m <sup>2</sup> ]	330-350	345-366	--
Stowed Volume Efficiency [kW/m <sup>3</sup> ]	10-15	--	--
Performance Degradation [%/year]	--	1.7 <sup>[35]</sup>	--
Temperature Range [C]	15 - 80	15 - 75	15 - 125

With a solar cell decision, the design of the solar array could advance. Estimating the solar-array area required an understanding on how much power,  $P_{sat}$ , the solar array must provide during daylight operations for the entire orbit. To do this:

$$P_{sat} = \frac{\left( \frac{P_e T_e}{X_e} + \frac{P_d T_d}{X_d} \right)}{T_d}$$

Where  $P_e$  and  $P_d$  are the spacecrafts' power requirements during eclipse and daylight respectively;  $T_e$  and  $T_d$  is the duration the eclipse and daylight;  $X_e$  and  $X_d$  represent the efficiency of the paths from the solar arrays through the batteries to the individual loads (subsystems.) Fire-LOC satellites plan to use be using the Electrical Power System offered by Nano-Avionics. This is a Maximum Power Point Tracking System with efficiency of 96% when generating power and 90% when using stored energy<sup>[38]</sup>. From this, the required power that the solar array must produce during daylight operations is  $P_{sat} = 12.7\text{ W}$ .



The energy-conversion efficiency of a solar cell is defined as the power output divided by the power input. To complete this step, we select the type of solar and their performance throughout the entire mission. For this, the following equation is used:

$$P_o = S e$$

Garcia Gordon

Where  $S$  is the solar irradiance averaged over a year in LEO at 1AU ~~.....~~, and  $e$  is the efficiency. For the NeXt XTJ solar cell, the power output was found to be  $P_o = 400.6 W$ . Continuing forward, the realistic power production of the manufactured satellite must be considered. In manufacturing solar arrays, inherent inefficiencies in solar array design such as shadowing, and temperature variations exist. These inefficiencies are collectively referred to as *inherent degradation*,  $I_d$  and were assumed to be 0.77 for the first design iteration.

The power required at the beginning-of-life (BOL) is defined as the product of the estimated power output, inherent degradation and the cosine loss where  $\theta$  is the angle between the sun incidence and the vector normal to the surface of the solar panel.

$$P_{BOL} = P_o I_d \cos \theta$$

For the first design iteration, a worst-case scenario of  $\theta = 45^\circ$  was assumed until a more accurate angle was found. The relation between the sun's incident angle and power generated at BOL is presented in the **Figure 39**. At the assumed worst case, the power at BOL was determined to be  $P_{BOL} = 218 W$ .

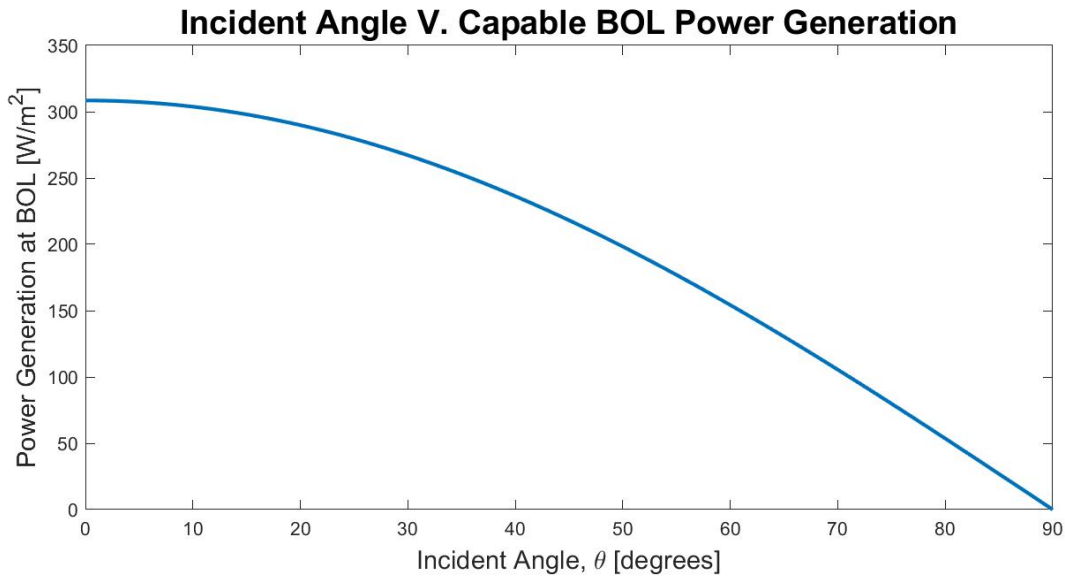


**Figure 39. Power generation at BOL as a function of the sun's incident angle.** As expected, the power generation decreases as the incident angle reaches  $90^\circ$ .

Degradation on the solar panel by radiation is a cause for the reduction of a solar array's output voltage and current. The *Life degradation*,  $L_d$ , occurs due to thermal cycling in and out of eclipses,



micrometeorite strikes, plume impingement from thrusters and material outgassing. The lifetime degradation can be estimated using the following:

$$L_d = \left(1 - \frac{\text{degradation}}{\text{year}}\right)^{\text{satellite lifetime}}$$

From this, the arrays performance per unit area at the end-of-life is:

$$P_{EOL} = P_{BOL} L_d$$

Provided the 1.7% performance degradation per year for the Spectrolab NeXt XTJ GaAs Solar cell for a 9-month (0.75 yrs) mission, the life degradation constant was found to be  $L_d = 0.9872$  with a resulting power at EOL of  $P_{EOL} = 215 \text{ W/m}^2$ . The solar array area required to support the spacecraft's power requirement is found by the ratio of the required satellite power to the power supplied at the end of life. This results in a solar array surface area of,  $A_{SA} = 587 \text{ cm}^2$ . Using the upper end of the specific weight listed in **Table 35**, the mass of the solar array was found to be  $M_{SA} = 0.1 \text{ kg}$ .

#### **12.4. SUN INCIDENCE AND SELF SHADING ANALYSIS**

The sun incidence angle is a key metric required for power related analysis, given that the sun incidence angle affects the power solar panels have available as a result of orbital geometry. Therefore, it required an investigation for computing the power generated from solar panels and the process of choosing the location of the solar panels. To accomplish this, a comprehensive simulation was created to reiterate over the calculations done in the power generation section, considering these additional parameters and factors.

For this investigation, the sun incidence angle for each of the faces containing solar panels, namely planes  $\pm X$  and  $\pm Y$  as well as panels on the  $\pm X$  and  $\pm Y$  that are deployed for all 22 satellites for all four seasons. The seasons affect the sun incident angle since the Earth orbits at a relative angle of 23.5 degrees. The simulation also ran for different deployable solar array lengths and angles to estimate solar array sizing.

Free Flyer by default has no built-in functionality to compute the sun incidence angle for all the faces. Therefore, a MATLAB simulation with the capability of being able to compute the sun incidence angle for different satellite orbits for each of its six different faces. The written program simulates a satellite given its Keplerian characteristics, the satellite propagates for a total timespan of 5 hours, roughly 3 orbits. These orbiting satellites are then analyzed for shading and illumination characteristics, as well as power generation assuming 29.5% efficient solar cells and the inherent degradation factor of 0.77.

There are two different scenarios that could cause a Fire-LOC satellite to be shaded. The first case would be if one of the satellite's faces are turned away from the sun. The effective area in sun was then computed by dotting the vector from the spacecraft to the sun with the plane's surface, which if positive, meant the face was illuminated, and if negative, meant the face was shaded. The second scenario that would lead to the spacecraft being shaded is when the satellite is in earth eclipse. This was determined off the location of the satellite in its orbit and was combined with the previous scenario to determine total power generation. This logic is illustrated in **Figure 40** where A. shows the earth shading case while B. depicts the self-shading case. The model also includes self-shading from deployable solar panels at varying lengths and deployment angles.



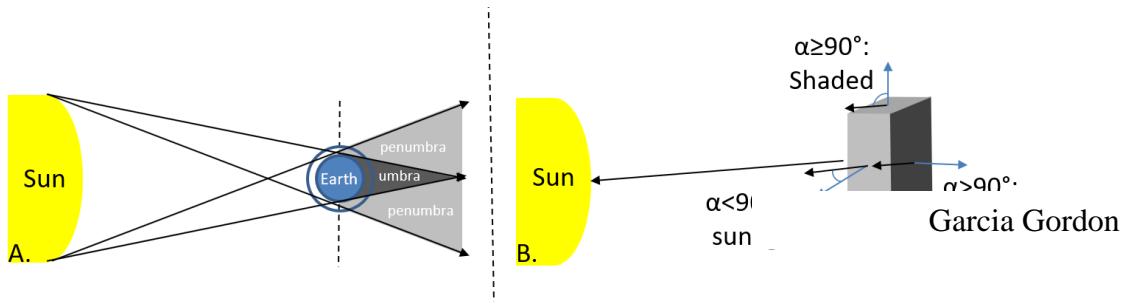


**Figure 40. Simulation calculation illustrations alliteration.** The sun-incident angle was calculated using the dot product of the sun vectors to the normal of the surface vector for all sides. The eclipse shading was computed by defining whenever the satellite-earth vector is negative and within the shadow region.

Found from orbital trade studies, the most time the payload would be collecting data (Phases A-D) was approximately 35.8% of the time. In addition, the maximum amount of power that can be used during this phase would be 8.2 W. The largest amount of power that can be used is 0.86 W when the payload is inactive, which can be rounded to 1 W to further increase the margin of safety. Now a possible worst-case power usage scenario can be calculated for 5 hours of orbit time, with an applied 1.5 margin of error to the payload “on” activity percentage to achieve the result below:

$$(8.2 [W]) (35.8 \%) (1.5) (5 [hr]) + (1 [W]) (1 - 35.8 \%) (1.5) (5 [hr]) = 24.332 [W \cdot hrs]$$

The computed 24.332 Whr, with a large margin of safety applied, still doesn't exceed the 25.62 Whr generated in the worst case found, an impossibly bad case where both normal vectors for  $\pm X$ -faces are always perfectly perpendicular to the rays of the sun shown in **Figure 41**. This analysis demonstrates that the power generated is enough to operate Fire-LOC subsystems as anticipated in orbit.

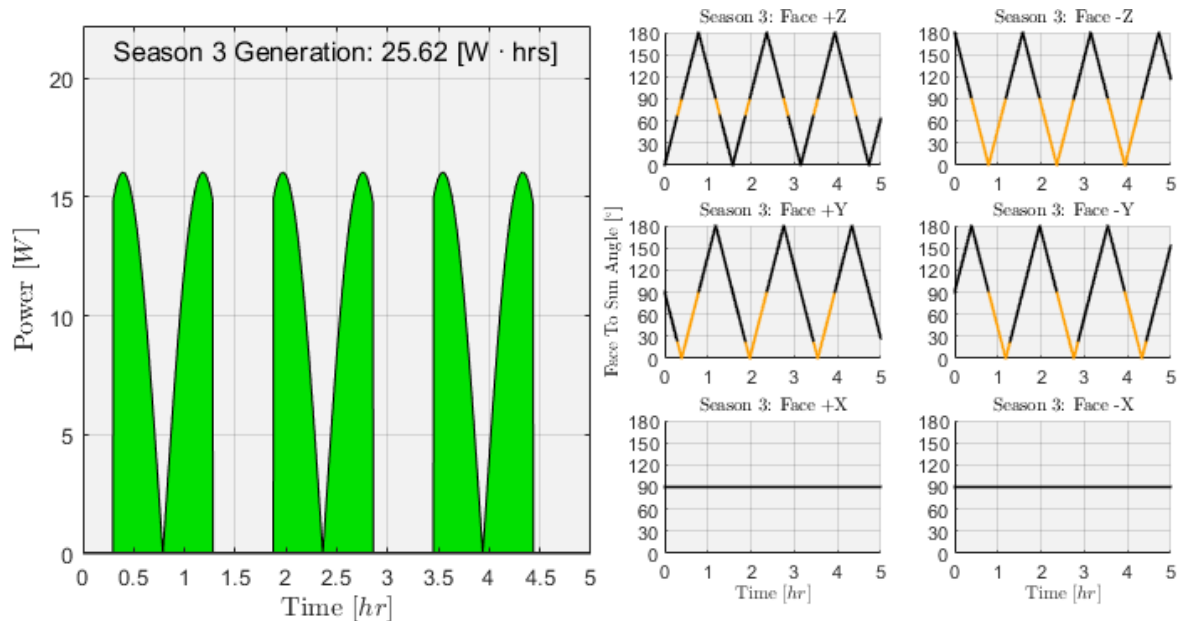


**Figure 41. Worst-case scenario for power generation.** By examining all the satellites in the orbit, season 3 for satellite 2 resulted in the worst power generation with 25.62 Whrs per every 3 orbits. This satellite had the following orbital parameters  $\Omega = 0^\circ$ ,  $\omega = 0^\circ$ ,  $f = 0^\circ$ ,  $i = 27^\circ$ .

## 12.5. POWER DISTRIBUTION AND STORAGE

Garcia Gordon

From previous orbital analysis, the eclipse frequency per day was found to be approximately 16 per day with a max eclipse duration of 36 minutes. Due to the high eclipse frequency, the secondary battery required a low depth of discharge. The *depth-of-discharge* (DoD) is the percent of total battery capacity removed during a discharge period. Higher percentages imply shorter cycle life. Li-Ion and LiPo batteries were the main battery types of focus due to their prevalent use in CubeSats. However, Given the current trend and research in Li-ion batteries in the CubeSat industry, the decision has been made to choose a Li-ion for the Fire-LOC satellites.

Sizing the secondary battery is simply a ratio of the orbital power requirements ( $P_e$ ) and average eclipse time ( $T_e$ ) to the DoD, transmission efficiency ( $n$ ) and number of batteries ( $N$ ) as shown in the following equation.

$$C_r = \frac{P_e T_e}{(DoD) N n}$$

Typically, a satellite is designed to need at least two battery cells for redundancy but no more than five to prevent over-complicating the electrical system.

The Fire-LOC satellites plan to use the NanoAvionics EPS Maximum Power Point Tracking power conditioning and distribution unit. The system offers up 96% output converter efficiency and accepts solar panel voltages within range of the selected panels and accepts inputs to at least 8 solar arrays. The EPS unit runs with minimal power consumption and operates at a bus voltage of 8.2V. The system also includes two internal NanoAvionics Battery Cells. This self-contained battery reduces the number of boards for power down to one while also providing ample storage capabilities. Using a transmission



frequency  $n = 0.96$  and a battery count of  $N = 2$ , the required storage capacity to provide stable power to Fire-LOC satellites is  $C_r = 2.7 \text{ Whr}$ . The NanoAvionics EPS board offers 23Whr of combined storage from its two internal batteries. While the board meets all the demands for distributing power, it also offered easy and reliable power storage capabilities making it the final choice for Fire-LOC satellites. In addition, this allows requirement **W:2.1** to develop such that the batteries when tested in the LASSI labs must store at least 5.5 W-hr of power.



### **13. STRUCTURES**

#### **13.1. SYSTEM REQUIREMENTS**

The structures system is one of the final design processes for this mission. Sizing and modeling relied on the final iterations of every other system to complete each section. The level one and level two system requirements in **Table 36** will detail the process needed to confirm the Fire-LOC satellite was flight ready. Included are the requirements from the CubeSat Design Specification Document that determine if the satellite is compatible with the Poly Picosatellite Orbital Deployer (P-POD).

**Table 36 Payload Requirements.** *Enumerated Level 1 and Level 2 Requirements for the Structures subsystem as specified by the Request for Proposal (RFP).*

Req. #	Requirement	Verification
<b>S:1</b>	<b>Satellite shall be compatible with cubesat.org specs</b>	<b>Inspection</b>
S:1.1	Satellites shall be a standard size CubeSat 3U	Inspection
S:1.2	Satellites shall have a top, bottom, and middle plate structure with four rails	Inspection
<b>S:2</b>	<b>Satellite shall be P-POD compatible</b>	<b>Inspection</b>
S:2.3	The satellites shall have a center of gravity located within 2 cm from its geometric center in the X, Y direction	Test
S:2.4	The satellites' structures shall be made of aluminum 6061	Inspection
<b>S:3</b>	<b>Satellites shall be structurally modeled</b>	<b>Test</b>
S:3.1	Satellites shall be a mass of 2.846 kg	Inspection
S:3.2	ADCS shall have a maximum mass of 0.720 kg	Inspection
S:3.3	C&DH shall have a maximum mass of 0.094 kg	Inspection
S:3.4	Power shall have a maximum mass of 0.438 kg	Inspection
S:3.5	Payload shall have a maximum mass of 0.595 kg	Inspection

#### **13.2. FIRST DESIGN ITERATION**

The initial values for the Fire-LOC satellite were determined using past Preliminary Design Reviews of CubeSat satellites. Using the values from the INSPIRESat-1, Phoenix Satellite, and Earth Science Mission, a mass distribution was created which can be seen in **Table 37**. The maximum mass for a 3U satellite is 4kg leaving 0.13 kg of extra mass for later stages of the design iteration.

**Table 37. Mass Distribution.** *Initial subsystem masses for preliminary research when choosing instruments.*

Subsystem	Nominal Mass (kg)
ADCS	0.35
C&DH	0.15
Communications	0.15
Power	0.20
Payload	2.00
Structure	0.82
Thermal	0.20
Propulsion	0.00
Total	3.87



### 13.3. SECOND DESIGN ITERATION

After final iterations were completed for each subsystem, a 3D CAD model was created. **Figure 42** shows the satellite deployed with two sides removed to view the inside of the satellite. **Figure 43** shows the satellite in its stowed position until it reaches orbit. This model will provide a visualization of the Fire-LOC satellite, provide moment of inertia and center of mass values, and create a thermal model to complete a second design iteration for the thermal subsystem.

**Figure 42. 3D CAD Model.** A model of the Fire-LOC satellite containing all systems in their deployed position.



**Figure 43. 3D CAD Model.** A model of the Fire-LOC satellite containing all systems in their stowed position.

General dimensions for the CAD model can be seen in **Figure 44**. The dimensions of the Fire-LOC satellite meet the requirements for P-POD compatibility.

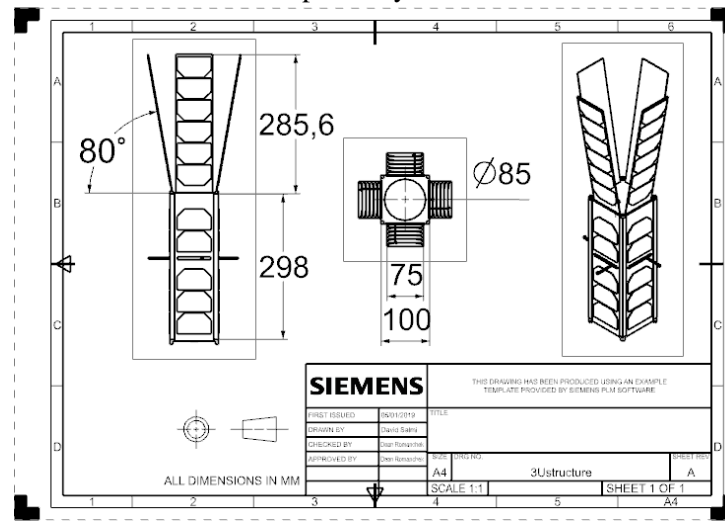


**Figure 44. CAD Schematic.** A schematic of the Fire-LOC satellite containing external dimensions of the deployed satellite



Solar panels will be deployed using thermal knives to cut a Kevlar strap attaching the solar panel to the bottom panel of the satellite. **Figure 45** shows the size and method a thermal knife will be used in the Fire-LOC satellite.



**Figure 45. Thermal Knife.** A thermal knife will be used to cut the Kevlar strap that keeps the deployable solar panels in their stowed position during launch.

After the completion of the 3D model, an analysis was run to calculate the moment of inertia and center of mass. The values can be seen in **Table 38**. The satellite was determined to be gravity gradient stable from the moment of inertia values and the center of mass values are within the acceptable range set by the CubeSat Design Specification Document.

With the model completed, volume and mass values for

**Table 39. Final Mass Values.** The final values for the

Subsystem	Volume (%)	Mass(g)	Values	Numbers
ADCS	0.247	700	I <sub>x</sub>	.403781 kg/m <sup>2</sup>
C&DH	0.039	94	I <sub>y</sub>	.404050 kg/m <sup>2</sup>
Communications	0.134	171	I <sub>z</sub>	.015563 kg/m <sup>2</sup>
Power	0.076	438	X <sub>c</sub>	-0.19 cm
Payload	0.384	595	Y <sub>c</sub>	-0.22 cm
Structure	0.117	833	Z <sub>c</sub>	18.91 cm
Thermal	0.004	15		
Propulsion	0.000	0		
Total	2736.7 cm <sup>3</sup>	2846		3445

each subsystem were calculated and added together to create the final volume and mass values. **Table 39** shows that the values of 2736.7 cm<sup>3</sup> and 2846 g are within the specifications of a 3U satellite. Extra room and mass are available if any changes should occur after the Preliminary

David Salmi



**THERMAL****13.4. SYSTEM REQUIREMENTS**

The thermal system requires the collaboration of all systems to provide temperature ranges for each instrument and determine what thermal control system is best suited for satellite's orbit. Therefore, the requirements of the thermal system discussed in **Table 40**. **Table 40** name each subsystem that needs thermal control and states the minimum and maximum operational temperatures of each subsystem. Systems must stay above the temperature values listed in order to operate.

**Table 40. Payload Requirements.** *Enumerated Level 1 and Level 2 Requirements for the Payload as specified by the Request for Proposal (RFP).*

Req. #	Requirement	Verification
<b>T:1</b>	<b>The thermal subsystem shall maintain specified operating temperature ranges for the satellite systems</b>	<b>Analysis</b>
T:1.1	ADCS shall operate within -10°C to 40°C thermal range NOTES: In accordance with ADCS requirement A:6.2	Test
T:1.2	C&DH shall operate within -25°C to 65°C thermal range NOTES: In accordance with C&DH requirement C:4.3	Test
T:1.3	Power shall operate within -60°C to 70°C thermal range NOTES: In accordance with Power requirement W:2.4	Test
T:1.4	Payload shall operate within -40°C to 70°C thermal range NOTES: In accordance with Payload requirement Y:6.1	Test
<b>T:2</b>	<b>The thermal subsystem shall incorporate into the satellite</b>	<b>Analysis</b>
T:2.1	Thermal subsystem shall have a maximum mass of 0.015 kg NOTES: In accordance with Structure requirement S:3.7	Inspection

**13.5. FIRST DESIGN ITERATION**

The first design iteration focused on the bulk thermal properties of the satellite. This determined the temperature ranges of each system inside the satellite during the aphelion and perihelion of our mission. These points of reference would offer the most extreme conditions that the satellite will face. To create a preliminary model, the following thermal equation was used:

$$\frac{dQ}{dt} = \sigma * e * A * T^4$$

Five sources of radiation need to be accounted for in the bulk heat analysis: direct solar flux, albedo, earth emitted infrared radiation, internal generated heat and emitted radiation. The four sources that cause heat to enter the system are accounted for in the equation below:

$$R = \frac{1414 * W * H}{10000} + \frac{241 * L * H}{10000} * \frac{r_{Earth}^2}{(a + r_{Earth})^2} + \frac{1414^2 * L * H}{10000} * \frac{r_{Earth}^2}{(a + r_{Earth})^2} + A * ssr * \varepsilon + sca * (1 - ssr) + E * 0.0001 * \sigma * T^4$$

Where W = width, H = height, L = length,  $r_{Earth}$  = radius of Earth, a = semimajor axis, A = Absorptance, ssr = solar side ratio,  $\varepsilon$  = solar panel efficiency, sca = solar cell absorptivity, E = Emissivity,  $\sigma$  = Boltzmann's Constant and T = Temperature.

The one source that cause heat to leave the system are accounted for in the equation below:

$$R = \frac{L * H}{10000} + \frac{2 * L * W}{10000} + \frac{2 * W * H}{10000} * (3^4 - (T + 273.15)^4) * (\varepsilon * (ssr + sce)) * (1 - ssr) * \sigma$$

Where W = width, H = height, L = length, T = temperature,  $\varepsilon$  = Emittance, ssr = solar side ratio, sce = solar cell efficiency, and  $\sigma$  = Boltzmann's Constant.



David Salmi  
David Salmi

The equations were used to create a bulk heat analysis of the Fire-LOC satellite. **Figure 46** shows the temperature vs time of the hot case perihelion and cold case aphelion scenarios. **Figure 47**, **Figure 48**, and **Figure 49** detail an example bulk heat analysis for the hot case perihelion thermal model including structural temperature, energy absorbed, and solar panel temperature respectively.

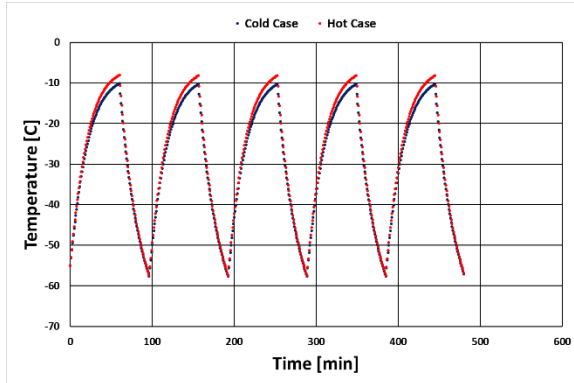


**Figure 46. Temperature vs. Time.** Hot case perihelion and cold case aphelion bulk heat analysis

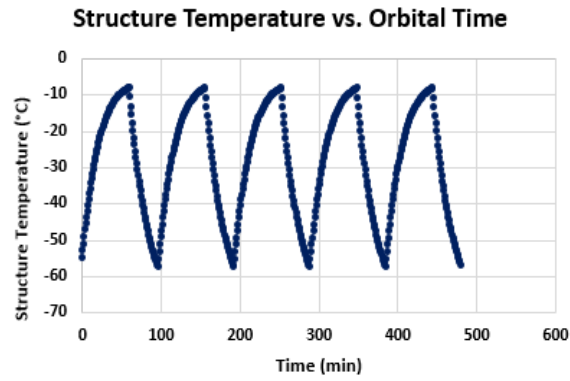


**Figure 47. Structure Temperature vs. Orbital Time.** Hot case perihelion structural temperature during orbit

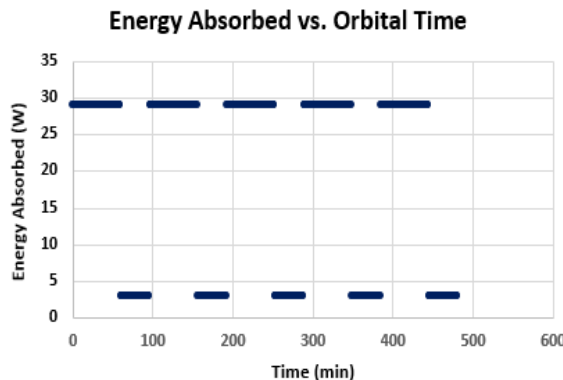


**Figure 48. Energy Absorbed vs. Orbital Time.** Hot case perihelion energy absorbed during orbit

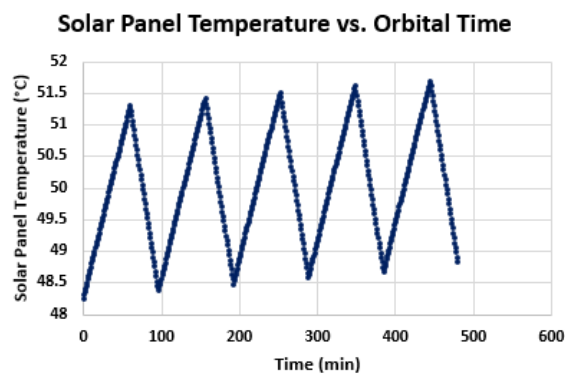


**Figure 49. Solar Panel Temperature vs. Orbital Time.** Hot case perihelion solar panel temperature during orbit



**14. COST**

The cost estimation process is heavily impacted by the design decisions, namely due to the fact that the choice of selecting the FLIR Neutrino LC Thermal Imagine Core to heavily modify to meet our needs may have adverse effects. The developmental costs associated with raising the technology readiness level (TRL) level from its current place as a TRL 4 (verified for Earth-based applications) to TRL 8 or TRL 9 to accommodate space flight may prove to be challenging as this device was not originally intended for space activity. Therefore, the cost of research, testing, and development must also be considered as the payload for each of the 22 satellite must be customized from a COTS parts. A larger constellation like Fire-LOC may be logically challenging for LASSI's facilities, thus outsourcing may be advisable. The outsourcing process may increase cost, but in order to maintain the reliability of the mission the possibility must be considered. However, only the payload may have to be tested this extensively as many of the other sub-system components are commercially available with a TRL of 8 or 9.

A major design decision that affects cost is the choice of communications systems. This mission requires not one, but three communications platforms. One for direct downlink, another for downlink via space-based networks, and a final package for receiving GPS information. While, direct space to ground communications are the cheapest option, the high downlink time makes it a less favorable option for fire detection due to the urgency of information transfer, thus space-based communications are considered. However, using a system such as Iridium increases the cost per unit data, a large expense considering the 9-month operations phase along with the presence of multiple satellites. With thousands of fires occurring globally every day, with an average burn time around six days, each of the 22 satellites would observe these fires dozens of times, especially with an imaging rate which allows for overlapping data. This would result in potentially dozens of warning signals being broadcast through space-based networks each day, which may prove to be excessive. Possible solutions to this problem involve using ground to satellite contacts to program latitude and longitude based flags of know, actively suppressed ground fires to avoid network saturation with already known data.

Ground associate costs also area a potential risk to drive the system cost up. Having a full-time staff would incur an additional \$8.25/person/hour, so if one attendant is used for each satellite for ten hours a week, this would add an additional \$70,979.57 to the mission budget without including overtime. This cost can be mitigated using ground automation strategies. If each warning signal is autonomously routed to a customer or a live-updating web page, then attendants only need to verify findings several times a week as opposed to constantly. This could reduce the number of required attends to four, reducing the nine-month budget to \$12,905.38, causing a 138.46% savings.



## 15. RISKS

To ensure mission success, Fire-LOC satellites, mission architecture and operation cost were all given strong considerations when performing risk analysis. To categorize mission risks, a traffic-light scale was utilized to quantitatively assess risks for the mission and spacecraft subsystems. In order to accomplish this task, a risk scale was established based on the NASA Systems Engineering Handbook shown in Table XXX.

Level	1	2	3	4	5
Probability	Very Low: Not Expected	Low: Less Likely Than Not	Moderate: May or May Not	High: More Than Likely	Very High: Expected
Severity	Negligible: No Measurable Impact	Minor: System Operating Close to Intended	Moderate: System Underperforms	Severe: Mission Detrimentally Impacted	Catastrophic: Total Mission Loss

Descriptions of potential risk scenarios identified for the Fire-LOC constellation can be seen in Table 41. Mission risk mitigation is primarily being implemented using COTS hardware, repetitive testing, and added redundancy. Minimizing unique technology developments for major subsystem function reduces the use of low-fidelity system architecture.

**Table 41. Risk Analysis and Mitigation:** This table uses the stoplight method to classify and mitigate risks.

Scenario	Type	Risk	Probability	Severity	Total	Mitigations
R1	Payload	Payload Shutter fails to open due to low temperature.	1	5	5	Thermal heaters will use emergency reserved power to heat the payload.
R2	Payload	Earth Albedo penetrates lens to overheat payload.	2	3	6	Close shutter and deactivate payload for cooldown.
R3	Payload	Solar Flux on panels causes the payload to overheat.	2	3	6	Close shutter and deactivate payload for cooldown.
R4	Payload	ADCS system does not retain prescribed pointing accuracy.	3	2	6	Gravity Gradient with periodic control can dampen the oscillations to achieve higher accuracy.
R5	Payload	Frequent eclipse periods cause the payload to become too cold.	3	4	12	Thermal heaters will use emergency reserved power to heat the payload.
R6	Orbits	Space debris crash	1	4	4	Track space debris where possible using space debris tracking system and attempt to change attitude accordingly.
R7	Orbits	Fail to get injected into the correct orbit	1	5	5	None.
R8	Orbits	Orbit degrades faster than expected	1	5	5	Increased margin significantly, the current design has a deorbit time of 816 days easily surpassing the required 9 months.
R9	Power	Failed solar array deployment	2	5	10	Testing to reduce likelihood of a failed solar array deployment and ensure reliability.
R10	Power	All systems initialize at the same time,	2	3	3	Design and test a sequence that powers up



		draining battery	<span style="background-color: #6aa84f; color: white; padding: 2px 5px;"> </span>	<span style="background-color: #ffcc00; color: black; padding: 2px 5px;"> </span>	<span style="background-color: #ff0000; color: white; padding: 2px 5px;"> </span>	systems necessary for power generation and power control first, proceeding to sequentially power on remaining systems, reducing power strain.
R11	Power	Damaged solar cell creates open circuit in solar array.	<span style="background-color: #6aa84f; color: white; padding: 2px 5px;">1</span>	<span style="background-color: #ff0000; color: white; padding: 2px 5px;">5</span>	<span style="background-color: #ffcc00; color: black; padding: 2px 5px;">5</span>	Utilize bypass diodes in solar array design to prevent open circuiting
R12	Power	Lower than expected solar cell efficiency values	<span style="background-color: #ffcc00; color: black; padding: 2px 5px;">3</span>	<span style="background-color: #6aa84f; color: white; padding: 2px 5px;">2</span>	<span style="background-color: #ffcc00; color: black; padding: 2px 5px;">6</span>	Sun simulator testing to characterize solar cell efficiencies, and other metrics
R13	Power	Improper battery environment results in damaged or destroyed energy storage system.	<span style="background-color: #6aa84f; color: white; padding: 2px 5px;">1</span>	<span style="background-color: #ff0000; color: white; padding: 2px 5px;">5</span>	<span style="background-color: #ffcc00; color: black; padding: 2px 5px;">5</span>	Thermal vacuum chamber and vibe testing to ensure reliability
R14	Thermal	Heaters Fail	<span style="background-color: #6aa84f; color: white; padding: 2px 5px;">2</span>	<span style="background-color: #ffcc00; color: black; padding: 2px 5px;">4</span>	<span style="background-color: #ff0000; color: white; padding: 2px 5px;">8</span>	Orient satellite to maximize external thermal absorption.
R15	Thermal	Temperature Sensors Fail	<span style="background-color: #ffcc00; color: black; padding: 2px 5px;">3</span>	<span style="background-color: #6aa84f; color: white; padding: 2px 5px;">2</span>	<span style="background-color: #ffcc00; color: black; padding: 2px 5px;">6</span>	Include multiple sensors and rely on working sensors. If no sensors are working, rely on best estimates from orbital situation.
R16	Structures	Solar Panels do not deploy	<span style="background-color: #6aa84f; color: white; padding: 2px 5px;">2</span>	<span style="background-color: #ff0000; color: white; padding: 2px 5px;">5</span>	<span style="background-color: #ffcc00; color: black; padding: 2px 5px;">10</span>	Include redundant thermal knives to ensure Kevlar ties are cut
R17	Structures	Antenna does not deploy	<span style="background-color: #ffcc00; color: black; padding: 2px 5px;">3</span>	<span style="background-color: #6aa84f; color: white; padding: 2px 5px;">3</span>	<span style="background-color: #ff0000; color: white; padding: 2px 5px;">9</span>	Rely solely on Space Comms. Do not transmit full size images
R18	Structures	Vibration from launch dislodges system	<span style="background-color: #ffcc00; color: black; padding: 2px 5px;">3</span>	<span style="background-color: #6aa84f; color: white; padding: 2px 5px;">3</span>	<span style="background-color: #ffcc00; color: black; padding: 2px 5px;">6</span>	Vibe test to ensure system does not dislodge during launch
R19	ADCS	Reaction wheel failure	<span style="background-color: #ffcc00; color: black; padding: 2px 5px;">3</span>	<span style="background-color: #6aa84f; color: white; padding: 2px 5px;">3</span>	<span style="background-color: #ff0000; color: white; padding: 2px 5px;">9</span>	Redundant fourth reaction wheel
R20	ADCS	Star tracker FOV interference	<span style="background-color: #ffcc00; color: black; padding: 2px 5px;">3</span>	<span style="background-color: #6aa84f; color: white; padding: 2px 5px;">1</span>	<span style="background-color: #ffcc00; color: black; padding: 2px 5px;">3</span>	Magnetometer for redundancy
R21	ADCS	Gyroscope failure	<span style="background-color: #ff0000; color: white; padding: 2px 5px;">5</span>	<span style="background-color: #6aa84f; color: white; padding: 2px 5px;">2</span>	<span style="background-color: #ffcc00; color: black; padding: 2px 5px;">10</span>	3-axes Magnetometer for redundancy
R22	COMMs	Space COMMs cannot connect	<span style="background-color: #6aa84f; color: white; padding: 2px 5px;">2</span>	<span style="background-color: #ffcc00; color: black; padding: 2px 5px;">4</span>	<span style="background-color: #ffcc00; color: black; padding: 2px 5px;">8</span>	Report failure & queue data at next GS Downlink
R23	COMMs	Ground COMMs cannot connect	<span style="background-color: #6aa84f; color: white; padding: 2px 5px;">2</span>	<span style="background-color: #ffcc00; color: black; padding: 2px 5px;">4</span>	<span style="background-color: #ffcc00; color: black; padding: 2px 5px;">8</span>	Report failure through Space, prepare for next GS downlink
R24	COMMs	Antenna Deployment Failure	<span style="background-color: #6aa84f; color: white; padding: 2px 5px;">1</span>	<span style="background-color: #ff0000; color: white; padding: 2px 5px;">5</span>	<span style="background-color: #ffcc00; color: black; padding: 2px 5px;">5</span>	Use patch antenna to transmit telemetry data in addition to payload data. May require multiple orbits to transmit data.
R25	Ground	Ground Station Failure	<span style="background-color: #6aa84f; color: white; padding: 2px 5px;">2</span>	<span style="background-color: #6aa84f; color: white; padding: 2px 5px;">1</span>	<span style="background-color: #ffcc00; color: black; padding: 2px 5px;">3</span>	Store data on craft, wait for different station
R26	Ground	Increase in Subscription Costs	<span style="background-color: #6aa84f; color: white; padding: 2px 5px;">2</span>	<span style="background-color: #ffcc00; color: black; padding: 2px 5px;">3</span>	<span style="background-color: #ff0000; color: white; padding: 2px 5px;">5</span>	Negotiate fixed price for duration of mission. Explore alternative ground stations.
R27	Ground	Image Processing Failure	<span style="background-color: #6aa84f; color: white; padding: 2px 5px;">2</span>	<span style="background-color: #6aa84f; color: white; padding: 2px 5px;">1</span>	<span style="background-color: #ffcc00; color: black; padding: 2px 5px;">3</span>	Store images locally until issue is fixed.
R28	C&DH	Kernel Panic	<span style="background-color: #6aa84f; color: white; padding: 2px 5px;">1</span>	<span style="background-color: #ff0000; color: white; padding: 2px 5px;">5</span>	<span style="background-color: #ffcc00; color: black; padding: 2px 5px;">5</span>	No mitigation
R29	C&DH	SD Card Failure	<span style="background-color: #6aa84f; color: white; padding: 2px 5px;">1</span>	<span style="background-color: #ff0000; color: white; padding: 2px 5px;">5</span>	<span style="background-color: #ffcc00; color: black; padding: 2px 5px;">5</span>	No mitigation
R30	C&DH	Not enough memory before next downlink	<span style="background-color: #6aa84f; color: white; padding: 2px 5px;">2</span>	<span style="background-color: #6aa84f; color: white; padding: 2px 5px;">2</span>	<span style="background-color: #ffcc00; color: black; padding: 2px 5px;">4</span>	Delete non-Payload telemetry data, keep a log



## **16. REFERENCES**

1. Thiessen, Mark. "Wildfires Information and Facts." *National Geographic*, 18 Jan. 2018, [www.nationalgeographic.com/environment/natural-disasters/wildfires/](http://www.nationalgeographic.com/environment/natural-disasters/wildfires/).
2. Hoover, Katie. "Wildfire Statistics." *In Focus*, Congressional Research Service, 16 Nov. 2018, [fas.org/sgp/crs/misc/IF10244.pdf](http://fas.org/sgp/crs/misc/IF10244.pdf).
3. "U.S. Fire Statistics." U.S. Fire Administration, 23 Oct. 2018, [www.usfa.fema.gov/data/statistics/](http://www.usfa.fema.gov/data/statistics/).
4. Ingraham, Christopher. "Wildfires Have Gotten Bigger in Recent Years, and the Trend Is Likely to Continue." *The Washington Post*, WP Company, 14 Aug. 2018, [www.washingtonpost.com/business/2018/08/14/wildfires-have-gotten-bigger-recent-years-trend-is-likely-continue/?noredirect=on&utm\\_term=.3a12529b2ded](http://www.washingtonpost.com/business/2018/08/14/wildfires-have-gotten-bigger-recent-years-trend-is-likely-continue/?noredirect=on&utm_term=.3a12529b2ded).
5. Evarts, Ben. "Fire Loss in the United States." *NFPA Report - Fire Loss in the United States*, Sept. 2018, [www.nfpa.org/News-and-Research/Data-research-and-tools/US-Fire-Problem/Fire-loss-in-the-United-States](http://www.nfpa.org/News-and-Research/Data-research-and-tools/US-Fire-Problem/Fire-loss-in-the-United-States).
6. "California's \$442 Million Fire Budget Is Exhausted-and Needs \$234 Million More to Keep Fighting." Fortune, Fortune, 6 Sept. 2018, [fortune.com/2018/09/06/california-fire-2018-cost-insurance-claims/](http://fortune.com/2018/09/06/california-fire-2018-cost-insurance-claims/).
7. "Ferguson Fire." Ferguson Fire, Sierra National Forest, 19 Sept. 2018, [inciweb.nwrgov/incident/5927/](http://inciweb.nwrgov/incident/5927/).
8. "Global Fire Monitoring." NASA, NASA, 22 Oct. 1999, [earthobservatory.nasa.gov/features/GlobalFire/fire\\_5.php](http://earthobservatory.nasa.gov/features/GlobalFire/fire_5.php).
9. "Fire." Earth Observatory, NASA, [earthobservatory.nasa.gov/global-maps/MOD14A1\\_M\\_FIRE](http://earthobservatory.nasa.gov/global-maps/MOD14A1_M_FIRE).
10. "California Statewide Fire Map." Fire Statistics, State of California, 4 Jan. 2019, [cdfdata.fire.ca.gov/incidents/incidents\\_details\\_info?incident\\_id=2164](http://cdfdata.fire.ca.gov/incidents/incidents_details_info?incident_id=2164). "Size Class of Fire." Size Class of Fire, The National Wildfire Coordinating Group, [www.nwrgov/term/glossary/size-class-of-fire%C2%A0](http://www.nwrgov/term/glossary/size-class-of-fire%C2%A0).
11. "Federal Fire Occurrence Map Viewer." Fire History, United States Geological Survey, [wildfire.cr.usgs.gov/firehistory/viewer/viewer.htm](http://wildfire.cr.usgs.gov/firehistory/viewer/viewer.htm).
12. "Fire Detection Maps." Remote Sensing Applications Center, USDA Forest Service, [fsapps.nwrgov/afm/activefiremaps.php](http://fsapps.nwrgov/afm/activefiremaps.php).
13. "IlliniSat-3 Request for Proposal." *LASSI*, Section L/M. 16 Jan. 2019. Microsoft Word file.
14. "CubeSat Electrical Power System 'EPS'." *NanoAvionics*, <https://nanoavionics.com/subsystems/cubesat-electrical-power-system-eps/>.
15. "ISIS On Board Computer." *Innovative Solutions in Space*, <https://www.isispace.nl/product/on-board-computer/>
16. "MCP2515 - Stand-Alone CAN Controller with SPI Interface." *Microchip Technology*, August 2012, <https://www.mouser.com/ds/2/268/21801G-76865.pdf>
17. "Low-power bridges for I2C or SPI to UART or IrDA or GPIO." *NXP Semiconductors*, September 2006, <https://www.nxp.com/docs/en/brochure/75015676.pdf>



18. NASA. "The Electromagnetic Spectrum." *Spectrum Properties*, 23 July 2007, [mynasadata.larc.nasa.gov/images/EM\\_Spectrum3-new.jpg](http://mynasadata.larc.nasa.gov/images/EM_Spectrum3-new.jpg).
19. Cafe, Tony. "PHYSICAL CONSTANTS FOR INVESTIGATORS." *T.C. Forensics*, PTY Limited, [www.tcforensic.com.au/docs/article10.html](http://www.tcforensic.com.au/docs/article10.html).
20. Wertz, James R, and Wiley Larson. *Space Mission Analysis and Design*. Springer, 2013.
21. AI solutions. "FreeFlyer® Software." *AI Solutions*, 2019, [ai-solutions.com/freeflyer/](http://ai-solutions.com/freeflyer/).
22. "Tracking Fires and Haze - Global Forest Watch Fires." *Fires.globalforestwatch.org*, 2019, [fires.globalforestwatch.org/map/](http://fires.globalforestwatch.org/map/).
23. Ullery, Dylan C., et al. "Strong Solar Radiation Forces from Anomalously Reflecting Metasurfaces for Solar Sail Attitude Control." *Nature News*, Nature Publishing Group, 3 July 2018.
24. "Attitude Determination and Control Subsystem." *Laboratory for Atmospheric and Space Physics*, [lasp.colorado.edu/home/csswe/system/subsystems/adcs/?doing\\_wp\\_cron=1555990680.6373319625854492187500](http://lasp.colorado.edu/home/csswe/system/subsystems/adcs/?doing_wp_cron=1555990680.6373319625854492187500).
25. Gravdahl, Jan Tommy, et al. *THREE AXIS ATTITUDE DETERMINATION AND CONTROL SYSTEM FOR A PICO-SATELLITE: DESIGN AND IMPLEMENTATION*. 7 Oct. 2003, [pdfs.semanticscholar.org/5341/6df42ae8a000dafcc121b5463e5c6e44df56.pdf](http://pdfs.semanticscholar.org/5341/6df42ae8a000dafcc121b5463e5c6e44df56.pdf).
26. "09. Communications." NASA, [sst-soa.arc.nasa.gov/09-communications](http://sst-soa.arc.nasa.gov/09-communications).
27. RBC Signals. "RBC Signals Global Ground Station Network." *RBC Signals*, [rbcsignals.com/](http://rbcsignals.com/).
28. Unidata@unidata.com.au. "Satellite Airtime Pricing Models." *Unidata*, [www.unidata.com.au/support/technical-white-papers/satellite-airtime-pricing-models/](http://www.unidata.com.au/support/technical-white-papers/satellite-airtime-pricing-models/).
29. "Satellite Ground Operations Automation - Lessons Learned and Future Approaches." NASA, 11 May 2001, <https://ntrs.nasa.gov/archive/nasa/casi.ntrs.nasa.gov/20020023390.pdf>
30. "Bit Fields in C." *GeeksforGeeks*, 23 Nov. 2017, [www.geeksforgeeks.org/bit-fields-c/](http://www.geeksforgeeks.org/bit-fields-c/).
31. "Passive Deorbit Systems – State of the Art of Small Spacecraft Technology." NASA, 12 Mar. 2019, <https://sst-soa.arc.nasa.gov/12-passive-deorbit-systems>
32. Spectrolab, "Ultra Triple Junction," Spectrolab -A Boeing Company, [https://www.spectrolab.com/photovoltaics/UTJ-CIC\\_Data\\_Sheet.pdf](https://www.spectrolab.com/photovoltaics/UTJ-CIC_Data_Sheet.pdf), Accessed 27 Apr. 2019.
33. Azurspace Solar Power GMBH, "30% Triple Junction GaAs Solar Cell," Azurspace. <https://www.spectrolab.com/pv/support/R.%20King%20et%20al.,%20IEEE%20PVSC%202000,%20Next-generation%20MJ%20solar%20cells.pdf>, Accessed 27 Apr. 2019.
34. Spectrolab, "29.5% NeXt Triple Junction" Spectrolab -A Boeing Company, [https://www.spectrolab.com/photovoltaics/XTJ-CIC\\_Data\\_Sheet.pdf](https://www.spectrolab.com/photovoltaics/XTJ-CIC_Data_Sheet.pdf) Accessed 27 Apr. 2019.
35. Spectrolab, "Production Ready 30% Efficient Triple Junction Space Solar Cells," Spectrolab -A Boeing Company, <https://www.spectrolab.com/pv/support/C.%20Fetzer%20et%20al,%2033%20IEEE%20PVSC%202008,%20Production%2030%20Percent%20Efficient%20Triple%20Junction%20Space%20Solar%20Cells%20.pdf>, Accessed 27 Apr. 2019.
36. Wertz, J. Everett, D., Puschell, J., "Space Mission Engineering : The New SMAD", Hawthorne, CA : Microcosm Press, 2011
37. Solar Power Management, "Iridium Qualifies Multijunction Solar Panel System", Solar Power Management



[https://solarpowermanagement.net/article/95152/Iridium\\_Qualifies\\_multijunction\\_solar\\_panel\\_system](https://solarpowermanagement.net/article/95152/Iridium_Qualifies_multijunction_solar_panel_system) Accessed 27 Apr. 2019.

38. Nano-Avionics, “*Electrical Power System (EPS)*”, <https://n-avionics.com/subsystems/cubesat-electrical-power-system-eps/>. Accessed 27 Apr. 2019.
39. Fisher, John. “A Preliminary Design for the InSPiRESat-1 Mission and Satellite Bus”. <https://pdfs.semanticscholar.org/cc10/479df2096429ec46966e54a6e7246f989e46.pdf>
40. Dhuyvetter, Eleanor. Parisi, Gianna-Maria. “Phoenix PDR”. 24 March 2017. [http://phxcubesat.asu.edu/sites/default/files/general/phoenix\\_pdr\\_part\\_2\\_1.pdf](http://phxcubesat.asu.edu/sites/default/files/general/phoenix_pdr_part_2_1.pdf)
41. Campbell, Mark. Henry, Daniel. Waydo, Stephen. “CubeSat Design for LEO-Based Earth Science Missions”. 2001. <https://pdfs.semanticscholar.org/cc10/479df2096429ec46966e54a6e7246f989e46.pdf>
42. “Size Class of Fire.” *The National Wildfire Coordinating Group*, NWCG, [www.nwcg.gov/term/glossary/size-class-of-fire](http://www.nwcg.gov/term/glossary/size-class-of-fire).



## Appendix A. Fire Classification

**Table 42. NWCG Fire Classification.** *The most commonly cited classification scheme for wildfires used in the US.*

Classification	Minimum Size	Maximum Size
<b>Class A</b>	0 acres ( $0 m^2$ )	< $\frac{1}{4}$ acre
<b>Class B</b>	$\frac{1}{4}$ acre (1,011.71 $m^2$ )	<10 acres
<b>Class C</b>	10 acres (40,468.6 $m^2$ )	<100 acres
<b>Class D</b>	100 acres (404,689 $m^2$ )	<300 acres
<b>Class E</b>	300 acres (1,214,056.926 $m^2$ )	<1,000 acres
<b>Class F</b>	1,000 acres (4,046,856.422 $m^2$ )	<5,000 acres
<b>Class G</b>	$\geq$ 5,000 acres (20,234,282.112 $m^2$ )	--

## Appendix B. Requirement Exemptions

**Table 43. Requirement Exemptions.** *A table consisting of all RFP requirements which the Fire-LOC system is exempt from with the subsequence reasons why.*

Requirement Exemptions	Purpose of Request
Fire-LOC requested use of Telecommunications constellations.	Given Fire-LOC's objective, the speed with which data is downlinked is vitally important. The Fire-LOC team would like to investigate constellations such as Globalstar for this purpose.
Fire-LOC requested use of non-US based ground Stations.	Fire-LOC wishes to compare the use of non-US based ground stations to telecommunications satellites, to ensure an effective and cost competitive decision is made.
Fire-LOC requested non-US based data gathering.	Fire-LOC wishes to locate, observe, and classify fires globally to increase its feasibility as a fire-detection system.
Fire-LOC requested an alteration of the global coverage requirement.	Oceanic coverage is unnecessary and historical fires rarely occur above 70°S or below 70°N.



## Appendix C. Iterative Design Approach

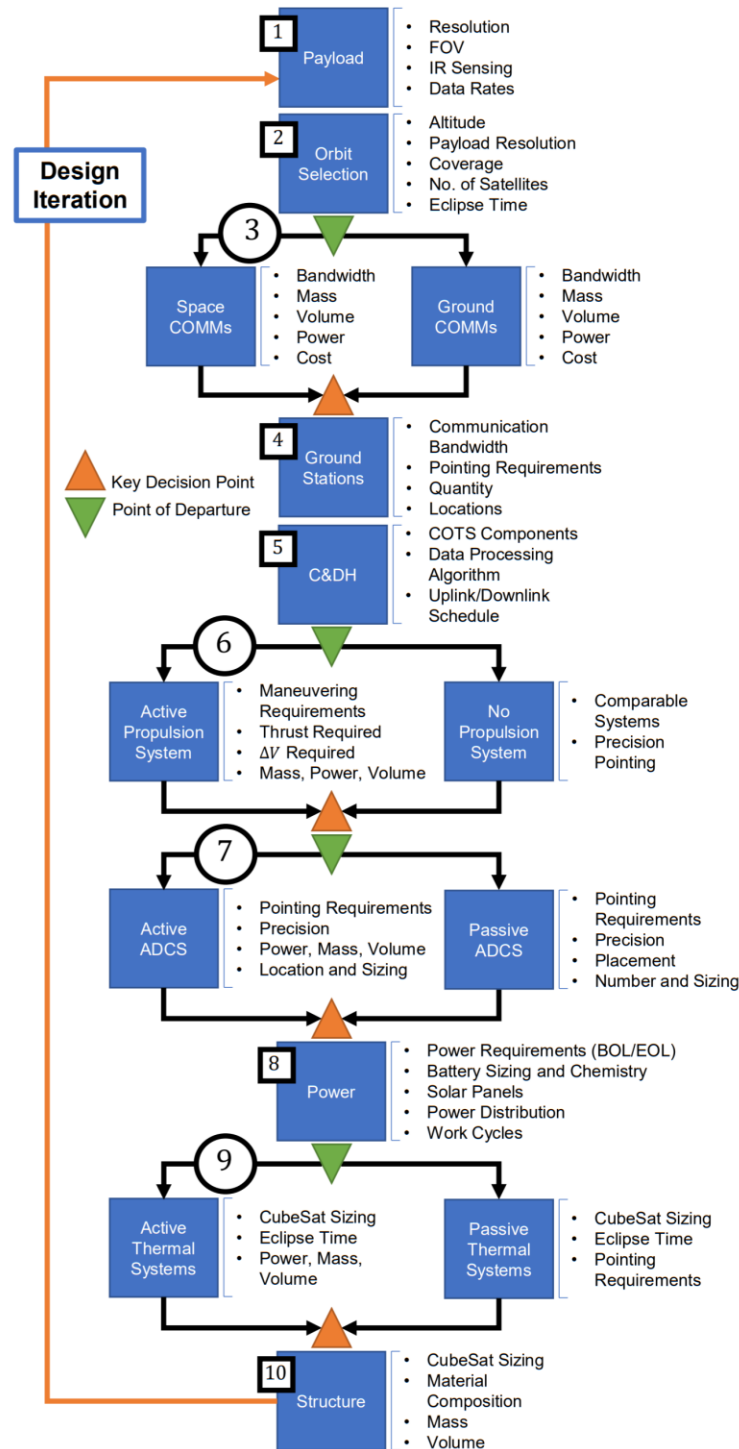


**Figure 50. Iterative Tree Diagram.** The iterative design approach developed for the FIRE Trade Study Documentation method.



## Appendix D. Concept of Operations

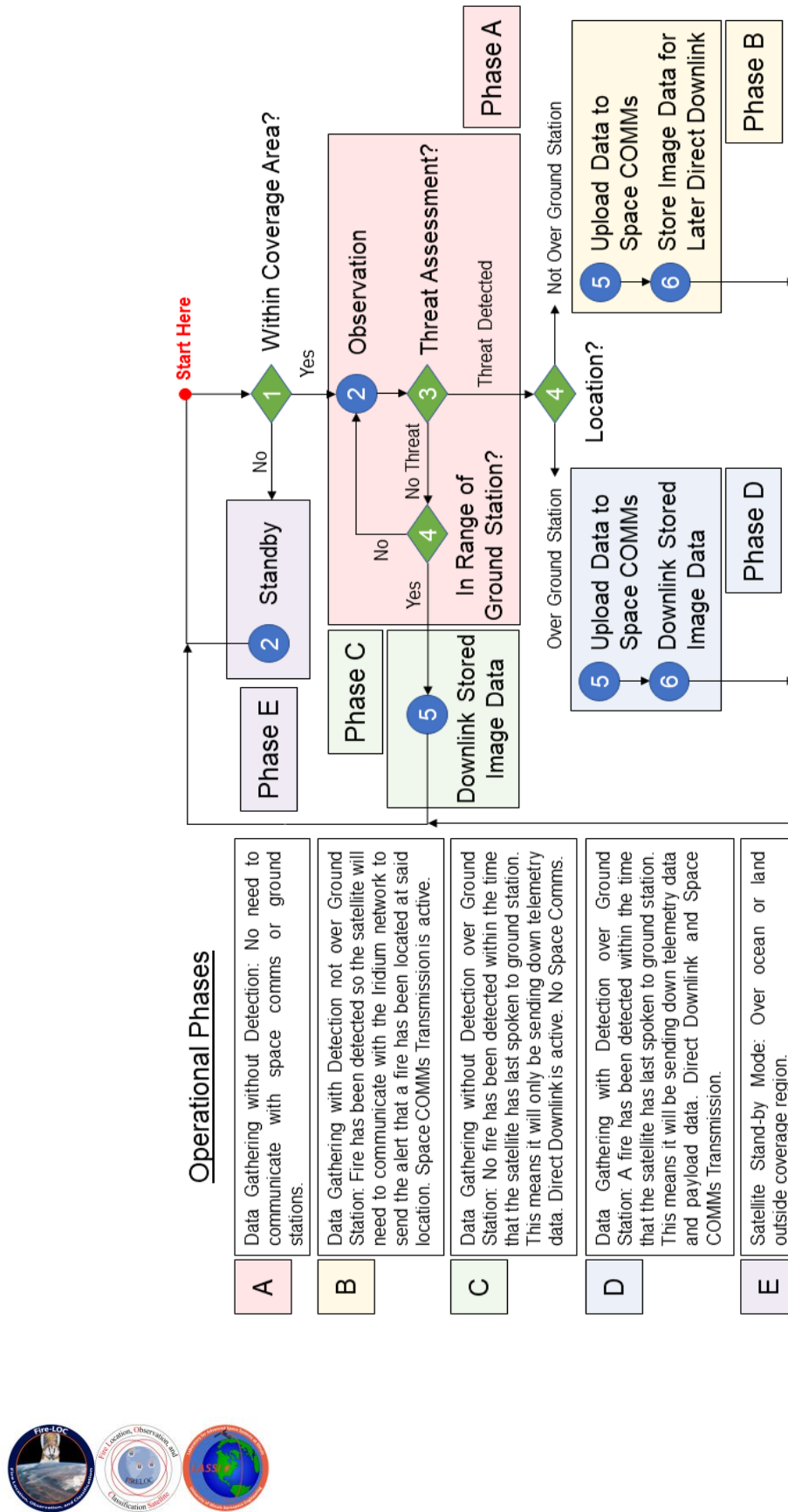
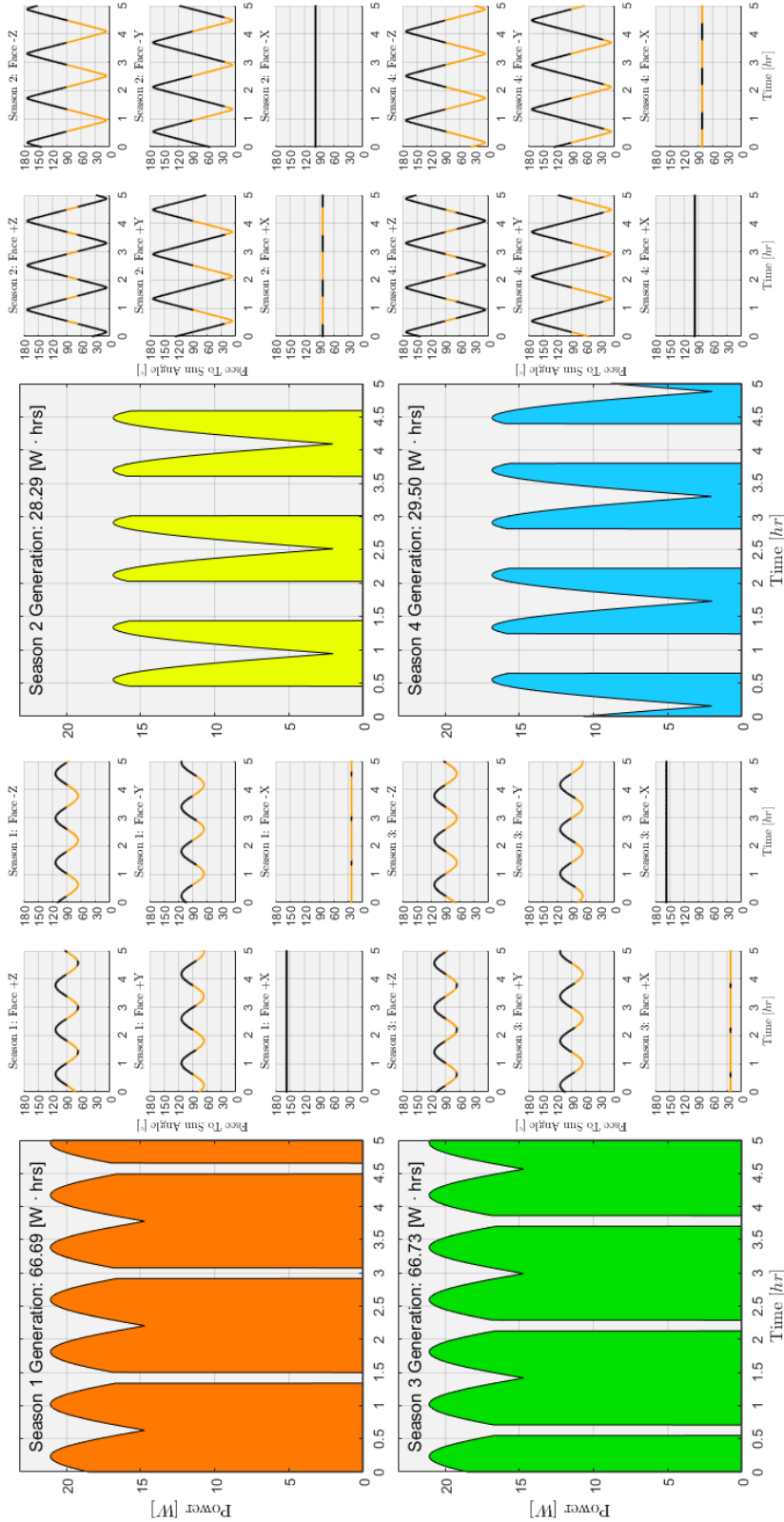


**Figure 51. Fire-LOC Concept of Operations.** The decision tree which relates the operational phases and all their interactions.



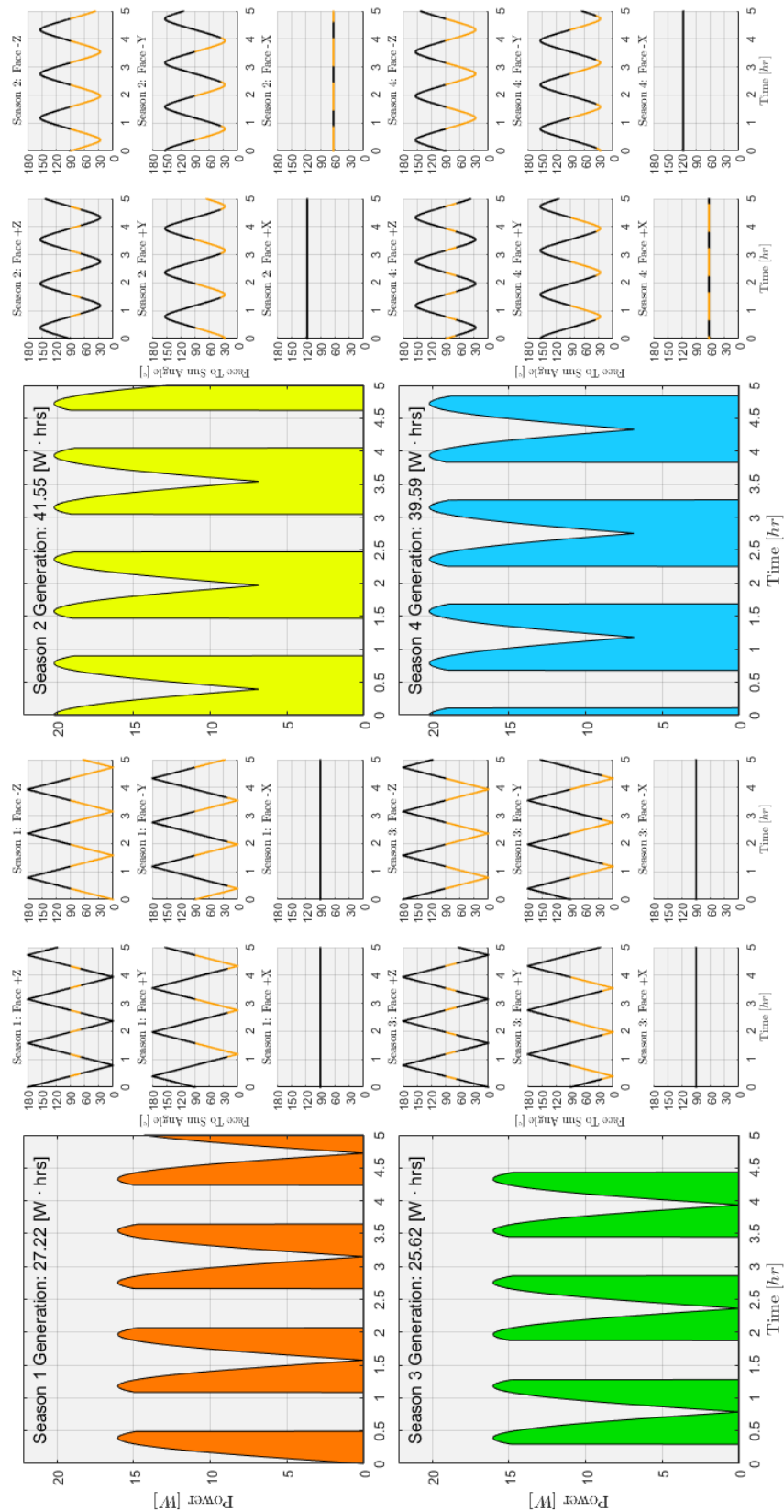
## Appendix E. Power Generation Figures



**Altitude: 500 km,  $\Omega = 261.82^\circ$ ,  $\omega = 327.27^\circ$ ,  $f = 0^\circ$ ,  $i = 68^\circ$**

**(best case: season 3)**





**Altitude: 500 km,  $\Omega = 0^\circ$ ,  $\omega = 0^\circ$ ,  $f = 0^\circ$ ,  $i = 27^\circ$**   
**(worst case: season 3)**



## Appendix F. Gantt Chart

